NASA CONTRACTOR REPORT

NASA CR-485

NASA CR-485

EVALUATION OF SELF-SEALING STRUCTURES FOR SPACE VEHICLE APPLICATION

by Philip J. D'Anna and Roger M. Heitz

Prepared by
NORTHROP CORPORATION
Hawthorne, Calif.
for

NATIONAL AERONAUTICS AND SPACE ADMINISTRATION • WASHINGTON, D. C. • MAY 1966

NASA CR-485

EVALUATION OF SELF-SEALING STRUCTURES FOR SPACE VEHICLE APPLICATION

By Philip J. D'Anna and Roger M. Heitz

Prepared under Contract No. NASr-102 by
NORTHROP CORPORATION
Hawthorne, Calif.

for

NATIONAL AERONAUTICS AND SPACE ADMINISTRATION

For sale by the Clearinghouse for Federal Scientific and Technical Information
Springfield, Virginia 22151 – Price $3.00

CONTENTS

EVALUATION OF SELF-SEALING STRUCTURES

FOR SPACE VEHICLE APPLICATION

By Philip J. D'Anna and Roger M. Heitz
Northrop Space Laboratories

SUMMARY

The concept of a self-sealing wall is investigated as a technique for ensuring the sealed integrity of pressurized space vehicle compartments in a micrometeorite environment. Experimental verification of the feasibility of this concept has been achieved with simulated space vehicle multi-sheet wall structures incorporating either mechanical, chemical or combined mechanical-chemical self-sealing techniques which were developed during the course of this investigation. Self-sealing capability of the candidate wall configurations has been established for a pressure differential of one atmosphere and three temperature conditions of the impact face sheet (R.T., -85°F and +300°F), by puncturing wall specimens with a 1/8-inch diameter steel sphere at impact velocities of 20,000 fps and above. However before effective self-sealing could be consistently achieved, at these higher impact velocities, it was necessary to develop impact damage control techniques for minimizing damage to the wall face sheets where sealing was to be effected.

Two basic self-sealing wall configurations evolved from this investigation. One configuration, the "Integral System Concept," incorporates the self-sealing feature into the space between the inner and outer shell of an aluminum structural wall. In this concept, the sealing action is achieved at the outer shell where impact damage is minimal and sealing more easily effected. The other self-sealing wall configuration utilizes a "Tile Concept" in which the self-sealing feature is incorporated into a nonmetallic open face tile which is then bonded to the inner shell of a double face sheet wall structure. In this concept, the sealing action is accomplished at the inner shell of the basic wall structure. The weight that had to be added to a basic multi-sheet wall geometry in order to give it self-sealing capability varied from 0.40 lbs/ft^2 for the mechanical concept to 1.04 lbs/ft^2 for the combined mechanical-chemical sealing system when applied to the integral wall concept. When the tile concept was used, a weight addition of 1.45 lbs/ft^2 was required. The final weight of the wall structure will, of course, depend on the specific structural and thermal requirements of the space vehicle. No attempt was made during the program to optimize the self-sealing techniques for minimum weight.

Ballistic test results confirm the fact that a multi-sheet wall structure possesses improved penetration resistance over that of a single sheet configuration of equivalent weight. However, it was observed that upon perforating a multi-sheet aluminum wall configuration at velocities of 20,000 fps or higher, blowout or petalling of the rear shell could be expected. Replacing the aluminum rear shell with a fiberglas-epoxy laminate, which is not susceptible to petalling, minimized the impact damage and permitted successful sealing at that face with the self-sealing tile concept. It was also determined that the front face aluminum sheet of a multi-sheet wall, when isolated from nearly incompressible materials, sustains a simple hole. Therefore, it is concluded that, for wall structures having metallic face sheets, self-sealing can best be accomplished at the outer shell where impact damage is minimal. However, while in conventional multi-sheet wall construction the inner shell is made airtight, the "integral" self-sealing wall requires that the outer shell be airtight. For the conventional type of wall construction, sealing must be achieved at the inner shell, therefore requiring that the self-sealing tile concept be used. This also requires that the inner pressure shell be fabricated with either a nonmetallic laminate or a bonded composite of nonmetallic laminate and metallic face sheet.

Based on current knowledge of the meteoroid environment and an estimated penetration flux, a preliminary comparative analysis, between non-self-sealing and self-sealing wall configurations, indicates that for a probability of zero penetration equal to 0.990, the weight tradeoff point will occur at a mission parameter $A\tau$* equal to 8.2×10^6 ft^2-days. If reliability considerations require a probability of zero penetration equal to 0.999, then the weight tradeoff point will occur at a value of $A\tau$ equal to 8.2×10^5 ft^2-days. For values of $A\tau$ larger than those indicated, both wall configurations can be expected to be punctured. However, while puncturing of the non-self-sealing wall will result in air leakage from a pressurized compartment, the self-sealing wall would seal the puncture and maintain the sealed integrity of the compartment beyond the mission parameters indicated. Even for one of the self-sealing wall configurations tested in which only partial sealing was achieved, it is shown that the time required to decompress a 10,000 ft^3 space station from 14.7 psi to 5.0 psi is increased from 1.3 days, for the unsealed punctured wall, to 580 days for the partially sealed wall. Therefore, while the possibility of an incomplete seal is recognized, the time gained by even a partial seal may mean the difference between a successful mission and a catastrophic failure.

INTRODUCTION

Recent limited findings from satellite experiments, although confirming the existence of a "micrometeoroid environment" have not as yet resolved the various conflicting opinions concerning the exact nature of the environment or the magnitude of its hazard to space vehicles. However, it is generally agreed upon by most investigators that, due to their extremely high velocities (36,080 to 236,160 fps or 11 to 72 Km/sec), micrometeoroids do present a real hazard to manned space vehicles, particularly those destined for long duration missions.

The potentially hazardous effects of micrometeoroid impacts, other than punctures followed by irreplaceable fluid losses, include physical injury to vehicle occupants and damage to critical components or subsystems by the resulting spray of impact-induced particles. For limited space missions in the near vicinity of the Earth, a number of punctures of the crew compartment with subsequent loss of atmosphere may be tolerated since the vehicle's proximity to the Earth makes it possible to abort the mission and return before the air supply is depleted. As space mission times and ranges from Earth are increased, the air leakage rates due to meteoroid induced damage or punctures may also be expected to increase. Though it is conceivable that some of these leaks may be located and sealed by the crew, a number of undetectable or inaccessible punctures would probably remain. This would ultimately result in a critical leakage rate and catastrophic failure of the mission, since all life supporting atmosphere would probably be lost or expended before the crew could return to Earth.

A representative technique for minimizing this hazard is the Whipple meteoroid bumper, or spaced sheet structure concept. At present, this concept is the one most frequently proposed by space vehicle designers. In this technique, the bumper vaporizes the meteoroid with the resulting spray of particles hopefully being stopped by the inner shell. It has been shown by numerous investigators that this configuration has greater penetration resistance than an equivalent weight single wall structure and is also highly effective in preventing the spray of impact-induced particles into the interior of a space vehicle compartment. However, damage to the inner shell by the spray of impact-induced particles may be severe enough to cause fluid leakage from pressurized compartments. Therefore, although the bumper shield concept may provide adequate protection for limited short duration missions it does not provide the "fail-safe" capability required for extended orbital, lunar, or interplanetary flights.

---

* A = Vulnerable area of space vehicle (ft^2)

τ = Exposure time in meteoroid environment (days)

Systems consisting of automatic leak detection, location, and manual repair have also been considered. However, the complexity of these systems plus the fact that the burden of sealing the puncture is placed on the astronauts, are considered to be serious drawbacks. In view of the above, it is appropriate that new concepts and techniques be developed and investigated to efficiently satisfy the "leak proof" pressurized wall requirements for future manned long-duration space missions.

With this objective in mind, the concept of a self-sealing structure wall has been proposed and its feasibility for enhancing the sealed integrity of a space vehicle investigated. In pursuing this goal various self-sealing techniques and self-sealing wall configurations were developed and their feasibility investigated. Initial wall concepts, while sealing effectively when punctured with 1/8-inch diameter steel spheres at impact velocities below 10,000 fps, proved ineffective when tested at higher impact velocities. In view of these initial results, modifications suggested by shock wave theory were incorporated into subsequent wall configurations (Reference 1) in order to minimize shock wave damage to the panel face sheets and increase their potential for successful sealing at higher impact velocities. These revised wall configurations have provided effective sealing at impact velocities above 20,000 fps with 1/8-inch diameter steel spheres.

As an additional task during this program, some exploratory experiments were conducted in which water-filled tanks were penetrated by high velocity particles. The purpose of this investigation was to develop and evaluate techniques for preventing explosive rupturing of thin shell pressurized tank walls under the ballistic conditions which normally create such failures. Details of these techniques and a summary of test results may be found in Reference 2 (classified Confidential).

The principles and concepts of the self-sealing wall structures investigated during the course of this investigation are summarized in the immediately following section. Succeeding sections contain discussions of: pertinent material and fabrication considerations related to the incorporation of self-sealing capability in a wall structure; summarization of the experimental program and evaluation of ballistic test results; analysis and comparative evaluation between self-sealing and non-self-sealing wall structures; conclusions and recommendations for future study.

PRINCIPLES AND CONCEPTS OF SELF-SEALING WALL STRUCTURES

The philosophy of self-sealing structures for space vehicles is based on the principle that air leakage control for meteoroid induced punctures may be achieved without resorting to an "absolute" puncture proof structure. The basic structural approach in this concept, though not primarily directed to the prevention of punctures, is oriented towards the development of structural wall configurations that will moderate penetration and shock induced damage to a pressurized compartment wall so that any resulting punctures may be effectively sealed by a "self-repair" system. In such a system, the self-repair mechanism is either attached to, or forms an integral part of the structural wall of the pressurized compartment to be protected. When leak provoking damage to a pressurized compartment occurs, a self-sealing action is initiated either mechanically by the local dynamic imbalance generated by the escaping fluid, or by the dynamic action of the penetrating particle causing an interaction between two chemical components that will expand in certain cases and then cure to form a solid polymeric mass.

During the course of this investigation, various self-sealing concepts and techniques were evaluated. A review and brief description of these basic concepts is given in the following subsections, together with pertinent remarks concerning their feasibility and/or limitations.

Mechanical System Self-Sealing Concepts

Systems activated by the mechanical response of elastomeric materials. — One of the earliest concepts investigated during this program depends on the mechanical response of cured elastomeric materials, following puncturing, to effect the sealing action. Figure 1A illustrates the basic components of this concept. The core cells of a double wall plastic honeycomb core sandwich are filled with an elastomeric sealant material (cured in place). The sealant is confined between the inside of the pressurized shell of a vehicle and a backup sheet of nonmetallic material. Upon perforation by a particle, the local dynamic imbalance causes the confined sealant to rebound or collapse into the hole and seal the puncture. In a modified version of this concept, a precompressed elastomeric core is inserted in the void between the face sheets of the wall structure. Precompression was achieved by using an elastomeric material that expands upon curing, and allowing it to expand and cure in the confined space of an assembled sandwich wall structure. Upon puncturing, the core would respond to the compression preload and close the hole. Both of these concepts sealed effectively when punctured with 1/8-inch diameter steel and glass spheres at impact velocities to 7000 fps. However, at higher impact velocities, shock wave induced damage to the face sheets and excessive sealant material removal along the pellet entry path reduced the self-sealing effectiveness of these two concepts. Further details on these two configurations may be found in Reference 3.

Systems activated by the escaping fluid. — The forces generated by the pressure differential across a puncture in a pressurized compartment may be used to move a sealing element into the hole to effect a seal. Three wall configurations using this principle of operation were evaluated.

The fiber mat concept: In the configuration depicted in Figure 1B, a mass of low density asbestos fibers is used as the sealing element. Following perforation of a pressurized compartment the fibers are drawn into the puncture and thereby restrict the flow of air through the hole. Testing of this configuration with 1/8-inch diameter steel spheres at impact velocities to 7000 fps yielded air leakage rates of approximately 5 lbs/day (against a pressure differential of 1 atmosphere) compared to 260 lbs/day for an unsealed 1/8-inch diameter hole. In an interesting modification of this concept, a mixture of asbestos fibers (6% by weight) and water was placed into the cavity of the panel similar to Figure 2 . Upon puncture by a 1/8-inch steel sphere at 7000 fps, complete sealing (zero leakage) was initially observed. After this initial sealing, the air leakage rate slowly increased until, at the end of three hours, it stabilized at a rate of 4 lbs/day. This can be explained as follows. At puncture, the fiber-water mixture formed a solid impermeable mass which was forced into the hole by the pressure differential. The water in the asbestos-water mixture freezes immediately upon exposure to a low pressure, creating a temporary complete seal. In a few hours the ice sublimes, thus yielding a partially sealed puncture.

Testing of the above two configurations at impact velocities above 10,000 fps resulted in a reduction in sealing capability. This is attributed to the fact that the greater intensity shock wave, although attenuated by the fibers, disperses them sufficiently from the pellet entry path to prevent their being drawn back to the hole and effecting a complete seal. Additional details on these configurations and further discussion of test results may be found in Reference 4.

The elastomer sphere concept: One of the simplest and minimum weight concepts which can be incorporated easily into a double wall structure is that shown in Figure 1C. Here the sealing elements are flexible impermeable rubber spheres. The sealing capability of this concept has been experimentally demonstrated by puncturing with a 1/8-inch diameter steel sphere at impact velocities to 20,000 fps and above. Effective sealing action results with residual air leakage rates (across one atmosphere pressure differential) varying from zero leakage to less than 2 pounds per day.

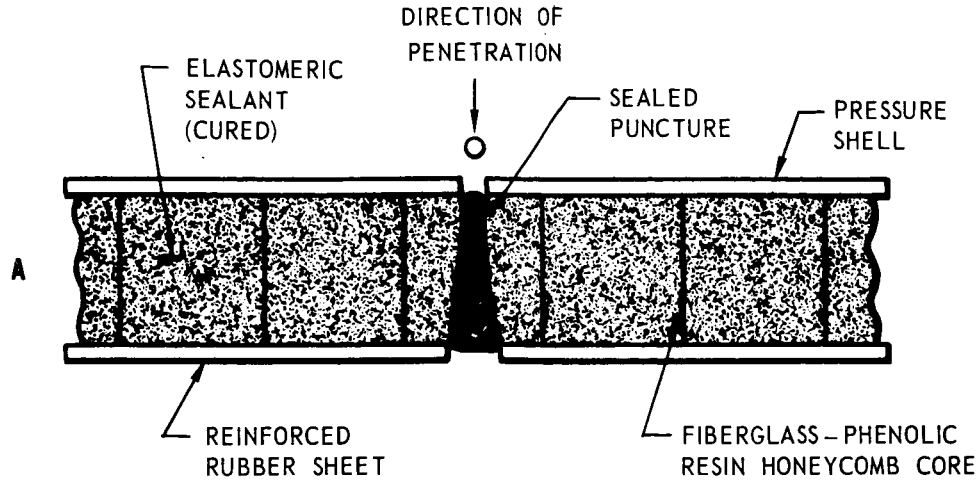

ELASTOMERIC SEALANT CONCEPT

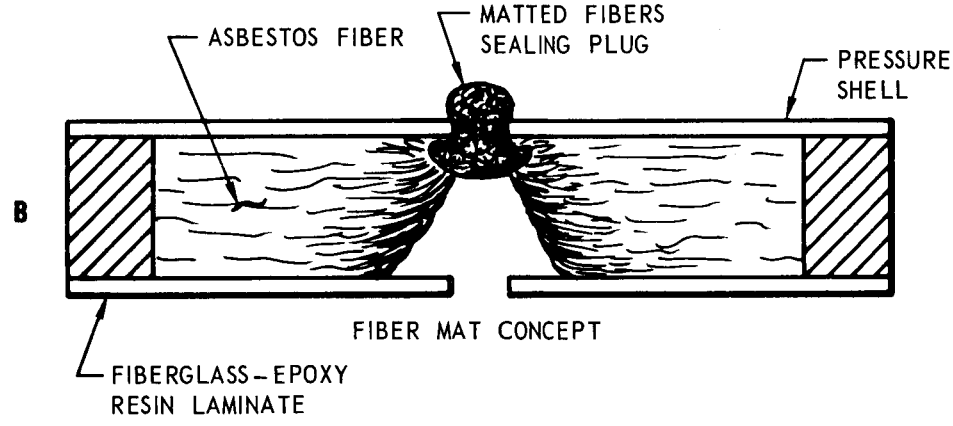

FIBER MAT CONCEPT

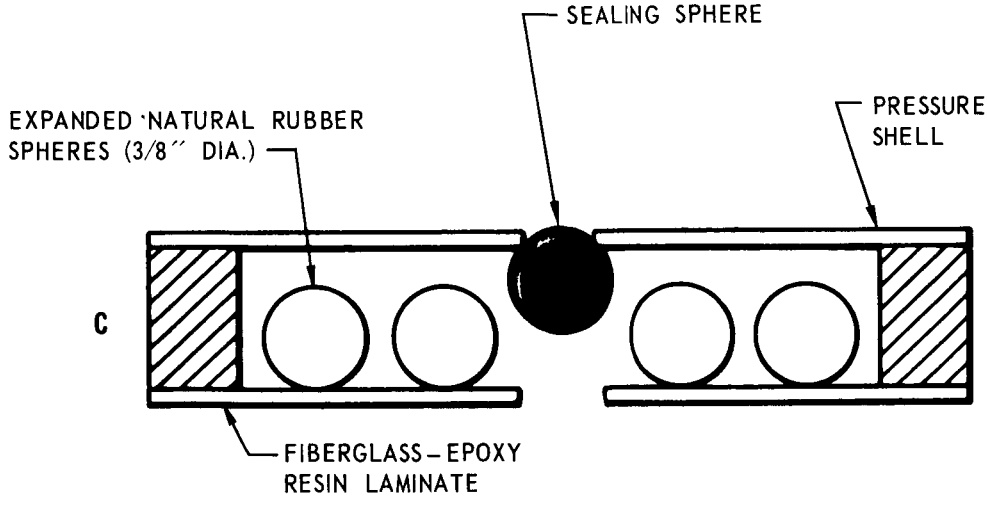

ELASTOMER SPHERE CONCEPT

FIGURE 1 MECHANICAL SYSTEM SELF – SEALING CONCEPTS

The membrane flap concept: The basic configuration of this concept consists of a molded elastomeric material sheet with staggered rows of thin membrane flap segments protruding from one surface. The other surface is then bonded to the inside face of the pressure shell. The theory of operation was based on the pressure differential across a puncture activating the flaps and forcing them across the hole to effect a seal. Three panel configurations were fabricated and tested with 1/8-inch diameter steel spheres at 7000 fps. None of the configurations tested sealed, due either to damage to the flaps local to the pellet entry path or insufficient flexibility of the membrane flaps thus preventing their activation by the pressure differential across the hole. Further details of this concept may be found in Reference 5.

Chemical System Self-Sealing Concepts

The dynamic action of a penetrating particle may be used to initiate a reaction between two initially separated chemicals such that a solid mass will be formed along the pellet entry path to effect a seal. Successful sealing was obtained with the following two basic chemical systems.

Uncured elastomer - catalyst system. — In this system, an easy flowing uncured silicone elastomer is initially separated from its curing catalyst either by a thin impermeable mylar membrane or by encapsulating the curing catalyst in mylar bags, as is illustrated in Figure 2. Following puncture, release of the catalyst local to the pellet entry path forms a solid cured plug of elastomeric material which effects a seal.

Rigid foam resin - catalyst system. — In this system the uncured elastomer is replaced by a rigid silicone foam resin (as indicated in Figure 2), which upon interacting with the catalyst expands and then cures to form a solid sealing plug. This system is preferred over the previous one because of its volume generating (foaming) capability which permits the replacing of removed material along the pellet entry path, thereby facilitating a complete seal of the hole.

Both of the above described chemical systems, when incorporated in wall configurations similar to that illustrated in Figure 2, provided complete sealing when punctured with 1/8-inch diameter steel spheres at velocities below 10,000 fps. At higher impact velocities, damage to the face sheets, particularly if they were metallic, became excessive due to the increased shock induced interfacial pressures. These pressures resulted in excessive loss of the chemical constituents and a reduction in sealing capability. Modifications of the wall configuration (discussed later - see pages 8 and 19) have alleviated this problem and give complete sealing at impact velocities to 20,000 fps and above.

Combined Mechanical-Chemical Sealing Concepts

It was found that a combination of both mechanical and chemical systems in a self-sealing wall structure exhibited considerable improvement over the individually applied concepts. In the separate concept configurations, either one of the sealing systems could effect a seal with a fair degree of reliability. However, by combining the two the mechanical sealing element acted to reduce the efflux of chemicals through the puncture thereby enhancing the chemical sealing action. Even if the mechanical system was only partially successful, the chemical system would complete the seal.

Combined fibers - chemical system. — The basic components of this concept are illustrated in Figure 3a. Upon impact, the incident shock wave is partially attenuated by the loosely packed asbestos fibers. Following puncture of the wall configuration some of the fibers are drawn towards the hole on the pellet entry face, while others intermix with the reacting chemical constituents. This tends to reduce the chemical efflux through the puncture until the sealing process is completed by the chemical system.

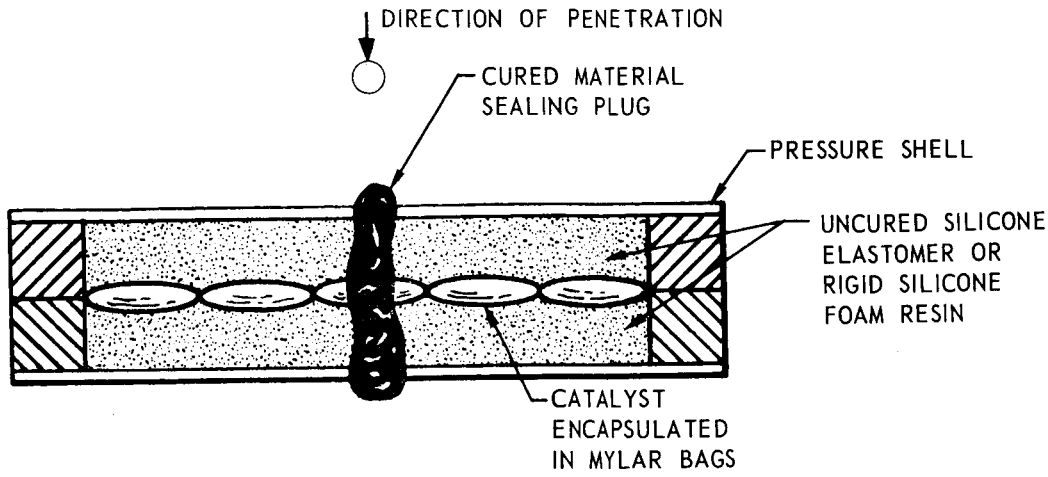

FIGURE 2 CHEMICAL SYSTEM SELF-SEALING CONCEPT

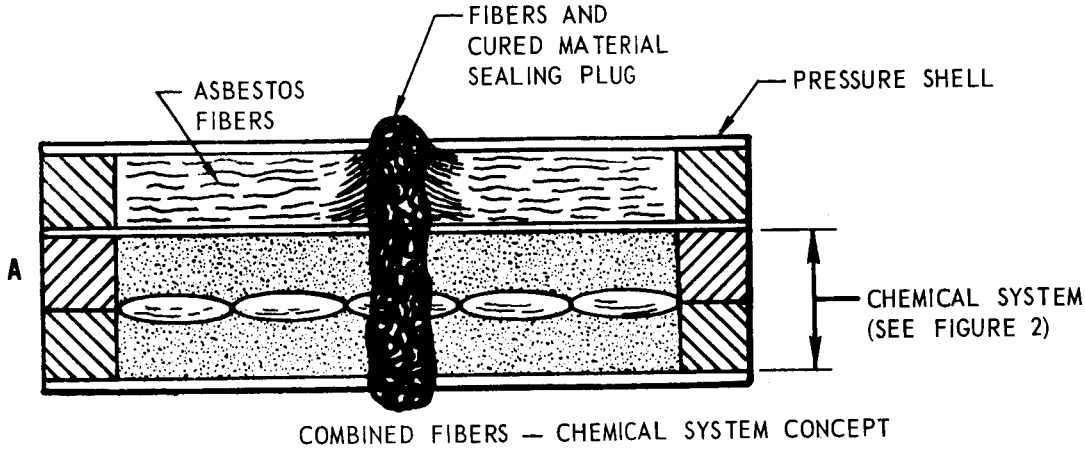

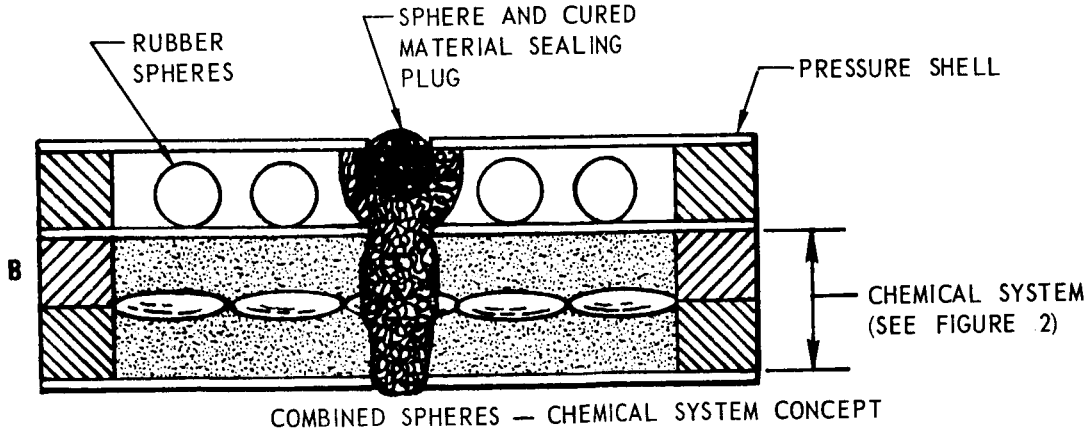

FIGURE 3 COMBINED MECHANICAL-CHEMICAL SELF-SEALING CONCEPTS

Combined spheres - chemical system. — In this concept, illustrated in Figure 3b, rubber spheres replace the asbestos fibers as the mechanical sealing element. The rubber spheres attenuate the shock wave and perform a partial or complete seal. If a partial seal occurs, the chemical reaction following puncture will form a solid mass which completes the sealing action and permanently sets the sphere in the punctured hole.

Both the fiber- and rubber sphere-chemical systems have provided successful sealing at impact velocities to 20,000 fps and above.

MATERIAL AND FABRICATION CONSIDERATIONS

Material Selection and Evaluation

The effectiveness of a self-sealing structure in space vehicles meteoroid hazard control depends largely upon the selection and use of suitable materials. It is realized that to realistically establish feasibility and space vehicle area applicability, the selection and evaluation of materials should be performed under simulated space environments such as combined temperature extremes, vacuum and radiations. The main objective of this research program was to investigate self-sealing concepts which provide effective sealing. Therefore, in the interest of simplification and efficiency, a major effort was devoted to the selection and evaluation of materials for minimizing detrimental high velocity shock wave effects. Thus, most of the tests performed consisted of impacting self-sealing structures with 1/8-inch diameter projectiles at velocities from 7000 fps to 24,000 fps at room temperature and with a pressure differential of one atmosphere across the self-sealing structure faces at the time of impact.

Since it is apparent, however, that certain space environmental conditions, particularly combined temperature extremes and vacuum, might be deciding factors in success of the self-sealing structures under investigation, a study program was established in which the temperature dependence of self-sealing capability was evaluated. It is known that in the course of lunar or interplanetary missions, spacecraft surface temperatures may fluctuate between +200°F and -270°F. These temperature extremes will have a direct effect on the self-sealing structure functional capability depending upon where the self-sealing elements are located with respect to the wall configuration outer shell, and the degree of thermal insulation. In addition, after impact, some sealing materials will be exposed to vacuum (10^{-14} mm Hg.). This factor may further degrade self-sealing reliability.

Another important environmental condition which should be considered is outer space radiation. Although a detailed discussion on this subject is beyond the scope of this report, it should be mentioned that polymeric materials would undergo varying amounts of changes either by cross-linking or scission processes, or by molecular rearrangements after prolonged exposure to such radiation. The degree of change will depend upon the type of polymeric material used, the shielding of the material against radiation, and the radiation exposure.

In the evaluation of the numerous self-sealing concepts various materials were investigated using projectile velocities up to 24,000 fps under room, elevated, and reduced temperature conditions. The variety of materials used in the fabrication of self-sealing panel structures performed one or both of the following: minimized the impact structural damage sustained by the panel face sheets, particularly the rear face sheets; and achieved a fast and effective seal. The most satisfactory materials for minimizing impact structural damage to the self-sealing configuration face sheets were found to be: wall composites of fiberglas-epoxy laminate bonded to a thin sheet of nitrile rubber, so as to inhibit delamination of the laminate; and highly compressible materials interposed between the face sheets and the more incompressible components. The epoxy laminate consisted of a multi-ply of fiberglas-cloth impregnated with versamide

catalyst and epoxy resin. Upon cure, this laminate was strong enough to reduce impact damage at the higher projectile velocities.

The most successful compressible materials for attenuating shock wave effects in the self-sealing wall configurations were found to be: low density asbestos fibers; elastomeric spheres made of various types of elastomeric materials; and flexible polyurethane foams (ρ = 1.5 lbs/ft^3). These materials, when interposed between the entry face sheet and the nearly incompressible materials, encourage expansion of the shock wave in the compressible material and permit some lateral dispersion of the incident energy. It is conceivable that sufficient energy is dissipated in this manner so that any puncturing of the sealing constituents will be accomplished at a lower residual velocity thereby resulting in minimum material removal and successful sealing.

From the three compressible materials tested, the elastomeric balls produced the best results. During fabrication of the spheres, different materials were evaluated such as a variety of RTV silicones and an expanded natural rubber foam. The latter material was found to be the best material in achieving successful mechanical seals. Spheres made with this material proved to be soft enough to conform to irregularities in the puncture, and yet strong enough to effect a seal. The elastomeric spheres (3/8-inch diameter) were selected so as to be larger than the largest anticipated puncture. The amount of oversize depends on the peripheral damage anticipated around the puncture. The spheres which sealed satisfactorily against damage when the pressure differential was 14.7 psi continued to seal against pressure differentials of less than 5 psi.

To perform a fast and effective chemical seal once a self-sealing wall configuration is punctured, selective chemical constituents meeting certain specific properties had to be employed. Briefly, the principle of chemical self-sealing is based upon the dynamic action of a penetrating projectile initiating chemical reactions which result in a fast chemical seal. The rate of the chemical reactions is increased appreciably by the existing pressure differential of approximately one atmosphere across the panel faces at the time of puncture. The principal considerations in selection of the chemical constituents were as follows.

(1) Upon mixing, curing and/or foaming should be fast in order to avoid heavy extrusion of the chemical constituents through the puncture.

(2) The mixing ratio of the chemical compounds involved in the self-sealing system should not be critical.

(3) The chemicals should have a viscosity compatible with proper flow and mixing inside the self-sealing panel configuration.

(4) The chemicals should form an elastomeric or foam material of sufficient strength and adhesion properties to withstand the pressure differential of 15 psi across the panel faces.

(5) The reactive components should have a low or nonexistent toxicity and should not undergo explosive reactions or highly exothermic reactions with the formation of highly volatile and toxic materials.

(6) The type of self-sealing panel configuration used should be considered in the selection of the chemical constituents.

During the course of this program the panel configurations evaluated changed from the single concepts (chemical or mechanical) to the combined concepts (mechanical-chemical). In the individual chemical concepts, the degree and rate of mixing, the viscosity of the reactive fluids, and the rate of reactions of the mixed reactive fluids, were of importance. These parameters dictated the amount of material being extruded from the punctured hole before curing and sealing took place. The rate of chemical reactions depended upon the degree and rate of mixing

which, in turn, was directly dependent upon the viscosity range and the temperature of the reactive constituents and the pressure differential existing across the structure face sheets.

In the case of the more successful combined concepts, the above parameters were still of importance but to a lesser extent due to the compressible materials, such as the elastomeric balls, partially or completely sealing the puncture and thus reducing the efflux of the chemical constituents. This afforded slightly more flexibility in the search for suitable reactive fluids. Among the materials evaluated, a rigid silicone foam was retained which gave the best results when ballistically tested at room, elevated, and reduced temperatures. For more details on the selection of the chemical constituents see Appendix C. When incorporated in self-sealing panel configurations, the rigid silicone foam resin, combined with a stannous type catalyst (T-9), gave excellent results. A very good chemical response was attained with fast formation of an impermeable mass which effectively sealed the pellet entry path. In these tests, excellent sealing assistance was provided by the elastomeric balls in addition to their serving as a very good shock wave attenuator. These results are fully illustrated and discussed later under "Experimental Test Results" (page 19).

To prevent the chemical components from reacting with each other before puncture a reliable means of pre-impact isolation had to be developed. After investigating several methods of isolation, two particular techniques appeared most favorable; encapsulation in plastic bags, and encapsulation in microcapsules. The former is a relatively simple method whereby rigid silicone foam resin and catalyst (T-9) are encapsulated in an appropriate plastic film. This method was highly successful as the tests illustrated in the subsection on "Experimental Test Results" indicate.

The method of encapsulating catalyst and uncured polymer resin in microcapsules was of a more complex nature. In the selection of microcapsules, several important factors had to be considered to insure successful operation.

(1) The shell material should be compatible with the encapsulated chemical, that is, the shell material should not dissolve or should not be affected chemically in any way by the encapsulated viscous fluid or the fluid in which it is suspended or immersed. The materials must be compatible for the anticipated exposure times.

(2) For a given capsule size, the wall thickness should be such that it would enable manual or mechanical mixing of the capsules in viscous materials ranging from 100 to 500 poises viscosity.

(3) The shelf stability of the chemical-containing capsules should be excellent. To attain this condition and in order to protect the encapsulated chemicals from the outside atmosphere, the shell material should be impermeable. Also, the shell material itself should be protected from the surrounding outside atmosphere.

(4) Finally, another important factor is the capsule payload. Enough chemicals will have to be present in the capsules to obtain the requisite ratio of resin to catalyst to effect initiation of the chemical reaction once the self-sealing panel is punctured. For a specific capsule size, the wall thickness determines the payload. On the other hand, the payload can be altered by varying the capsule size and keeping the wall thickness constant.

By taking the above factors into consideration, Southwest Research Institute (San Antonio, Texas) was able to prepare two capsule samples. In one case, the catalyst (T-9) was encapsulated in an algin-gelatin PVA blend shell composition with a payload of 33 to 35 per cent and approximately 1000 micron diameter size. In the other case, the rigid silicone foam resin was encapsulated in approximately the same shell composition (algin-gelatin PVA blend) with a payload of 85 per cent and approximately 1500 micron diameter size. For more details on the preparation of the microcapsules see Appendix C.

Some of the advantages of the microcapsule method were as follows.

(1) Simplification of the self-sealing structure chemical compartment.

(2) Greater ease of handling the chemical constituents.

(3) More localized chemical reaction, thereby enabling additional sealing of nearby punctures within the same self-sealing cell.

(4) More thorough mixing of the chemicals, giving an even faster reaction and a better quality end-product.

(5) The use of higher viscosity chemical constituents, while allowing adequate mixing.

The validity of these five points was checked experimentally by preparing several self-sealing panel configurations containing the microcapsules. Three different capsule combinations were investigated.

(1) Combination whereby the catalyst was encapsulated only and capsules mixed with the rigid silicone foam resin giving a slurry.

(2) Combination whereby both catalyst and resin were encapsulated giving a solid mixture.

(3) Combination whereby the resin was encapsulated only and capsules coated with the catalyst giving a wet solid.

Shock Wave Damage Control

Initial candidate self-sealing wall configurations were successfully tested with 1/8-inch diameter steel projectiles at impact velocities to 7000 fps. At these relatively low impact velocities, the face sheets of wall configurations enclosing cured elastomeric materials or chemical constituents of low compressibility, sustained simple punctures (holes) and minimal material removal along the pellet entry path. Following these initial tests an attempt was made to verify the results with impact velocities above 15,000 fps. These tests, with similar wall configurations, were conducted at the NASA Ames Research Center Ballistic Facility (Reference 3). One-eighth inch diameter pyrex projectiles were fired at impact velocities to 23,140 fps. Results of these tests indicated that when a high velocity particle impacts a compartment containing a nearly incompressible material (liquid or solid), the incident shock wave induces extremely high interfacial pressures which may exceed the dynamic rupture strength of the penetrated wall. In the case of aluminum face sheets, this resulted in crack propagation and petalling of the face sheets local to the pellet entry path. Figure 4 illustrates the type of damage sustained, at two different impact velocities, by a honeycomb core sandwich panel with the core cells filled with a cured elastomer sealant of low compressibility.

On the basis of these initial high velocity tests, it was concluded that those concepts in which sealing capability was dependent solely upon the mechanical response of precured elastomeric materials (e.g. Figure 1A) would not seal at the higher puncturing velocities, due principally to the increased shock wave effects causing excessive material removal along the pellet entry path. For the other mechanical and chemical concepts, control of shock wave damage to the face sheets would be a prime prerequisite for obtaining a successful seal. In view of this, modifications suggested by shock wave theory were incorporated into subsequent wall configurations in order to minimize shock wave induced damage. The following two damage control techniques were found to be the most effective in minimizing impact damage and permitting successful sealing at impact velocities above 20,000 fps.

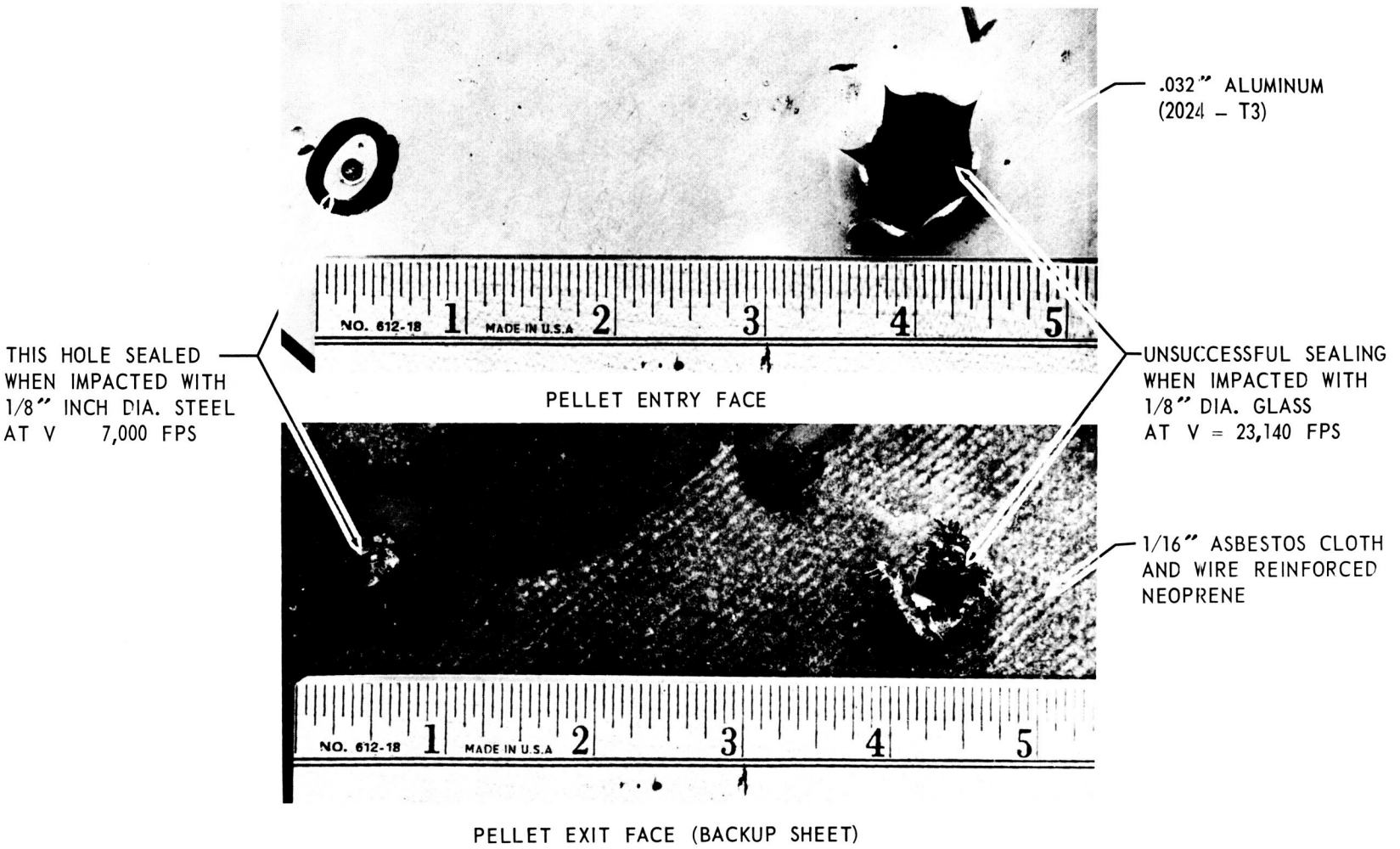

FIGURE 4 COMPARISON OF DAMAGE AT TWO IMPACT VELOCITIES — HONEYCOMB – ELASTOMER CONFIGURATION

(1) The use of nonmetallic face sheets (fiberglas-epoxy resin laminates) in the wall construction.

(2) Isolation of the wall face sheets from nearly incompressible materials (liquid or solid) by air gaps or the interposition of low density and highly compressible materials.

It was determined that an aluminum face sheet could be tolerated as the pellet entry face of a wall if isolated from low compressibility materials by an air gap. The damage in such cases was limited to a simple hole slightly larger in diameter than the penetrating projectile. The air gap proved effective in attenuating shock wave transmission into the wall panel and permitting expansion of the cloud of impact induced particles over a larger area of the inner shell and thereby diminishing its penetration capability. For walls where the aluminum front face sheet was placed adjacent to a low compressibility material (either solid or liquid), petalling of the sheet material local to the projectile entry hole occurred as is illustrated in Figures 4 and 5.

When aluminum rear face sheets were used in self-sealing wall configurations, crack propagation and petalling of the sheet material local to the rear face impact area usually occurred whenever the ballistic limit of the rear sheet was exceeded. The fragmented projectile, impacted face sheet, and enclosed filler material (which is set in motion by the impact) subjects the aluminum rear sheet to a high intensity distributed impulsive load. This type of loading, particularly when preceded by perforation, provokes outward petalling of the aluminum sheet. This is not surprising, since metals in general are more sensitive than nonmetals to rapid crack propagation and/or petalling when subjected to this type of loading.

Fiberglas-epoxy laminates, when used as the rear face sheet, were found to absorb the impact energy with less destructive consequences than metals. Figure 6A shows the punctured nonmetallic rear face sheet of a combined sphere-chemical self-sealing panel configuration in which the rear sheet was separated from the chemical compartment by a 1/4-inch air gap. This wall permitted a successful seal when punctured with a 1/8-inch diameter steel sphere at an impact velocity exceeding 20,000 fps. For purposes of comparison, Figure 6B illustrates the punctured metallic rear face sheet of a similar panel, except for the nonmetallic sheet which was replaced by a 0.020-inch aluminum sheet. This wall was tested with a similar projectile at approximately the same impact velocity. Excessive loss of the chemical constituents through the damaged rear sheet resulted in only partial sealing of the pellet entry hole on the front face. However, subsequent panel configurations were modified by placing a nonmetallic sheet (hole size controller) adjacent to the rear side of the chemical compartment, but separated from the metallic rear face sheet by an air gap or a low-density plastic sponge. This minimized the efflux of chemical constituents from the petalled hole in the aluminum rear sheet and restored the self-sealing capability of this wall configuration.

Self-Sealing Wall Configurations

The initial self-sealing wall specimens tested were basically breadboard prototypes in which the primary purpose was to evaluate various self-sealing concepts for sealing capability. In later tests the more successful self-sealing concepts were integrated into multi-wall metallic structures which were more realistic from an applied point of view. For this task, a wall geometry resulting from a study conducted by NASA, MSC, was selected as being representative of a space vehicle non-self-sealing wall structure. As originally proposed, this wall structure consisted of a 0.020-inch aluminum bumper, a 0.050-inch aluminum pressure shell, and a 2-inch layer of flexible polyurethane foam bonded between the two face sheets. This basic aluminum wall geometry was then modified to incorporate self-sealing capability and shock wave damage control resulting in the following two self-sealing wall configurations.

Integral self-sealing wall. — In this configuration, the self-sealing components are interposed between the metallic face sheets. The space between the face sheets not specifically

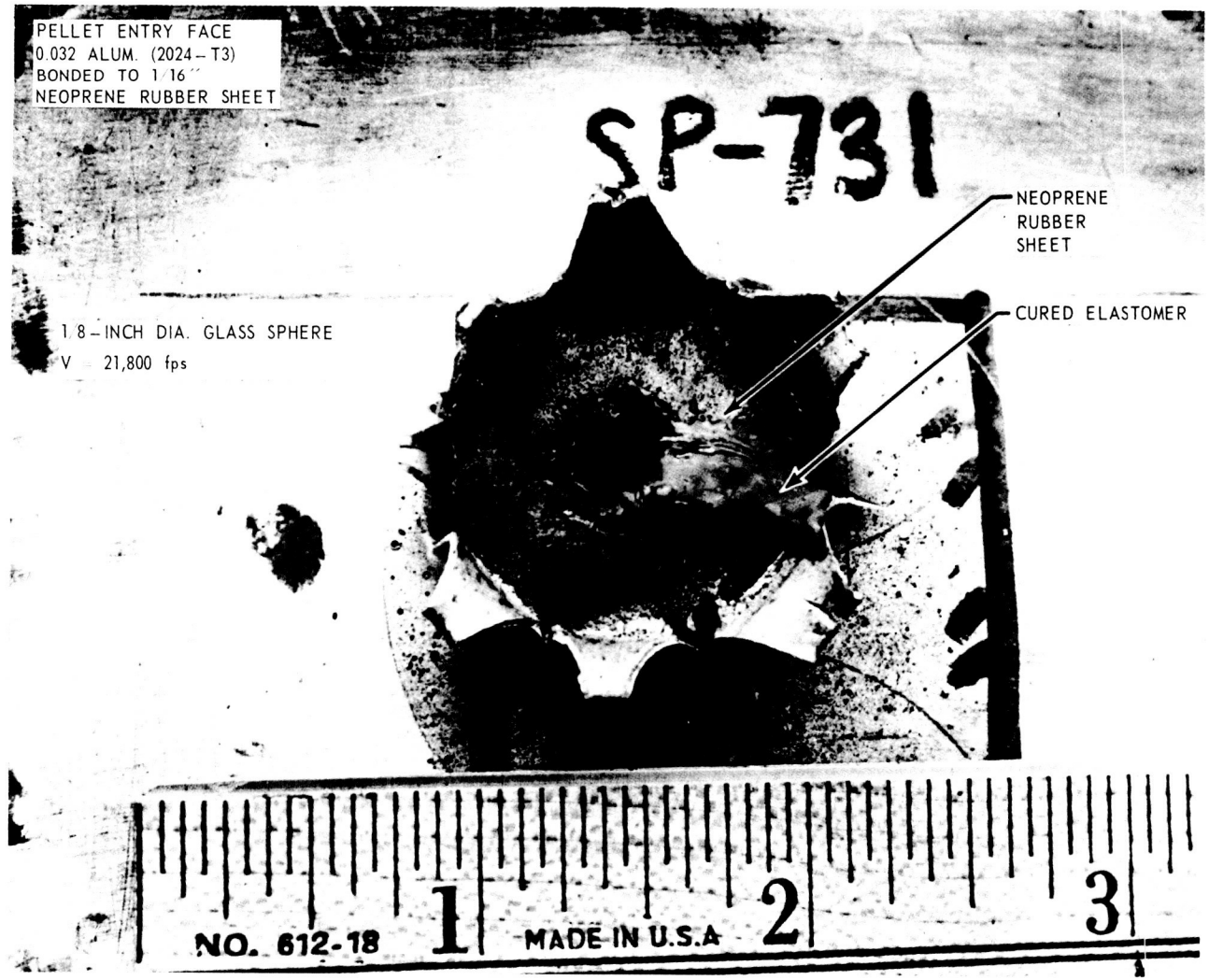

FIGURE 5 IMPACT DAMAGE TO FRONT FACE SHEET OF CHEMICAL SELF – SEALING PANEL CONFIGURATION

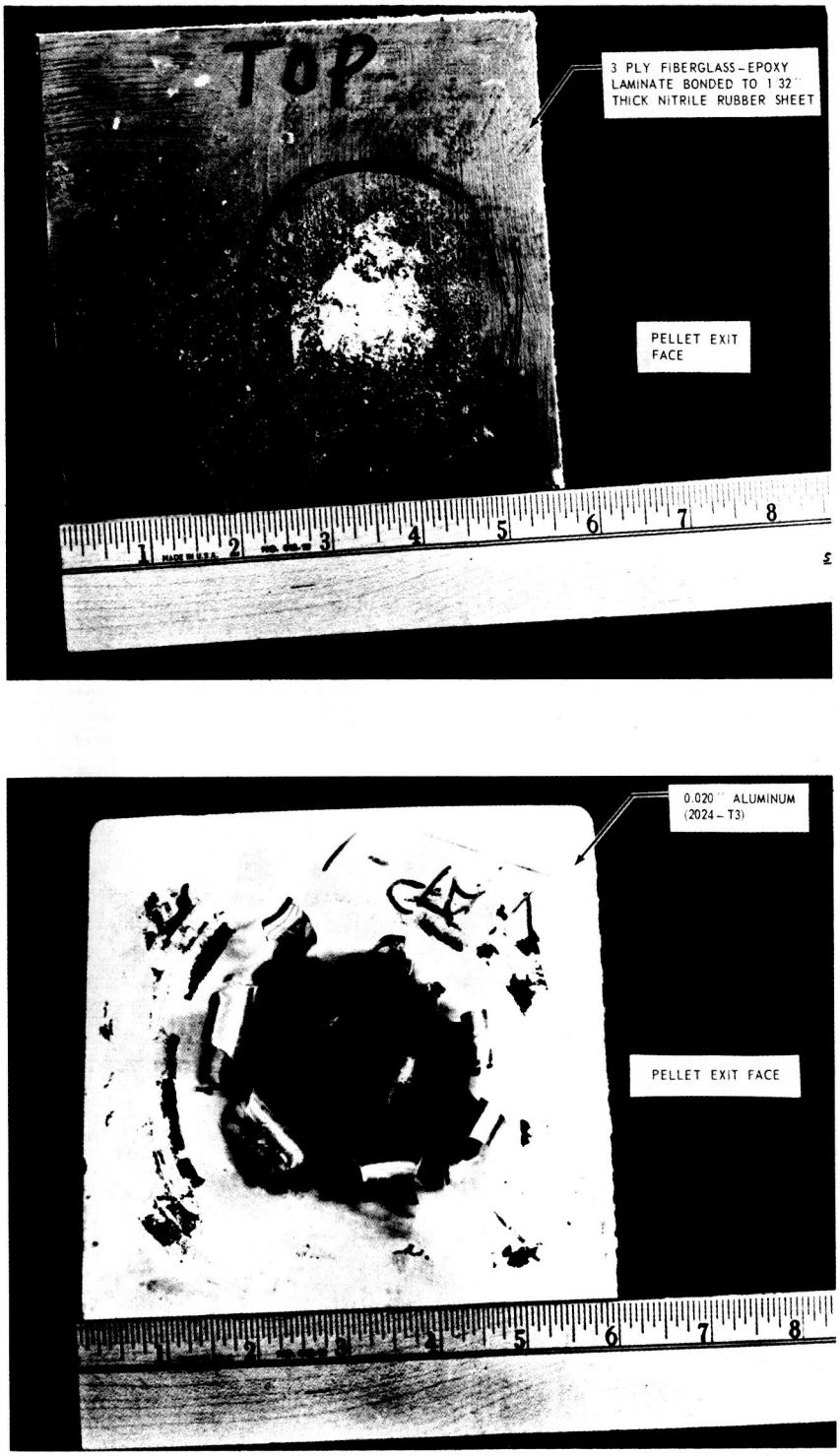

FIGURE 6 COMPARISON OF IMPACT DAMAGE TO NONMETALLIC AND METALLIC REAR FACE SHEETS OF SELF-SEALING PANEL CONFIGURATIONS

used by self-sealing components may then be filled with a low density insulative material to satisfy space vehicle thermal requirements. Two such specimens, one using the elastomer sphere sealing concept and the other the combined sphere-chemical concept, successfully sealed when perforated with 1/8-inch diameter steel spheres at impact velocities to 20,000 fps and above.

Multi-sheet wall configurations of current space vehicles have been conventionally constructed with the inner shell airtight and the outer shell vented to the surrounding atmosphere. However, in the integral self-sealing wall configuration it is a prerequisite that the outer shell be airtight, since sealing is achieved at that face. Now, while the sealing effectiveness of this concept does not require that the inner shell be airtight, reliability and "fail-safe" considerations for manned missions suggest that both shells be made airtight. For such a wall configuration, the ability to resist leak provoking damage would be increased since the inner shell would also have to be perforated before the pressurized compartment became susceptible to fluid leakage. In addition, while the self-sealing system would be maintaining a complete or partial seal on a perforation in the outer airtight shell, manual repairs, if required, could be made to the inner pressure shell, under normal operating cabin pressure, without having to first decompress the pressurized compartment. Should the thermal protection requirements for a space vehicle specify that a vacuum be maintained between the inner and outer shell, provisions could be made for venting any air entrapped during fabrication of the wall (by means of a valve once the vehicle is in space) or following puncture and repair of the inner pressure shell. This problem would be nonexistent with thermal protection systems that do not require a vacuum environment.

If the outer shell only is made airtight, then the primary function of the inner shell would be to contribute to the structural strength of the wall configuration for nonpressure loading conditions (e.g. launch and maneuvering loads). On the other hand, with both shells airtight, the pressure load would be divided between the two. In such a case the distribution of the pressure load and resultant hoop tension stresses in each shell will depend on the ability of the wall structure core or interior structural components to transmit pressure loads to the outer shell. Figure 7 illustrates the core stiffness requirements of a sandwich wall structure as a function of its ability to transmit pressure loads to the outer shell. The ratio of the stress in the outer shell σ_2 to the average stress σ_{AV} is plotted against a parameter representing the crushing stiffness of the core. It should be noted that as the core stiffness parameter increases, the efficiency of the wall structure to act as a unit in carrying pressure loads also increases until the outer shell carries the same stress as the inner shell. The area labeled "conventional sandwich construction" indicates the range of core stiffness for which a sandwich behaves as a structural unit in carrying compressive and shear loads. Therefore this range of core stiffness will also be the most effective for carrying pressure loads. For purely rigid foam cores, the efficiency for transmitting pressure loads decreases thereby requiring the inner shell to carry a greater portion of the total pressure load.

Due to the above considerations, it becomes apparent that in order to make the self-sealing concepts compatible with a wall structure, the sealing components should be incorporated in such a manner that the structural and thermal requirements of the wall are not compromised. Figure 8 illustrates two proposed wall configurations in which the sealing, structural, and thermal requirements may be satisfied. The thickness of the structural components will depend upon the specific application and load requirements for the wall structure.

Self-sealing tile. — In this concept the self-sealing components are fabricated into a nonmetallic single face tile and then the open face of the tile is attached to the inner airtight shell of the pressurized wall compartment. With the tile concept, sealing is achieved at the inner shell and therefore the outer shell of the basic wall structure need not be airtight. However, in order to achieve successful sealing, impact damage to the inner shell must be limited to a sealable type of puncture. This has been accomplished by using a nonmetallic laminate or a composite of nonmetallic laminate and metallic sheet as the pressure shell. In the case of the composite shell configuration, the metallic sheet, used basically for structural considerations, can be

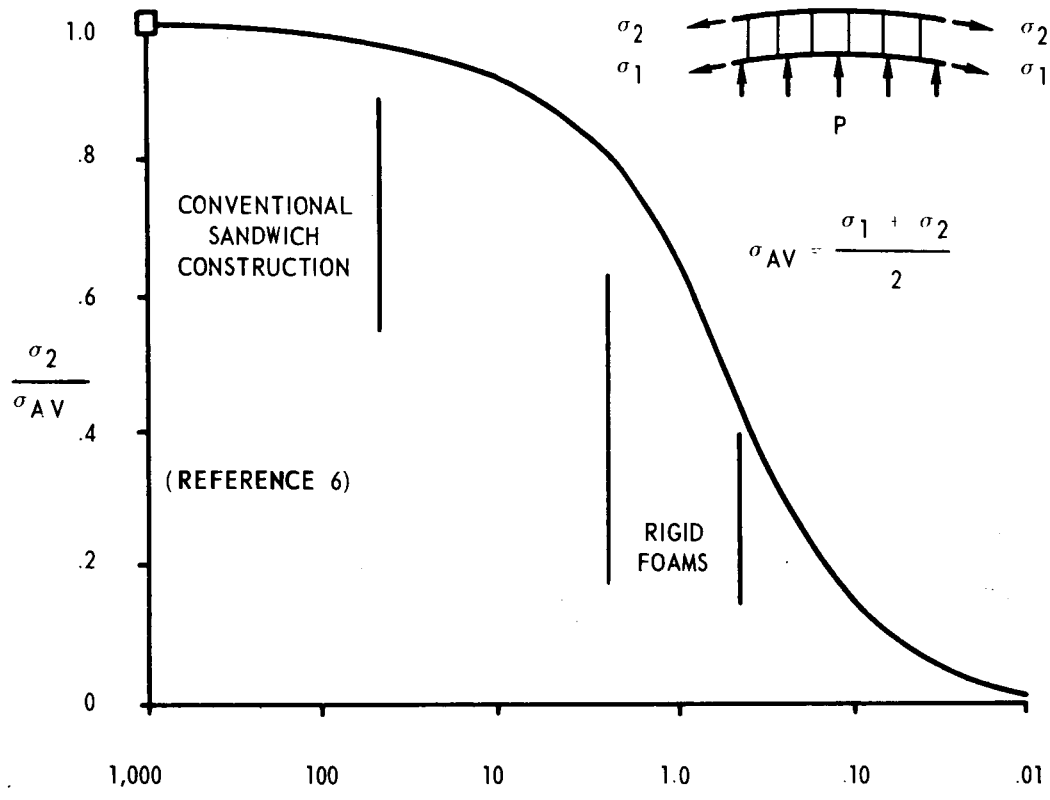

ψ — ELASTIC MODULUS OF SANDWICH CORE MEASURED IN DEPTHWISE DIRECTION

r — RADIUS OF CYLINDER

h — DEPTH OF SANDWICH

E — YOUNG'S MODULUS OF ELASTICITY

t_S — THICKNESS OF ONE FACE SHEET OF SANDWICH

FIGURE 7 EFFICIENCY OF PRESSURIZED SANDWICH SHELLS

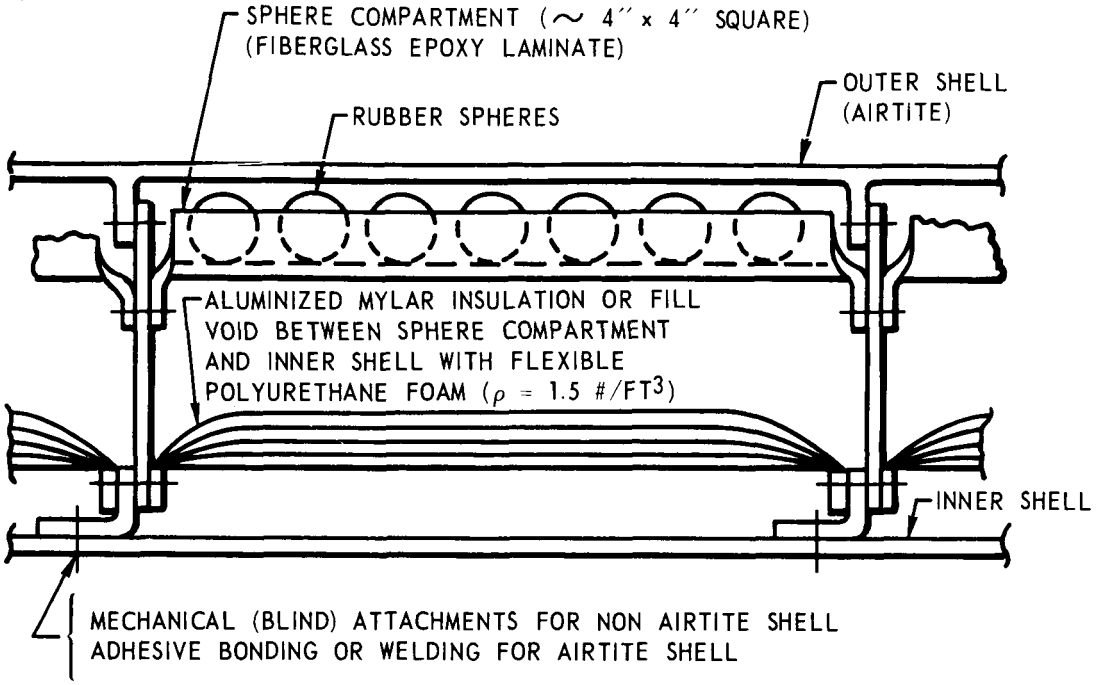

MECHANICAL SELF-SEALING CONCEPT

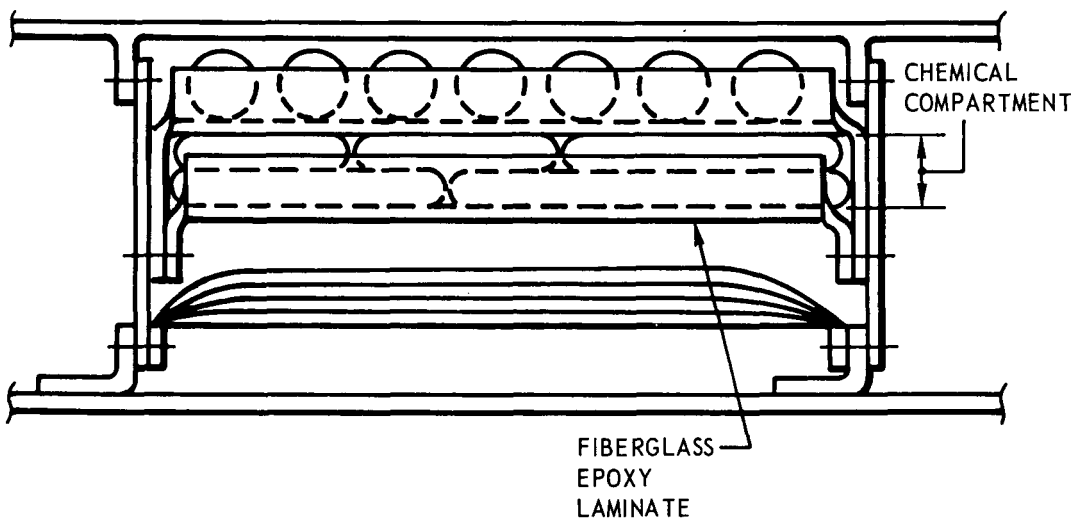

COMBINED MECHANICAL-CHEMICAL SELF-SEALING CONCEPT

FIGURE 8 PROPOSED INTEGRAL SELF-SEALING WALL CONFIGURATIONS

expected to petal once its ballistic limit is exceeded. The sealing in this instance is achieved at the puncture produced in the nonmetallic laminate. Since the puncture in the laminate is usually an irregular shaped hole, complete sealing can be obtained more consistently when the combined sphere-chemical system is used in the tile configuration.

Figure 9 illustrates a proposed self-sealing tile wall configuration in which the sealing, structural, and thermal requirements may be satisfied. As is indicated in the sketch, the individual tiles can be easily removed for making repairs to the pressure shell or for replacing expended tiles. For increased "fail-safe" reliability, the outer shell of the basic wall structure could also be made airtight and some loosely packed elastomer spheres incorporated adjacent to it. This would permit sealing at the outer shell should the tile sealing system fail or provide only a partial seal. In such a situation, manual repairs to the inner pressure shell, if required, could be made under normal cabin pressure conditions and without fear of cabin decompression.

EXPERIMENTAL PROGRAM AND EVALUATION OF TEST RESULTS

Equipment and Test Procedure

The experimental phase of this research program was conducted both at Northrop Space Laboratories and outside ballistic facilities such as NASA Ames Research Center and McGill University, Montreal, Canada. The facilities most frequently used during this work were those at McGill University and NSL. A brief description of the apparatus and test procedure used follows.

The Northrop Space Laboratories' particle accelerator. — This particle accelerator is capable of propelling 1/8-inch diameter projectiles down a 2-foot long barrel at velocities up to 8000 fps by an explosive gun powder discharge from a modified 25-caliber rifle cartridge. Projectiles smaller than 1/8-inch diameter can be propelled using an appropriate sabot-pellet separation technique. Projectile velocities are obtained by means of a velocity measuring trigger break screen circuit associated with a Tektronix 545 oscilloscope. The gun barrel muzzle is enclosed in one end of a transparent plexiglass chamber while the other end of the plexiglass chamber has an opening on which one face of the self-sealing test specimen is mounted. In an actual test, the chamber is evacuated to between 0.2 and 0.3 mm Hg to give a pressure differential across the specimen of approximately one atmosphere. An airtight seal is obtained between the test specimen and the vacuum chamber. Upon impact of the self-sealing structure, the sealability of the structure can be checked by means of a leak detection apparatus consisting of flowmeter gauges connected to a metallic chamber which in turn is attached to the other face of the test specimen.

The Northrop light gas gun facility. — Initial high velocity tests with 1/8-inch diameter steel projectiles were conducted at the light gas gun facility at the Nortronics Division of Northrop Corporation. Although most of the usable data were obtained at medium velocities (10,000 - 16,000 fps), valuable data were recorded regarding panel structural damages due to shock wave effects.

The light gas gun is a two-stage system, using one piston launch tube and one model launch tube. The compressed gas utilized is either helium or hydrogen. The design of both gun and vacuum chamber has been predicated on multi-purpose use. For example, provisions exist for extending the gun launch tube and for changing launch tubes to provide various bore diameters. Lexan sabots of 1/4- or 1/2-inch diameter were used for carrying 1/8-inch diameter or smaller projectiles. The 41-cubic foot vacuum chamber is capable of achieving a vacuum of 0.5 mm Hg with mechanical pumps after one-half hour of pumping time. Projectile velocity was measured with a Flexitron 720 three-channel flash X-ray unit, a trigger break screen circuit, and a Tektronix 545 oscilloscope. The gun has achieved velocities in excess of 22,000 fps with a 1/8-inch diameter steel projectile.

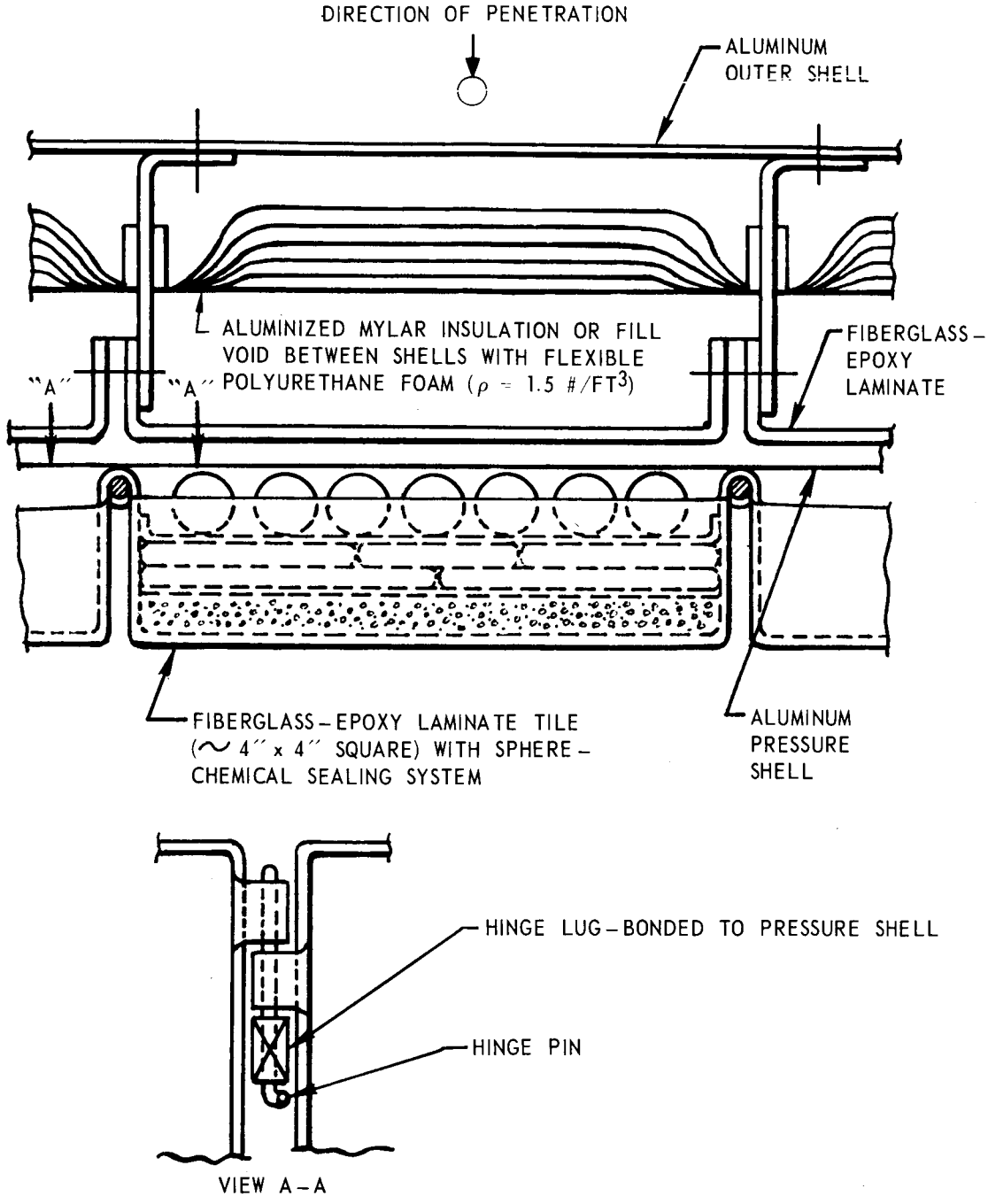

FIGURE 9 PROPOSED SELF-SEALING TILE WALL CONFIGURATION

The McGill University light gas gun facility. — In comparison with the Northrop light gas gun, the McGill gun is a three-stage system. The barrel has a bore of 0.5-inch and is fired with a black powder charge of 500 to 850 gr. Hydrogen is used as the compressed gas in the two pressure chambers using different diameters polyethylene pistons. Full bore lexan sabots carry the type and size projectiles selected. At the end of the evacuated barrel, the sabot and projectile are separated by a short travel in air at one atmosphere. Subsequently, the sabot is deflected by hitting a deflector plate while the projectile travels about 12 feet in a chamber evacuated to 3 mm Hg. The facility can attain velocities exceeding 20,000 fps consistently.

Projectile velocities are accurately determined by the use of a counter which is triggered as the projectiles traverse a light screen and stops as a vacuum phototube records the impact flash. In order to determine whether the projectiles triggered the light screen properly, flash X-ray pictures of the projectile and sabot in flight are taken. If for some reason the sabot, rather than the projectile, triggers the light screen, corrections to the velocity can be made by noting their relative positions in the picture.

Northrop Space Laboratories gun facility for ballistic testing of heated and cooled targets. — The temperature effect (reduced or elevated) on the self-sealing capability of the test structures was determined with the equipment illustrated in Figure 10. This setup uses the NSL particle accelerator described earlier. In an actual test at elevated or reduced temperature the panel specimen is mounted against the target vacuum chamber in such a way as to obtain an airtight seal.

Experimental Test Results

As discussed in the sections on "Principles and Concepts of Self-Sealing Wall Structures" (page 3) and "Shock Wave Damage Control" (page 11), a multitude of self-sealing concepts were evaluated experimentally during this research program. A systematic study and testing was undertaken whereby panel configurations and materials were investigated as the impact conditions and damages to the panel structures changed. Most of the self-sealing panels tested, with the mechanical as well as the chemical concepts, showed excellent self-sealing capabilities when impacted by 1/8-inch diameter steel projectiles at low velocities (up to 7000 fps) under ambient temperatures conditions. However, at higher impact velocities and identical environmental conditions, increased shock wave damage to the face sheets reduced their self-sealing capability. In view of this, modifications suggested by shock wave theory were incorporated in subsequent wall configurations which proved successful in restoring self-sealing capability at impact velocities of 20,000 fps and above.

During a typical mission a spacecraft will be exposed not only to meteoroid hazards, but also to other environmental conditions such as temperature extremes, radiation and reduced pressures. Because of this it was felt that tests should be performed under temperature variation conditions combined with vacuum. Experimental results of the more successful mechanical and chemical self-sealing concepts when impacted by 1/8-inch projectiles at low and high velocities is discussed in the following three subsections. Impact tests at room, elevated, and reduced temperature conditions are described and summarized.

Room temperature tests. — Highly significant results at room temperature were obtained with the more realistic multiwall metallic structures. These structures incorporated all the techniques and results derived from the preceding panel configuration breadboard models. The more successful mechanical and chemical self-sealing concepts were integrated into a double wall metallic structure to attain a more representative structure for space vehicle applications. Two basic configurations were investigated: the integral self-sealing panel configuration (IS);

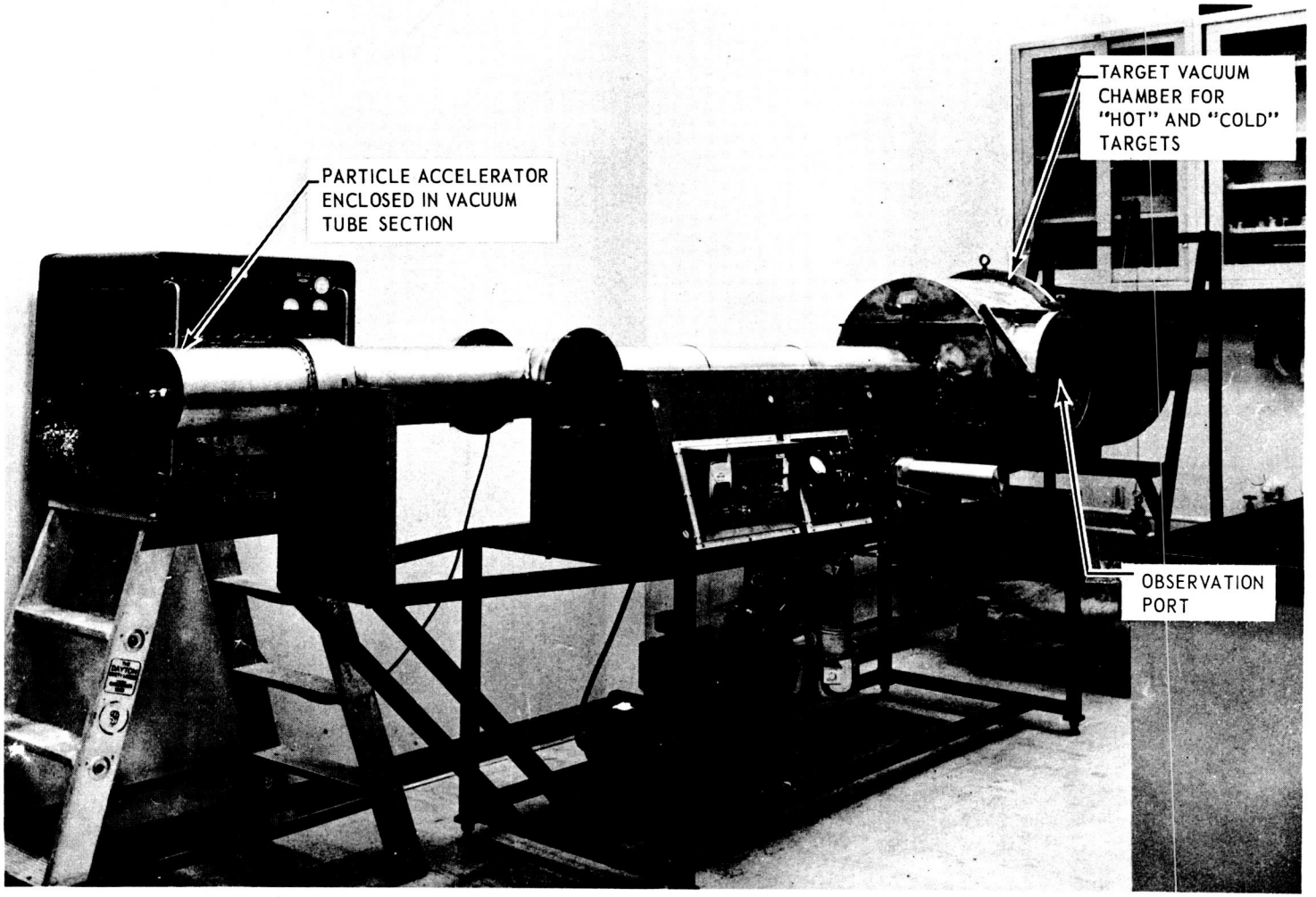

FIGURE 10 GUN FACILITY FOR BALLISTIC TESTING OF HEATED AND COOLED TARGETS IN A HIGH VACUUM

and the self-sealing tile configuration (SST). In both cases, the metallic outer and inner face sheets were used to conform with the up-to-date preference of metallic space vehicle cabin walls.

In the "Integral System" (IS) panels, as illustrated in Figure 11, the purely mechanical self-sealing configurations (IS-B and IS-C) functioned successfully and the entry face hole was easily sealable; however, in both panels the rear face sheet was heavily damaged as shown in Figure 12. Loss of the sealing spheres through the pellet hole of the rear face sheet was prevented by the use of a nonmetallic fiberglas epoxy laminate sheet which was incorporated between the sealing elastomeric balls and the rear face sheet. The impact velocity for these two panels, with a 1/8-inch steel pellet, was in the 20,000 fps range.

Among the combined integral chemical-mechanical systems evaluated, the panel configuration IS-E (Figure 13) using the plastic film encapsulation method, showed excellent sealing capability. Upon impact by a 1/8-inch steel projectile at a velocity of approximately 20,000 fps, instantaneous effective sealing was recorded, as illustrated in Figure 14. As shown, sealing was obtained all along the pellet entry path with the exception of the rear face sheet which suffered heavy damage and was unable to seal. Additional tests with this particular panel configuration revealed that the isolation of the rubber spheres from the entry face was not a necessary requirement to obtain a successful seal.

In using the microencapsulation method for the encapsulation of one or both chemical components, three different combinations were investigated as described in the section entitled "Material Selection and Evaluation" (page 8). A thorough study was performed using the first combination where only the catalyst is encapsulated. For this combination the weight ratio of microcapsules (containing the catalyst) to resin of 1:0.75 was considered optimum. The self-sealing panel configuration illustrated in Figure 15 shows show these microcapsules were incorporated within the self-sealing structure. In some preliminary tests, this configuration demonstrated excellent sealing capability at low velocity ($\approx$7000 fps) and at room, elevated, and reduced temperatures. Figure 16 depicts the panel configuration impacted at low velocity by a 1/8-inch diameter steel pellet and at room temperature. The predicted localized chemical reaction is well demonstrated and the unaffected area is shown. Similar results were obtained at elevated and reduced temperatures with the results at elevated temperatures being even more successful as expected. Further details on the elevated and reduced temperature tests are presented later under subsections entitled "Elevated Temperature Tests" (page 31) and "Reduced Temperature Tests" (page 36).

Incorporating this microencapsulation concept in an integral system panel configuration as shown in Figure 17 resulted in successful sealing action upon impact by a 1/8-inch steel pellet at the higher velocities and at room temperature. In an actual test, a panel impacted at 18,400 fps demonstrated this effective sealing action along the pellet entry path. Similar to the panel shown in Figure 14, heavy petalling of the rear face sheet was noted with only a 3/16-inch diameter hole in the front face sheet. Between the two face sheets the mechanical and chemical self-sealing mechanisms performed very well as evidenced by dissection of the panel. The predicted localized sealing action was obtained and the sealing pattern looked very similar to the one illustrated in Figure 16.

The preliminary results obtained with the second combination (where both catalyst and resin were encapsulated such that the weight ratio of encapsulated catalyst to encapsulated resin was 1:2.5) indicated partial success. Upon impact by a 1/8-inch diameter steel pellet at 7000 fps (in a panel configuration similar to the one illustrated in Figure 15 and containing the microcapsules in the ratio indicated above), the membrane separating the capsules from the elastomeric balls sealed, whereas the front face sheet did not seal. At higher impact velocities, it is expected that the larger hole in the separating membrane will allow passage of the sealing components through the membrane and the formation of a seal at the front face sheet.

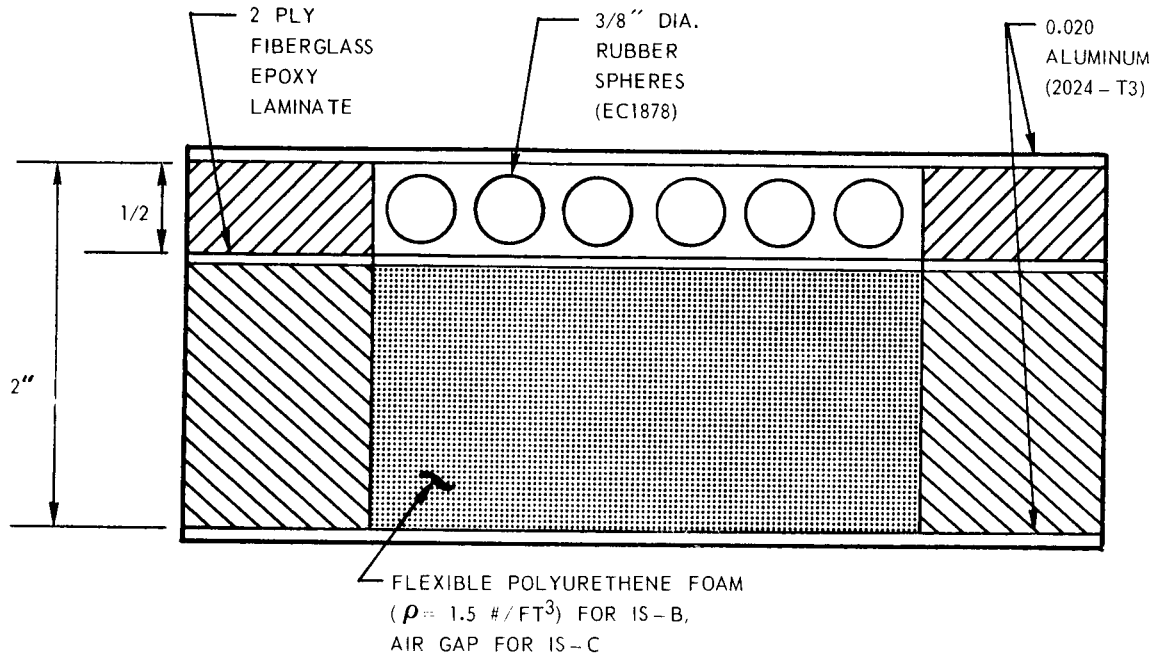

FIGURE 11 INTEGRAL SYSTEM – MECHANICAL SEALING CONCEPTS (IS-B AND IS-C)

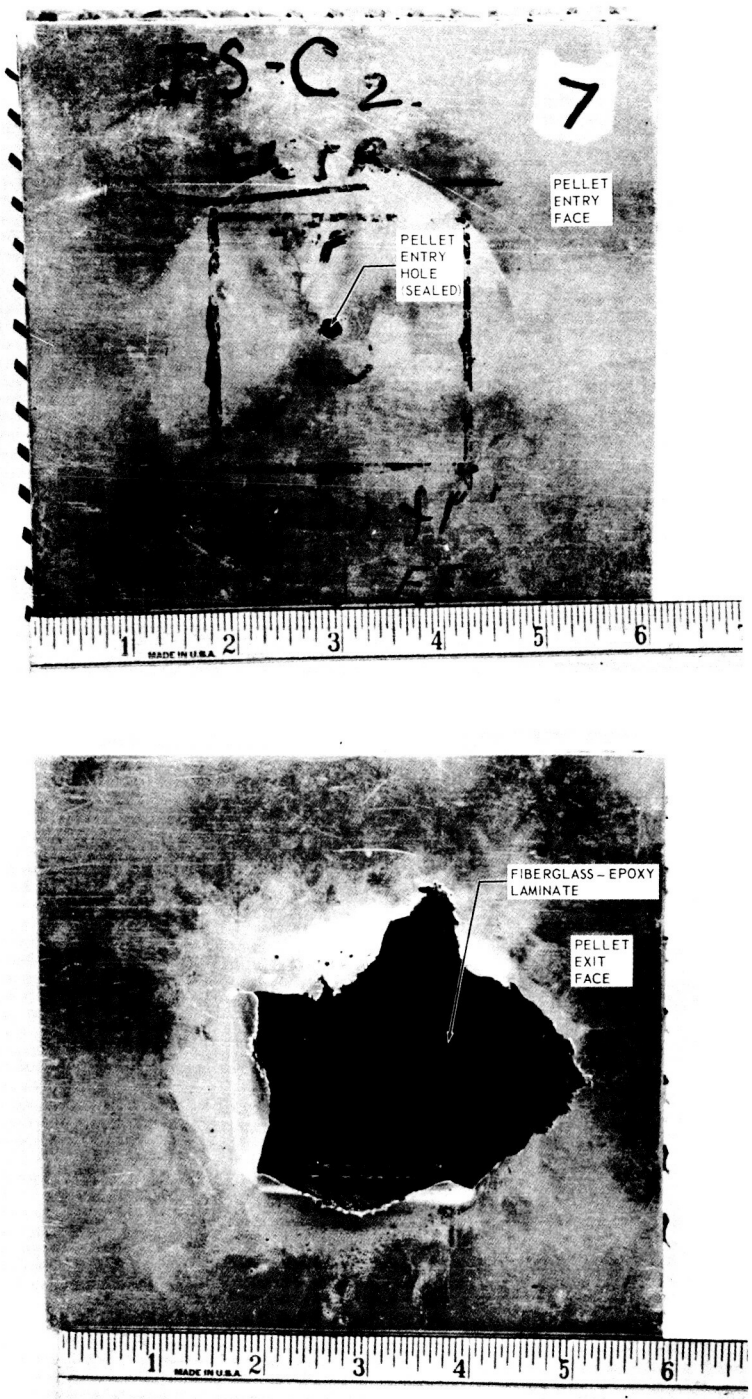

FIGURE 12 MECHANICAL SELF – SEALING CONCEPT — AIR GAP/SPHERES CONFIGURATION (TYPE IS – C)

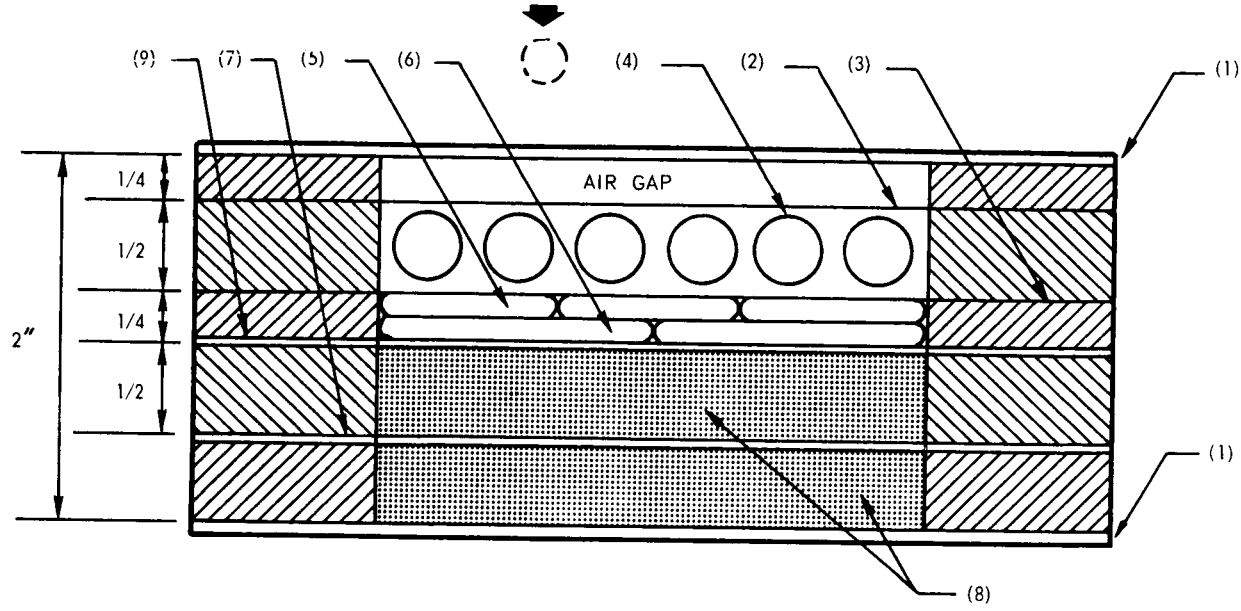

MATERIAL CODE

NO.		NO.	
1.	0.020" ALUMINUM (2024 – T3)	6.	1/16" THICK CATALYST (T–9), ENCAPSULATED IN HEAT SEALABLE PLASTIC FILM
2.	3 MIL MYLAR	7.	3 PLY FIBERGLASS–EPOXY LAMINATE
3.	9 MIL MYLAR	8.	FLEXIBLE POLYURETHANE FOAM (ρ = 1.5 #/FT^3)
4.	3/8" DIA. RUBBER SPHERES (EC1878)	9.	1/64" NITRILE SHEET
5.	3/16" THICK RIGID FOAM RESIN (XR–6–3700) ENCAPSULATED IN HEAT SEALABLE PLASTIC FILM		

FIGURE 13 INTEGRAL SYSTEM — COMBINED MECHANICAL — CHEMICAL SEALING CONCEPT (RIGID FOAM RESIN/RUBBER BALLS)

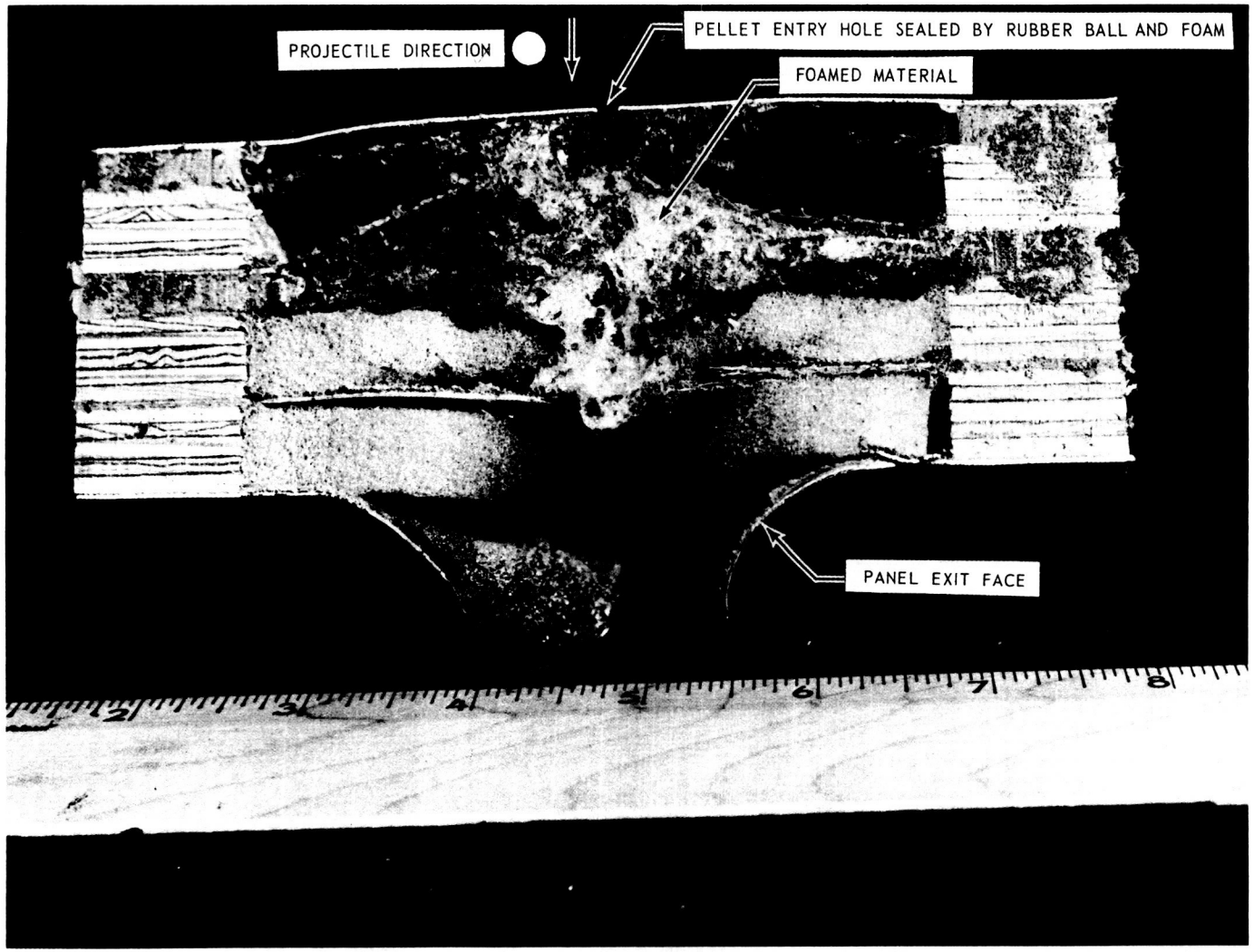

FIGURE 14 CROSS SECTION OF PANEL AFTER TEST — INTEGRAL SYSTEM — RIGID FOAM RESIN/RUBBER BALLS CONCEPT V ~ 20,000 FPS

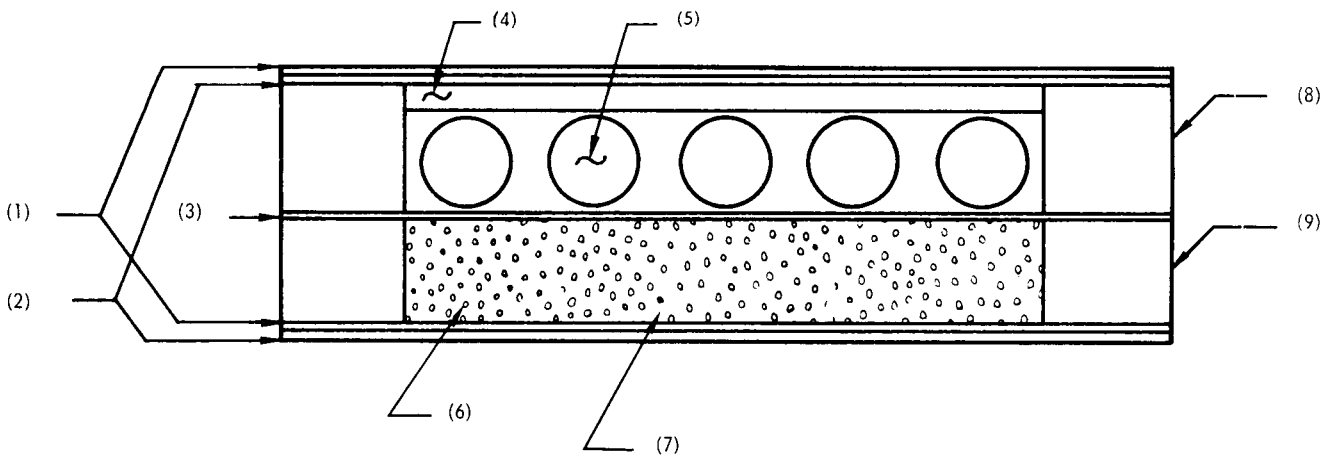

MATERIAL CODE

(1) EPOXY LAMINATE (2 PLY FIBERGLASS; 55% VERSAMIDE 125, 45% EPON RESIN 828)

(2) NITRILE RUBBER SHEET (AMS 2312J), 1/32" THICK

(3) MYLAR SHEET (9 MIL THICK)

(4) SOFT VINYL SPONGE, 1/8" THICK

(5) RUBBER BALLS, 3/8" DIA (EC 1878 NATURAL RUBBER)

(6) MICROCAPSULES (SAMPLE NO 1-722) CONTAINING T-9 CATALYST

(7) RIGID FOAM RESIN (XR-6-3700)

(8) HONEYCOMB STRUCTURE, 5/8" THICK

(9) HONEYCOMB STRUCTURE, 5/16" THICK

FIGURE 15 COMBINED CONCEPT — MICROENCAPSULATION/RUBBER BALLS CONFIGURATION

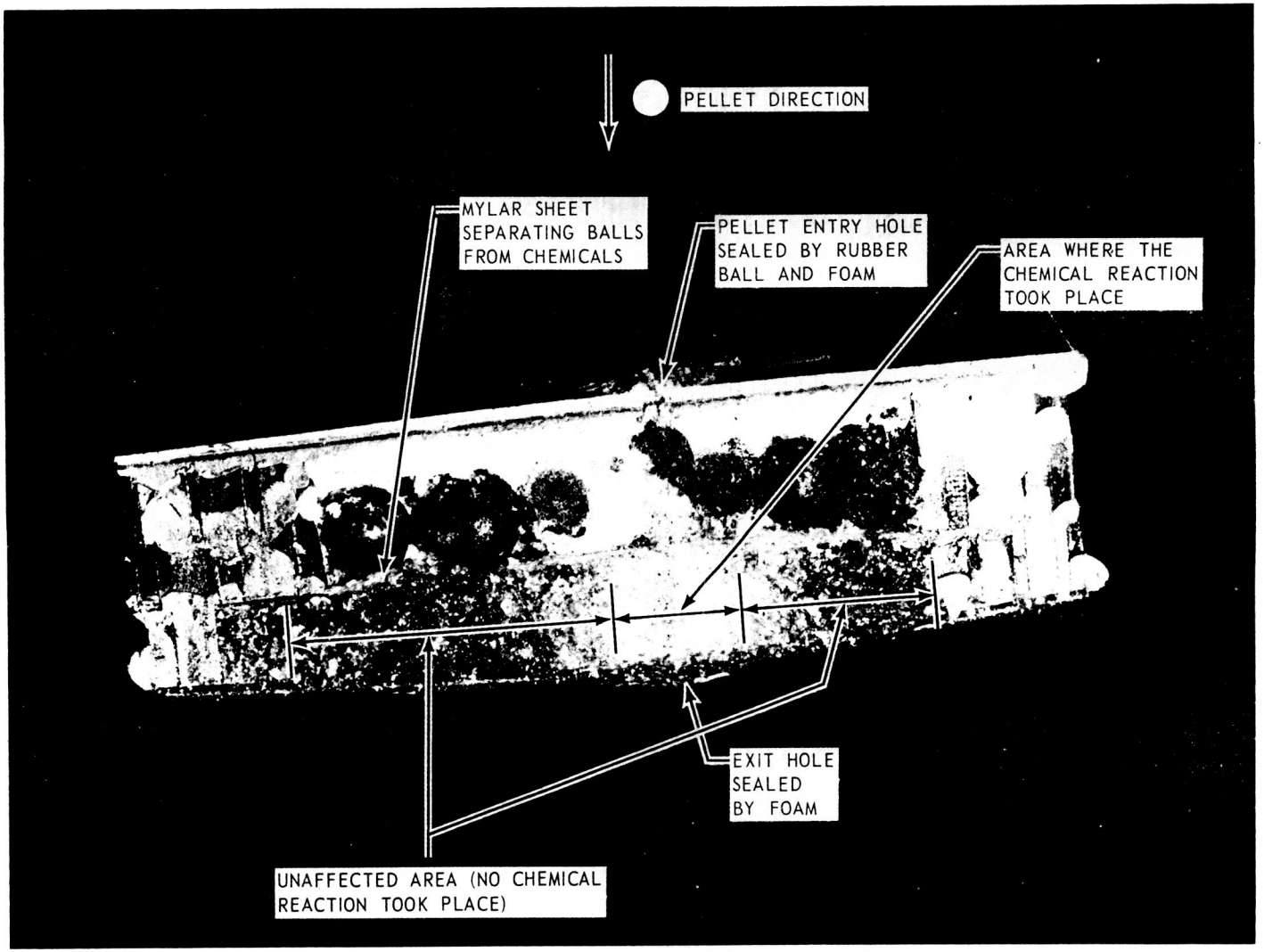

FIGURE 16 CROSS SECTION OF PANEL AFTER TEST — MICROENCAPSULATION / RUBBER BALLS CONCEPT V ~ 7,000 FPS

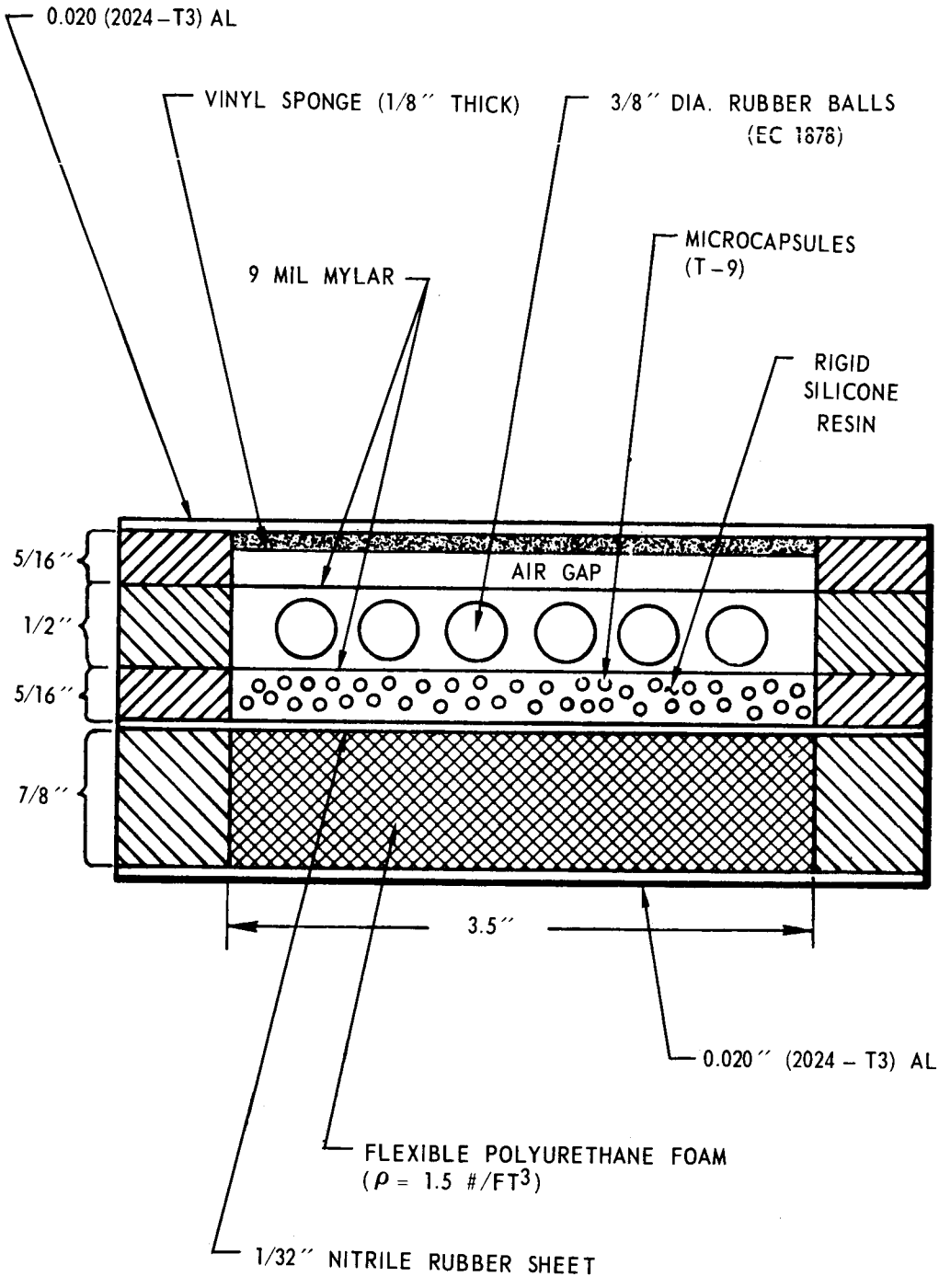

FIGURE 17 INTEGRAL SYSTEM — MICROENCAPSULATION/RUBBER BALLS CONCEPT

The third combination, where only the resin was encapsulated, gave excellent results when incorporated in a panel configuration similar to the one shown in Figure 15. The weight ratio of microcapsules (containing the resin) to catalyst was 4:1. Results obtained at the low velocity tests were very similar to the ones obtained with the panel configuration using the first combination. No high velocity impacts were performed, but performance at the higher impact levels is expected to be excellent.

To achieve sealing at the inner wall of the MSC panel configuration, the "Self-Sealing Tile" (SST) panel configurations were investigated. One of the configurations tested is shown in Figure 18 and the results are illustrated in Figure 19. As can be seen, the 1/4-inch diameter hole produced in the front sheet was sealed mechanically with one of the elastomeric balls. The rear sheet could not be sealed due to heavy damage. The panel was impacted by a 1/8-inch diameter steel pellet at a velocity of 18,500 fps.

Using the results obtained initially with the SST configuration, improved reinforced fiberglas-epoxy laminates and combination of these laminates with aluminum sheets for use as the inner wall of the panel configurations were evaluated. The objective was to minimize impact damage to the inner wall so that sealing will be achieved on that face. This was done successfully with the panel configurations (SST-E and SST-I) shown in Figure 20, which were impacted by 1/8-inch diameter steel pellets at velocities of 18,000 fps and 20,710 fps, respectively. In the case of the SST-E configuration where the composite laminate was composed of an aluminum sheet bonded to nonmetallic layers such as reinforced epoxy laminate and nitrile rubber, it was noted (see Figure 21) that petalling of the rear metal sheets was still severe. In spite of the heavy damage suffered by the aluminum sheet, successful sealing was obtained at the nonmetallic sheets bonded to the metal sheet. In this case only chemical sealing was obtained due to the fact that the balls could not move freely in the hole because of heavy petalling of the aluminum sheet. This situation is correctable by reversing the chemical and elastomeric ball compartments.

In the case of the SST-I panel configuration where an 8-ply reinforced fiberglas-epoxy laminate was used as the rear face sheet, an excellent sealing action was obtained. No petalling occurred and a hole not exceeding 1/4-inch in diameter sealed both mechanically and chemically. Heavy foaming occurred behind the rear face sheet, sealing effectively along the pellet entry path and setting the sealing rubber balls permanently in place. Thus, considering the last series of tests, it is possible to make the inner shell airtight and effectively sealed upon impact by a 1/8-inch diameter steel pellet at velocities exceeding 20,000 fps.

In summary, both basic self-sealing panel configurations (IS and SST) provide excellent self-sealing capability and permit sealing at either the front or rear face sheets when impacted in the manner described above.

Elevated temperature tests. — In the series of impact tests conducted at an elevated temperature, the materials used within the most successful self-sealing structures performed very well. The elevated temperature improved the self-sealing action, particularly in the case of the chemical sealing system where the chemical reaction rates increased with temperature, subject to the limitations of degradation of the component materials. Regarding the mechanical sealing action at elevated temperature, the sealing was not necessarily faster but it was more effective due to the softening of the elastomeric balls material.

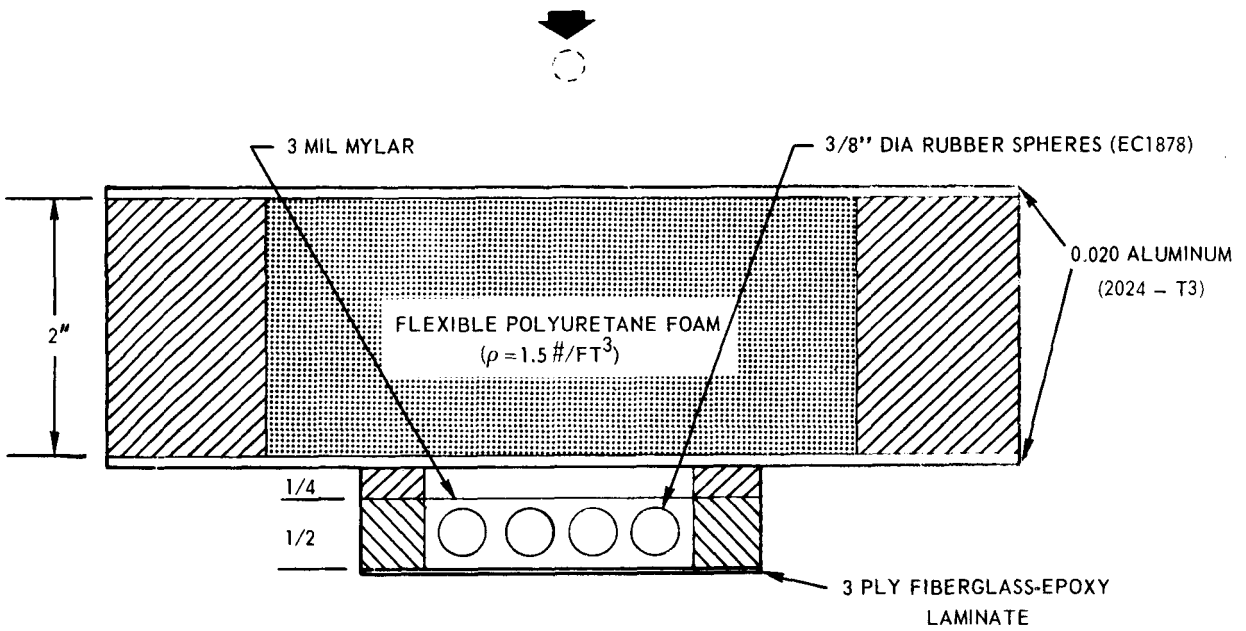

FIGURE 18 SELF-SEALING TILE — MECHANICAL SEALING CONCEPT (TYPE SST-B)

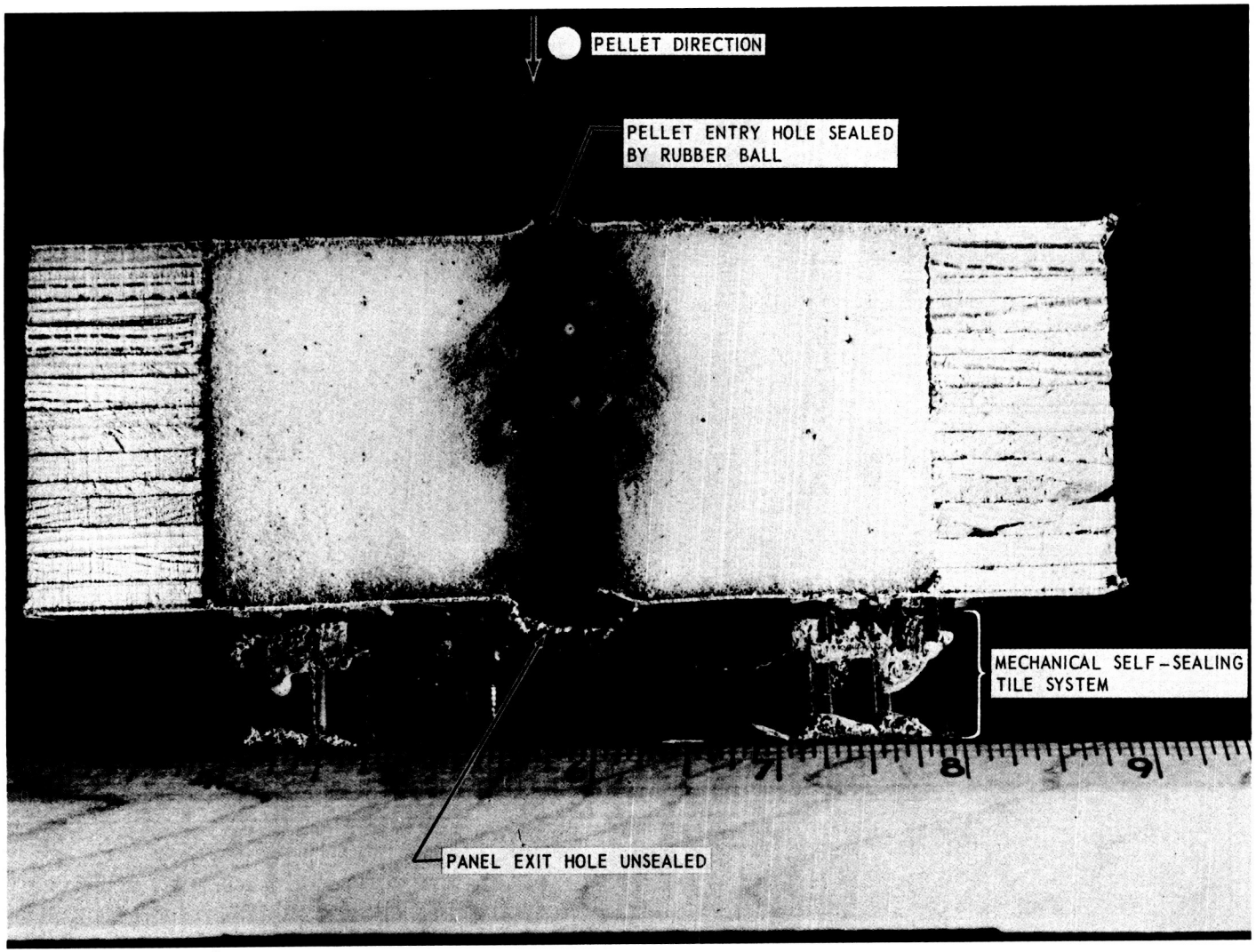

FIGURE 19 CROSS SECTION OF PANEL AFTER TEST — SELF-SEALING TILE — RUBBER BALLS CONCEPT

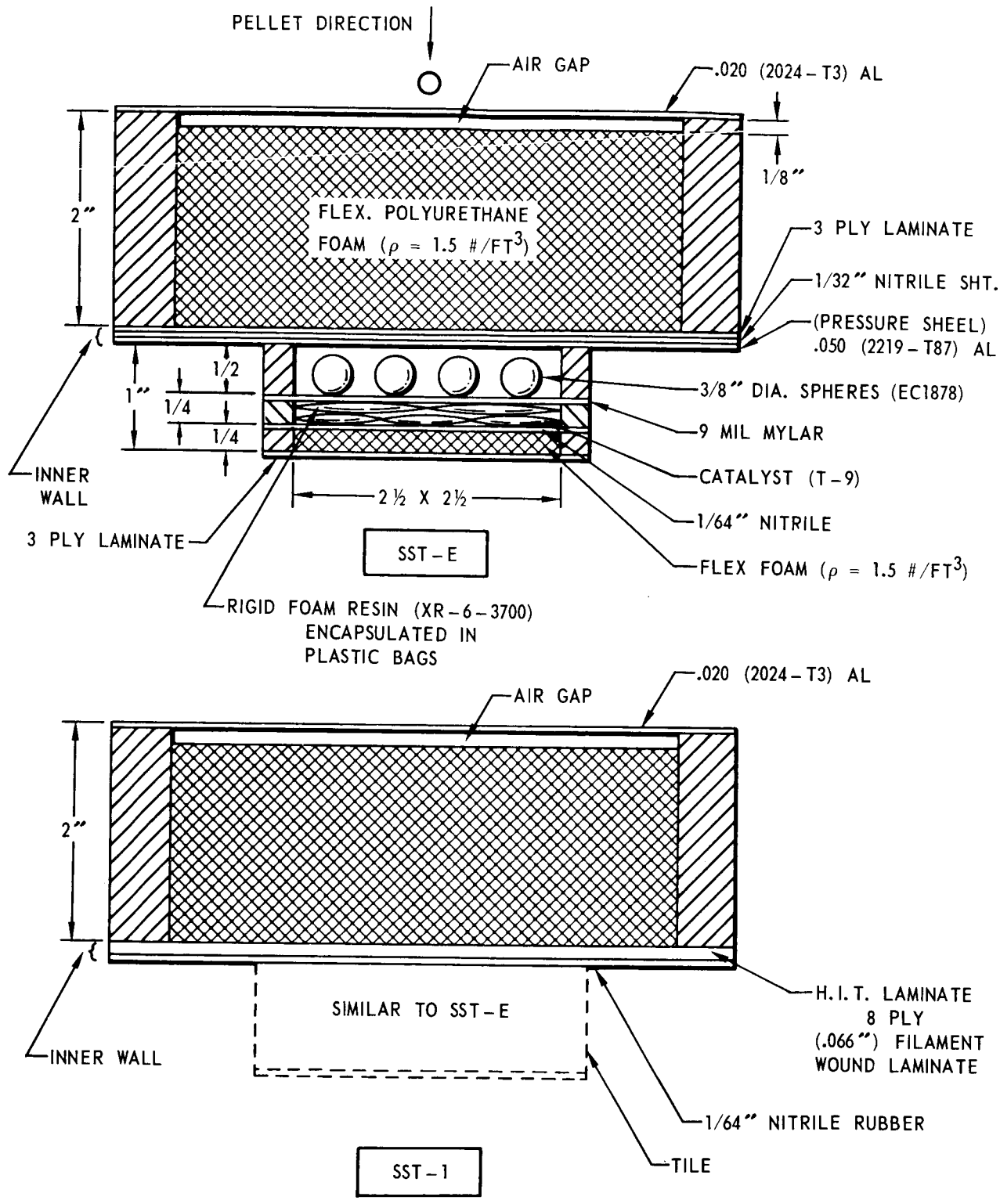

FIGURE 20 SELF – SEALING TILE — COMBINED MECHANICAL – CHEMICAL CONCEPTS (RIGID FOAM RESIN/RUBBER BALLS) SST – E AND SST – 1

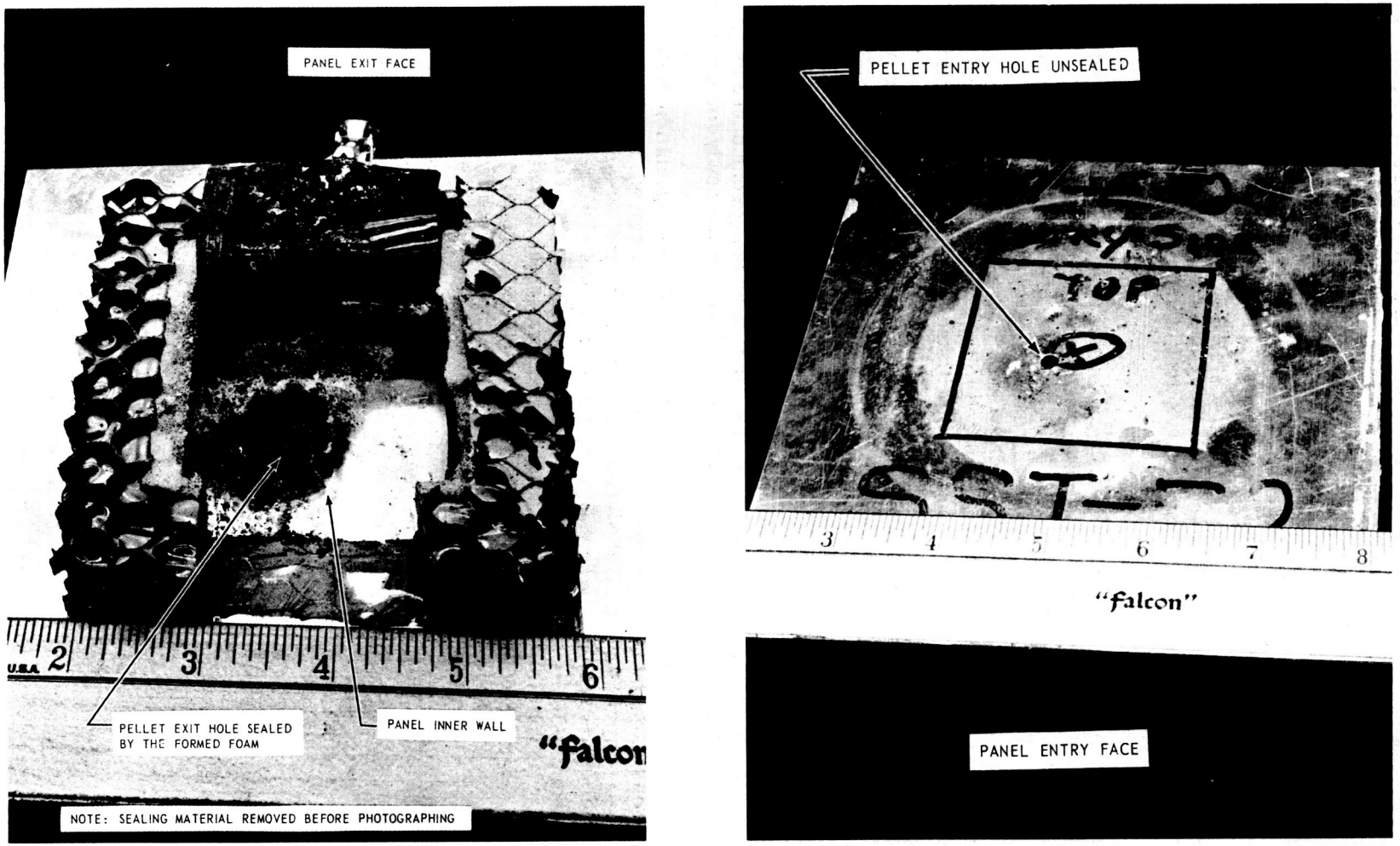

FIGURE 21 STRUCTURAL DAMAGE ON PANEL OUTER AND INNER FACE SHEETS — SELF-SEALING TUBE CONCEPT-TYPE SST-E

In actual tests two representative self-sealing panel structures were impacted by a 1/8-inch diameter steel pellet while exposed to an elevated temperature. The panel configurations in question are identical to the ones illustrated in Figures 17 and 13 which represent "Integral Systems" with a chemical microencapsulation concept and a chemical bag concept, respectively, both combined with the elastomeric spheres mechanical concept.

In the testing procedure each panel was attached to a heating source as shown in Figure 22 which assembly in turn was adapted to the NSL gun facility for ballistic testing of heated and cooled targets illustrated in Figure 10. The panel outer sheet was heated to 300° F and kept constant throughout the test giving a temperature gradient of 150° F inside the chemical compartment and 80° F at the inner sheet surface.

Upon impact of the panel using the plastic bag encapsulation method by a 1/8-inch diameter steel pellet at 18,400 fps, instantaneous (within one second) sealing was recorded. The chemical and mechanical self-sealing actions performed very effectively as it was evidenced upon dissection of the panel. The appearance of the final seal was very similar to the one illustrated in Figure 14. Since the chemical reaction rates increased at these higher temperatures, the self-sealing system performed even better when compared to the sealing at room temperature. Sealing was accomplished along the pellet entry path with the exception of the aluminum rear face sheet which was heavily petalled. However, as experienced in previous tests, this damage could be reduced by replacing the aluminum rear face sheet by epoxy laminates or other composites as was previously discussed for the tests at room temperature. The damage could be reduced sufficiently so as to enable a successful seal of both entry and rear faces. Other materials such as the Mylar and the nitrile rubber sheets inside the panel were not affected by these elevated temperatures and performed well. During the penetration process a large chunk of the polyurethane foam layer behind the rear face sheet was removed along the projectile entry path either by tearing action or oxidative degradation, the latter being considered as predominant. However, the volume of foam removed was completely replaced by the newly formed rigid foam.

Similar results were obtained with the panel using the microencapsulation method (see Figure 17) where one of the chemical constituents (catalyst T-9) is contained in microcapsules. Prior to impact, the temperatures measured at the panel front face sheet, inside the chemical compartment, and at the rear face sheet, by means of thermocouples, were 300° F, 150° F and 80° F, respectively. Upon penetration by a 1/8-inch diameter steel pellet at a recorded velocity of 19,000 fps, the panel sealed within one second. The seal was highly effective, mechanically as well as chemically. Localized chemical reaction took place along the pellet entry path and unreacted chemical components were still present away from the projectile trajectory. A new puncture in the unaffected area of this panel could have been sealed again mechanically and chemically. A panel similar to the one above but using the plastic bag encapsulation method had a large chunk of the polyurethane foam layer located behind the rear face sheet removed either by tearing action or oxidative degradation. The rear and front face sheets sustained similar damage.

The elevated temperature did not affect the rubber balls to the point of interference with the sealing action. To the contrary, the sealing action was enhanced. This was due to a slight softening of the rubber balls which were kept from sticking together by coating them with talcum powder. The other materials used within the panel configuration such as the vinyl sponge behind the entry face, the mylar sheets separating the rubber balls from the chemical components and the air gap, and the nitrile rubber sheet separating the microcapsules from the polyurethane foam performed very well under high temperatures.

Reduced temperature tests. — At sub-zero temperatures, the self-sealing capabilities of the panels were not affected seriously when properly selected materials were used. With the original chemical components little or no chemical sealing action was obtained. Careful selection of materials led to more successful results. It was noted that the chemical reaction rates

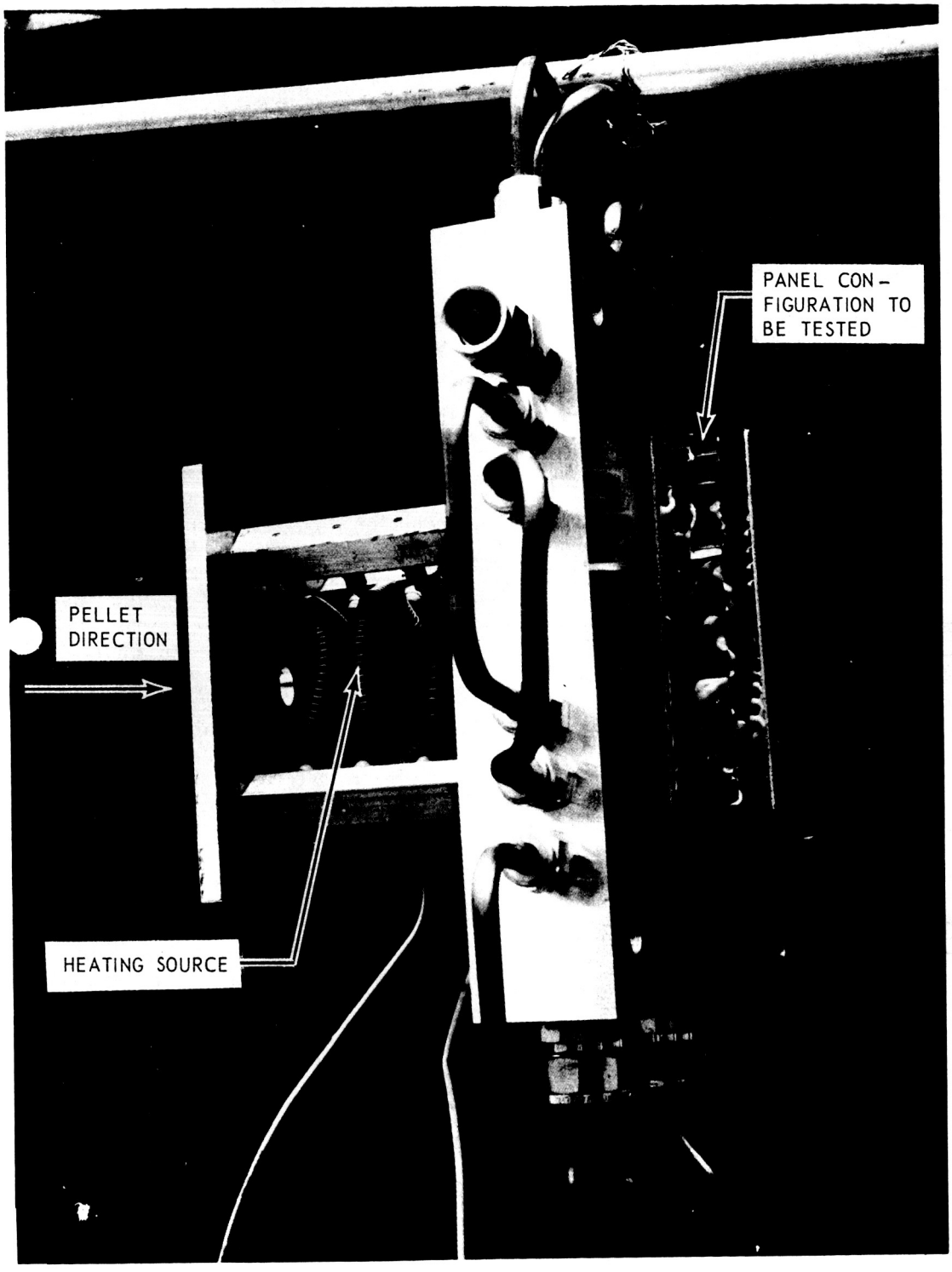

FIGURE 22 HEATING SOURCE APPARATUS FOR ELEVATED TEMPERATURE TESTS

decreased with decreasing temperature and the ideal ratio of resin to catalyst was shifted so that the foam obtained was of poorer quality, thus degrading the quality of the seal. After investigating more suitable chemical materials, a combination of products was selected for which the ratio shifting was minimized. The feasibility of these new materials was proven at even lower temperatures. They performed particularly well when combined self-sealing panel configurations were used. Among the combined concepts investigated, the one giving the best results was the "Rigid Silicone Foam/Elastomeric Balls" concept. Good insulation is obtained with this combination and the temperature of the liquid chemical components was kept above their freezing point. The elastomeric ball material selected also performed very well under these conditions.

Due to a filled schedule at the McGill University hypervelocity testing facility, no high velocity impacts were performed at reduced temperatures. A large series of preliminary tests were accomplished, however, at lower velocities (≈7000 fps). In these temperature dependent self-sealing tests, the objective was to determine the material's capability to resist temperature extremes combined with vacuum and still give an effective seal. Thus, it was felt that high velocity impact tests were actually not mandatory to demonstrate the material's behavior.

From the selective screening process of materials and self-sealing panel configurations discussed in the subsection entitled "Material Selection and Evaluation" (page 8), two breadboard self-sealing panels were retained for tests at reduced temperatures using the "Elastomeric Spheres Concept" and the "Rigid Silicone Foam/Elastomeric Spheres Concept" where the catalyst is either encapsulated in a plastic bag or in microcapsules. For each configuration two panels were prepared wherein one case nonmetallic front and rear face sheets were utilized and in the other case a metallic front face sheet and a nonmetallic rear face sheet were utilized. These panel configurations were penetrated by a 1/8-inch diameter steel pellet at velocities up to 7000 fps using the NSL gun facility. In a general testing procedure, the panel was placed in contact with a cooling source which, in turn, was mounted on the back of the vacuum chamber as shown in Figure 23. The cooling source consists of an aluminum plate having interwoven hollow passageways in which liquid nitrogen can be circulated. The temperature of the plate can be regulated and kept constant by controlling the flow of the liquid nitrogen. For cold tests, the temperature was set at -85° F at the panel front face which meant that the vinyl sponge was -35° F, the rubber balls at 0° F, the chemical compartment at 10° F, and the rear face sheet at 35° F. This temperature gradient differed by only a few degrees for the panels with nonmetallic front and rear face sheets.

Upon impact of the panel configuration using the "Elastomeric Spheres Concept" with the metallic face sheet, instantaneous sealing was obtained. At these low temperatures, the rubber balls and the vinyl sponge layer (1/8-inch thick) behind the entry face remained soft and flexible enough to successfully seal a 3/16-inch hole. A similar panel, but with a nonmetallic front face sheet (epoxy laminate reinforced with fiberglas), did not suffer any cracks and the hole size was kept to a minimum.

Upon impact one of the panel configurations using the "Rigid Foam/Elastomeric Spheres Concept" with the chemicals either encapsulated in plastic bags or microcapsules sealed very effectively. Nevertheless, in the case where the microcapsules were used, the chemical sealing reactions were more localized. At least two-thirds of the chemicals were unaffected upon penetration and remained unreacted after several weeks indicating that foaming and curing had remained localized. A similar panel was submitted to three punctures to check its ability to seal three holes approximately one inch apart. The results obtained showed good mechanical and chemical sealing in all three cases.

The viscosity of the rigid foam resin and the catalyst used as the foam chemical constituents increased appreciably, particularly in the case of the resin, under these reduced temperatures. However, they still remained fluid enough to allow good mixing and subsequent fast

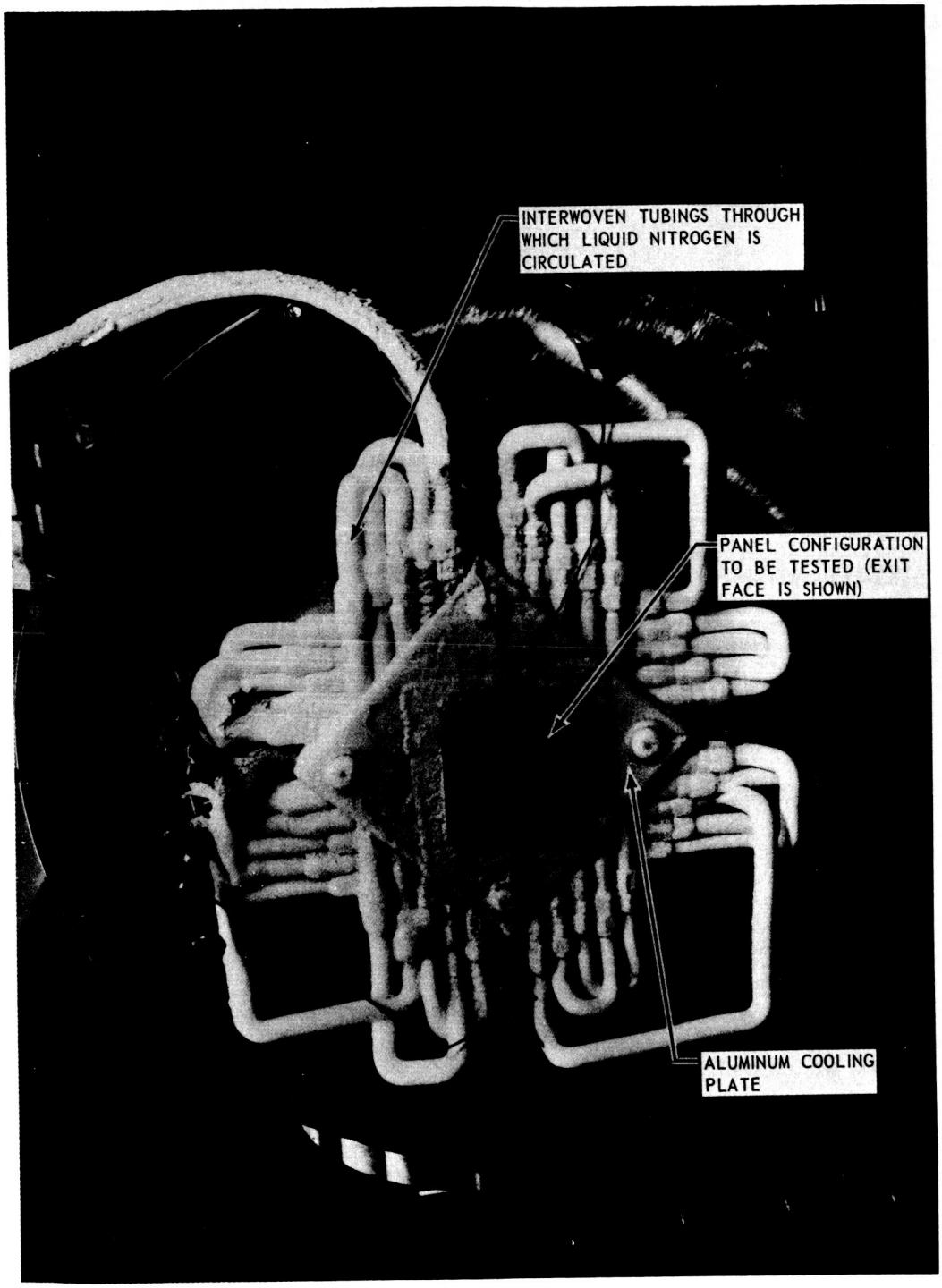

FIGURE 23 COOLING SOURCE FOR REDUCED TEMPERATURE TESTS

chemical reactions. Since these reactions are exothermic, their rates will be accelerated after initiation and produce a foam which will effectively contribute to the successful sealing of the punctured panel. No loss of materials was recorded during these tests.

TECHNICAL DISCUSSION AND ANALYSIS

Meteoroid Penetration of Single Wall Structures

In an analytical study conducted by Davidson and Sandorf (Reference 7), it was indicated that the meteoritic puncture rate in a single homogenous sheet will vary inversely as the cube of the thickness. By using a modified meteoroid flux, somewhat more optimistic than Whipple's 1961 estimate, and Bjork's penetration equation (for aluminum projectiles impacting an aluminum shield) the authors formulated the following penetration flux equation:

$$\psi = 4 \times 10^{-10} t^{-3} \tag{1}$$

where ψ is the average penetration flux in penetrations per square foot per day and t is the effective skin thickness in inches. This equation is plotted in Figure 24

The average number of punctures is given by

$$m = \psi A \tau \tag{2}$$

where A is the exposed area (ft^2) and τ the exposure time (days). Substituting equation (1) into equation (2) and rearranging terms yields

$$t = \left[\frac{4 \times 10^{-10} A \tau}{m} \right]^{1/3} \tag{3}$$

In reference 8, a statistical test of the puncture data obtained from the Explorer XVI micrometeoroid satellite experiments indicated that the occurrence of punctures follows a Poisson distribution. The Poisson distribution function has the form

$$P(n) = \sum_{j=o}^{n} e^{-m} \frac{m^j}{j!} \tag{4}$$

where, for our consideration, P(n) is the probability that a single wall structure will sustain n punctures or less and m is the average number of punctures that may be expected. For any specified value of P(n) and n, the corresponding average number of punctures (m) may be determined from the tables and computational procedure given in Reference 9. If values of m determined in the above manner are substituted in equation (3) the values of t determined from the equation will represent the corresponding aluminum single wall thickness required for the specified values of P(n), n and mission parameter ($A\tau$).

Equation (3) is plotted in Figure 25 for values of n varying from zero to five and a P(n) = 0.99. The vertical line shown in the figure indicates the design restraint that would be imposed by air pressurization load requirements of 14.7 psi and an assumed allowable design stress of 36,000 psi for a 20-foot diameter single wall aluminum cylindrical-shaped vehicle. Therefore, for the given example, only those portions of the curves that lie to the right of the vertical line would be used for design purposes.

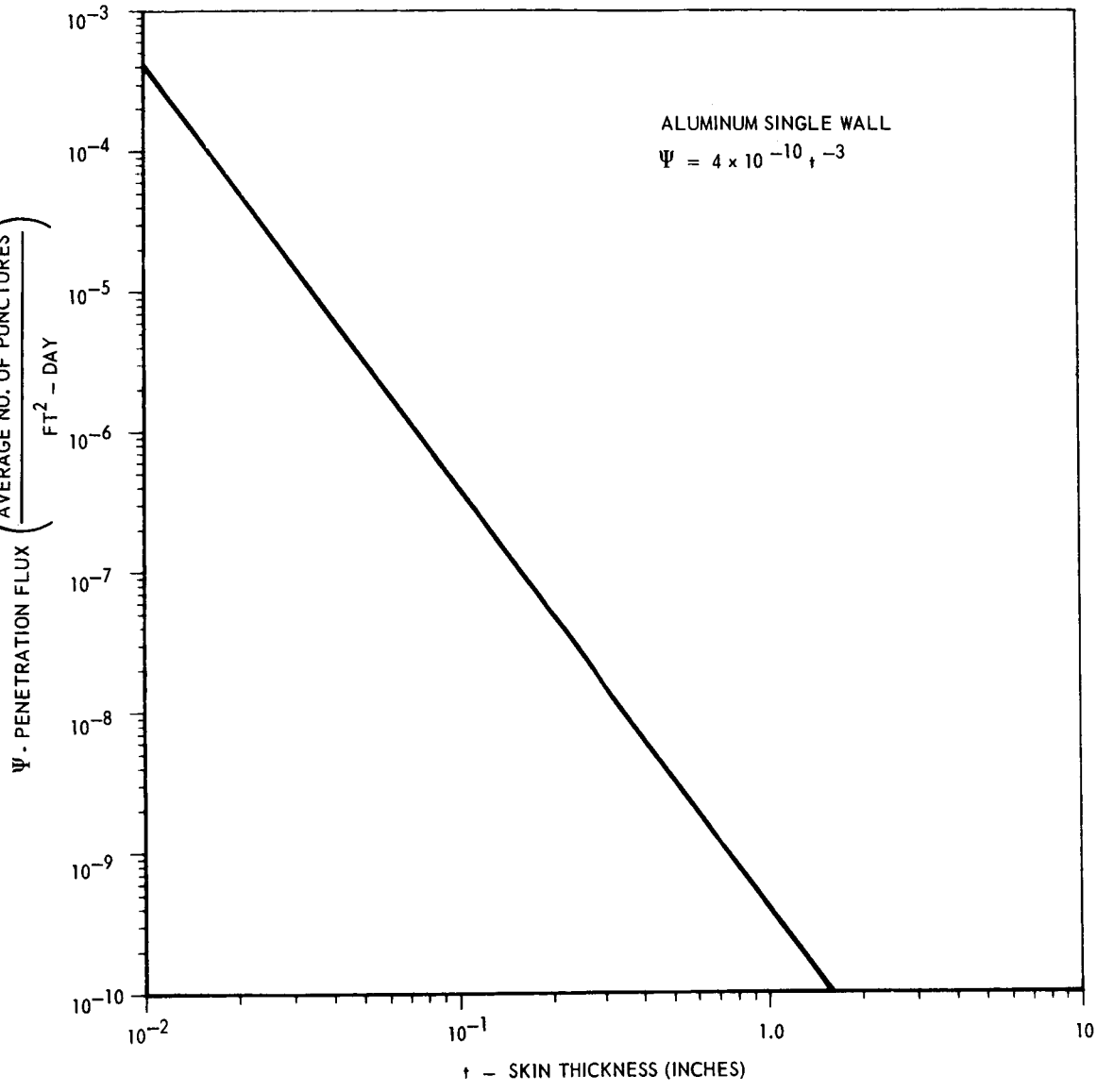

FIGURE 24 PENETRATION FLUX VS SKIN THICKNESS

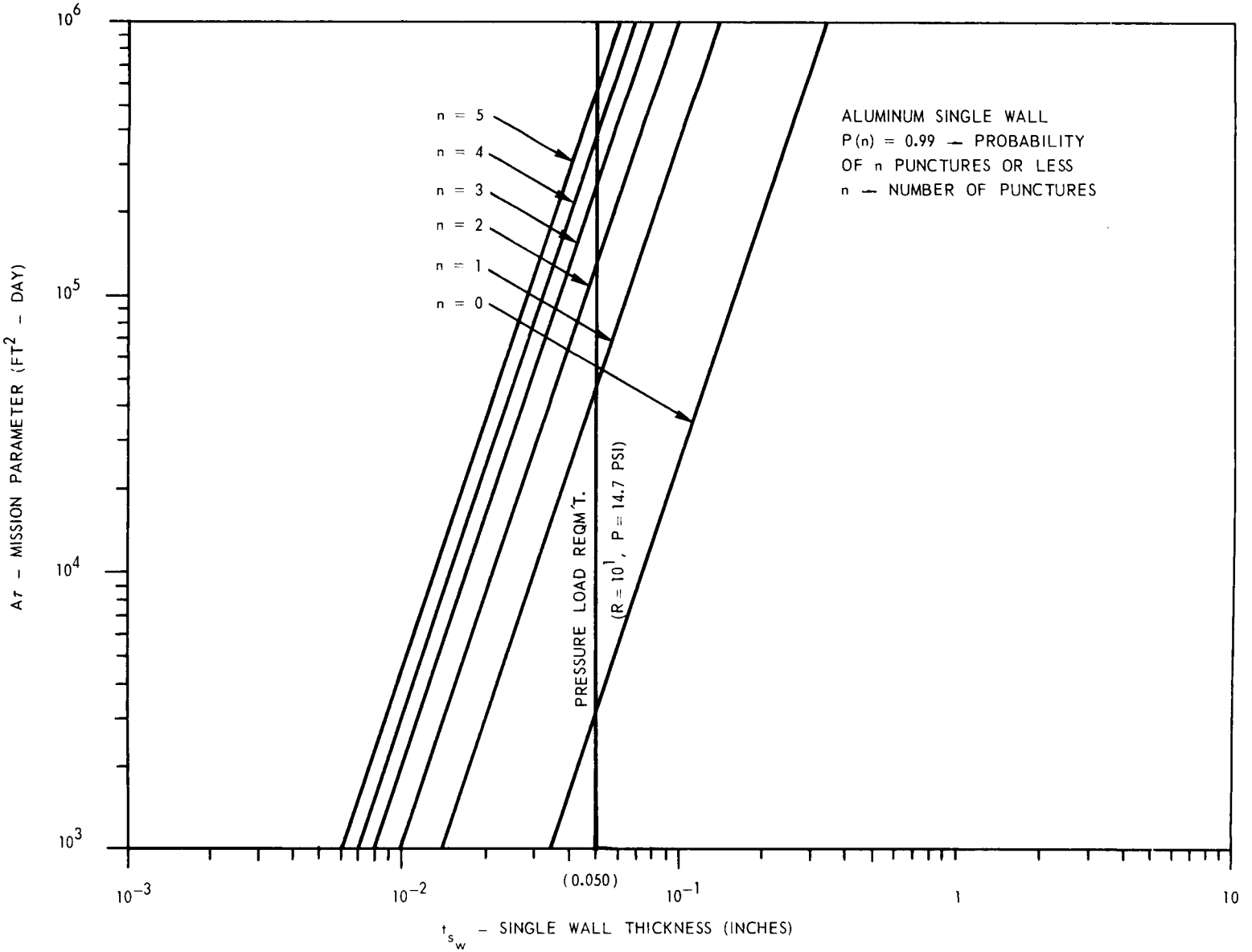

FIGURE 25 MISSION PARAMETER (Aτ) VS SKIN THICKNESS

Meteoroid Penetration of Multiwall Composite Structures

Current meteoroid satellite penetration experiments have been limited to single wall homogenous materials. Therefore the procedure outlined in the previous section cannot be directly applied to analyzing the penetration resistance of multiwall composite structures. However, a reasonable first order approximation of the penetration resistance capability of these structures may be obtained by determining, with ground tests, the relationship between their stopping power (ballistic limit) and that of a representative single wall homogenous structure. This of course makes it necessary to assume that the relative stopping efficiencies among the configurations is the same for meteoroids as for the ground impact tests.

In order to perform a penetration analysis of composite structures it will first be necessary to determine experimentally the ballistic limit of each candidate composite configuration. The area density of a single wall homogenous structure having the same ballistic limit as the composite structure may also be found experimentally or the following procedure may be used to arrive at a reasonable estimate.

The Herrmann and Jones Logarithmic Penetration Equation (Reference 10) for a semi-infinite thick target can be used for determination of the penetration resistance of homogenous single wall materials. In view of the limited physical significance of the logarithmic fit, extrapolation to higher velocities produces remarkable agreement with Bjork's theoretical points at the higher velocities (~ 72 km/sec) (Reference 10). The general form of the equation is

$$P^{\infty} = k_1 K^{2/3} \ln \left\{ 1 + \frac{K^{2/3} B}{k_2} \right\} \tag{5}$$

where k_1 and k_2 were found to be close to 0.6 and 4.0, respectively, for most material combinations tested, $K = \frac{\rho_p}{\rho_t}$ and $B = \frac{\rho_t V^2}{H_t}$. Equation (5) may be converted for use with thin single wall targets by applying the experimentally determined relationship $t_{sw} = 1.5\ P^{\infty}$, where t_{sw} is the thickness of a single wall target that will just be perforated (ballistic limit) for the same ballistic conditions that will penetrate a semi-infinite thick target of the same material to a depth of P^{∞}.

Substituting the above values for the constants and conversion factor into equation (5) yields

$$t = t_{sw} = 0.9\, d_p \left(\frac{\rho_p}{\rho_t}\right)^{2/3} \ell n \left\{ 1 + \left(\frac{\rho_p}{\rho_t}\right)^{2/3} \left(\frac{\rho_t V^2}{4 H_t}\right) \right\} \tag{6}$$

where ρ_p and ρ_t are the density of the projectile and target, respectively, d_p and V the projectile diameter and impact velocity, respectively, and H_t the brinell hardness of the target material.

If the ballistic conditions (d_p, ρ_p, V), prevailing at the experimentally determined ballistic limit of a multiwall composite structure, are inserted into equation (6), one can determine the equivalent homogenous single wall thickness of a representative material (e.g., aluminum) having the same ballistic limit as the composite. Multiplying this wall thickness by the material density would then give the area density or wall unit weight of the equivalent single wall shell.

$$\text{Let } r = \frac{\left(W/A\right)_{s.w}}{\left(W/A\right)_c} = \frac{\left(\rho t\right)_{sw}}{\left(W/A\right)_c} \tag{7}$$

be the ratio of the area density of the single wall (s.w.) structure and the multiwall composite (c) structure which have the same ballistic limit. This factor r can then be considered to be the efficiency factor of a multiwall composite structure when compared to a homogenous single wall structure.

Equation (4) converted to give the area density required for a probability of zero puncture equal to 0.99 reduces to

$$(W/A)_{sw} = 49.25 \times 10^{-3} \ (A\tau)^{1/3} \tag{8}$$

where $(W/A)_{sw}$, given in lbs/ft^2 is the area density or panel unit weight of an aluminum single wall structure.

Using the relationship given by equation (7) the area density of a multiwall composite structure satisfying the same conditions for zero puncture would then be

$$(W/A)_c = \frac{1}{r} \times 49.25 \times 10^{-3} \ (A\tau)^{1/3} \tag{9}$$

The value of the area density $(W/A)_c$, as determined from equation (9), will in general, be different from that of the configuration used in establishing the value of r. In making use of equation (9), one must assume that, in any new configuration of a specific composite panel concept in which the area density is different than that used in determining r, it is possible to readjust each new component weight so as not to affect the value of r as originally determined.

In Reference 6, data from penetration studies, conducted at NASA Ames Research Center, are presented in which the ratio of the weight of some double wall structures required to stop a projectile to that of a single sheet wall are given. By converting these to efficiency factors r as defined by equation (7) they are found to vary from 1 for the single sheet aluminum wall to approximately 6 for a double wall aluminum structure with a polyurethane foam filler.

Since attempts to experimentally determine the ballistic limits for the composite wall specimens used in our program were not successful (see Appendix D), it was not possible to calculate their efficiency factor r by the procedure outlined. Therefore, for purposes of this analysis, we have assumed an efficiency factor of 6, which appears reasonable in view of the results obtained by NASA Ames Research Center with the composite aluminum double wall structure.

Figure 26 illustrates how the area density of an aluminum face wall structure (for both single sheet and multi-sheet composite walls) designed for a probability of zero punctures equal to 0.99, would vary as a function of the mission parameter $A\tau$. For comparison purposes, efficiency factor lines for values of r equal to 1, 2 and 4 are also included. In addition, the efficiency factor line for r = 6 is also shown for a probability of zero penetration equal to 0.999 so

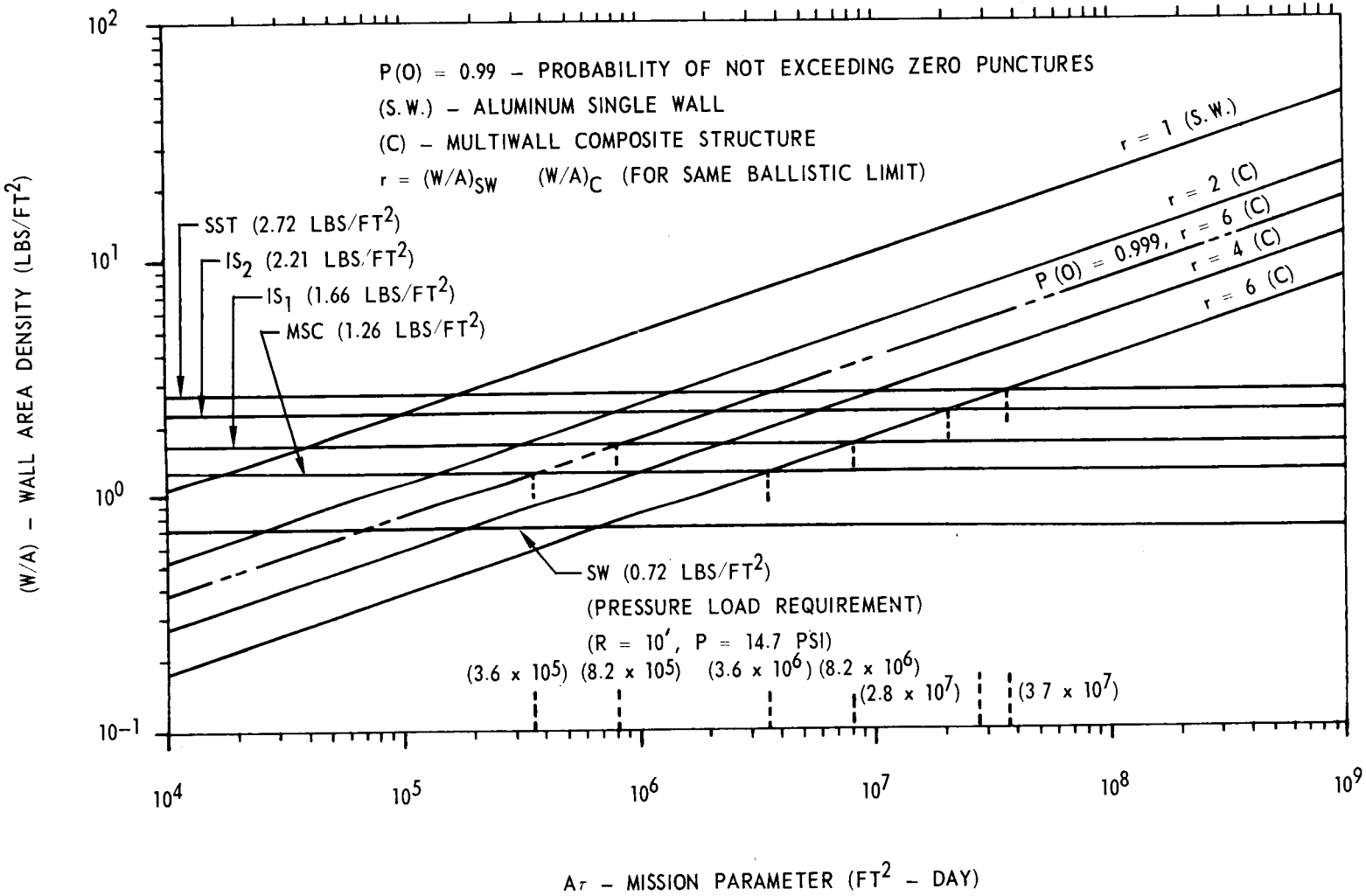

FIGURE 26 WALL AREA DENSITY VS MISSION PARAMETER (A τ)

that the effect of varying the reliability requirements may be considered. Also shown in the figure are the basic area density lines of the following wall structure:

(a) An aluminum single wall structure (SW) required to satisfy the pressure load requirements indicated.

(b) A composite non-self-sealing wall configuration (from NASA, MSC*).

(c) Two integral self-sealing wall configurations. Wall configuration IS_1 with the elastomer sphere sealing concept and IS_2 with the combined sphere-chemical sealing concept. Both of these configurations have similar exterior face sheets and wall depth as the MSC wall configuration with some of the polyurethane foam filler replaced by the self-sealing components.

(d) A self-sealing tile wall configuration (SST) in which the tile is bonded to the inner shell of a 2-inch flexible polyurethane foam (ρ = 1.5 lbs/ft^3) sandwich, fabricated with a 0.020-inch aluminum outer shell and an 8-ply fiberglas-epoxy laminate inner shell.

From the intersection of the basic area density lines with the efficiency factor line for r = 6 and P(0) = 0.990, it is determined that the MSC non-self-sealing wall configuration will satisfy the requirements of zero penetration up to a mission parameter of $A\tau$ equal to 3.6×10^6 ft^2-days while the lightest weight self-sealing wall configuration (IS_1) will satisfy this requirement up to a value of $A\tau$ equal to 8.2×10^6 ft^2-days. If the reliability requirement is increased to P(0) = 0.999 then these values will become 3.6×10^5 ft^2-days and 8.2×10^5 ft^2-days, respectively. For a 10,000 ft^2 space station these mission parameters translate into mission times of 360 days and 2.24 years respectively for a P(0) = 0.990 and 36 days and 82 days respectively for a P(0) = 0.999. Therefore, for the indicated space station and a reliability of P(0) = 0.990 the weight tradeoff point between non-self-sealing and self-sealing structures will occur at a mission time of 2.24 years, while for the more stringent requirement of P(0) = 0.999, this point will be reached at a mission time of 82 days. Beyond these mission times the probability of sustaining punctures in the respective wall configurations will increase. However, while puncturing of the nonself-sealing wall would result in air leakage from a pressurized cabin, the self-sealing wall configuration would seal the puncture and permit safe operation of the mission beyond the times indicated.

The results of the above analysis indicate that if the reliability requirement for the sealed integrity of a pressurized compartment is kept relatively low (P(0) = 0.990), the non-self-sealing wall structure would demonstrate a weight advantage over a self-sealing wall configuration, for a 10,000 ft^2 vehicle, for mission times up to 2.24 years. However, future manned space missions of long duration which may require these larger vehicles, will also require greater reliability for their pressurized compartments so that a specified reliability of P(0) = 0.999 would not be uncommon or unreasonable. For such mission requirements, the self-sealing wall would then demonstrate a weight advantage over the non-self-sealing structure for mission times exceeding 82 days for a 10,000 ft^2 vehicle or 2.24 years for a 1000 ft^2 vehicle. Figure 27 illustrates how the mission time for the weight tradeoff point varies with vulnerable vehicle area for the above two reliability requirements for zero penetration.

---

*The MSC wall configuration, selected as a representative non-self-sealing wall structure, consists of a 2-inch thick flexible polyurethane foam (ρ = 1.5 lbs/ft^3) sandwich with aluminum face sheets (0.020-inch front face, 0.050-inch rear face).

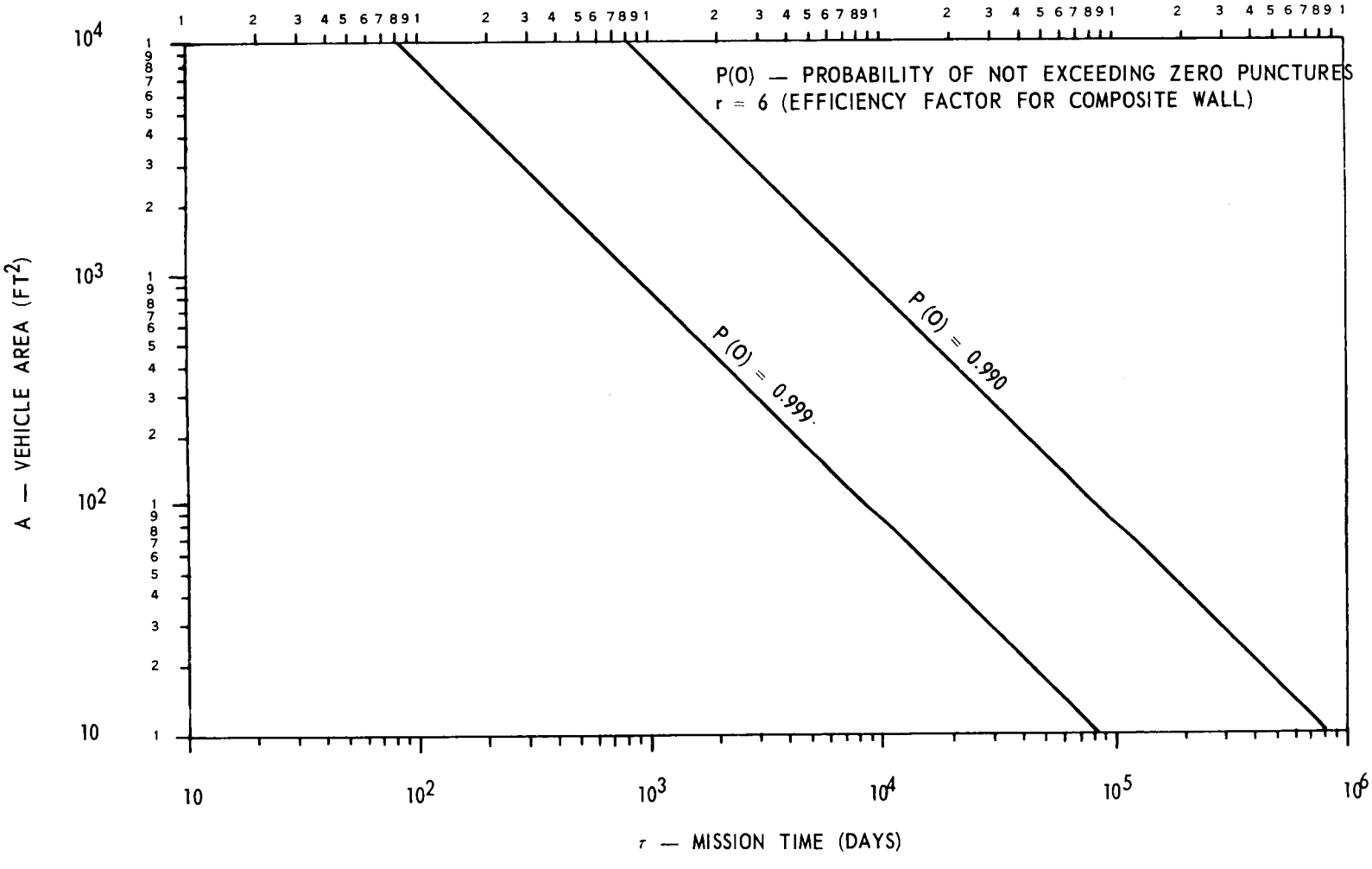

FIGURE 27 MISSION TIME VS VEHICLE AREA AT WEIGHT TRADEOFF POINT BETWEEN SELF-SEALING AND NON SELF-SEALING WALL STRUCTURES

Decompression of Punctured Pressurized Compartments

In the above analysis it was assumed that the self-sealing concepts would be 100 per cent reliable in providing a complete seal. This assumption, although recognized as being optimistic, was based on the consistent complete sealing that has been obtained with the latest self-sealing wall configurations evaluated. While the possibility of a partial or incomplete seal cannot be ignored, the advantages of a leak control system, even though not perfect, are still worthy of consideration. This will become more evident when one compares the times required (with and without leak control) to decompress a 10,000 ft^3 compartment from 14.7 to 5 psia, a pressure below which a crew could not long survive without increasing the oxygen content of the atmosphere. For this comparison we have considered one of the earlier elastomer self-sealing wall configurations which, upon being perforated by a 1/8-inch diameter steel sphere at an impact velocity above 20,000 fps, partially sealed the resulting 3/16-inch diameter hole (Reference 1, Part I). The residual air leakage rate for this wall configuration was recorded at 1.3 lbs/day for a pressure differential of 14.7 psi.

As is indicated in Figure 28, the unsealed punctured wall, without the leak control feature (elastomer sphere), would decompress the compartment to a dangerous level in 1.3 days (no air augmentation assumed), whereas, the self-sealing feature increases this time to 580 days. For those wall configurations in which complete self-sealing is achieved, this time would, of course, be increased indefinitely.

CONCLUSIONS AND RECOMMENDATIONS

Conclusions

Based on the evaluation of ballistic tests with various self-sealing wall concepts and an analysis of the factors associated with integrating these concepts into space vehicle wall configurations, the following conclusions have been reached.

(1) The self-sealing wall concept is a feasible technique for ensuring the sealed integrity of a pressurized compartment that has been punctured by a hypervelocity particle impact. This has been experimentally verified by ballistic tests with 1/8-inch diameter steel spheres at impact velocities exceeding 20,000 fps.

(2) Of the various self-sealing concepts evaluated, the two most successful techniques were determined to be the elastomer sphere and the combined sphere-chemical (rigid foaming resin) concept. While each of the above techniques sealed punctures effectively, the latter concept has the added advantage of a chemical backup system for achieving a complete seal should the elastomer sphere give only a partial seal.

(3) Of the two basic metallic wall configurations investigated in which the above sealing techniques were incorporated, the "integral self-sealing wall" configuration, where sealing is achieved at the outer shell, proved the most successful. However, while in conventional multi-wall space vehicle wall construction the inner shell only is made airtight, the above self-sealing wall requires that the outer shell be airtight. Although this wall concept does not require the inner shell to be airtight, it is concluded that if both shells were made airtight, a more reliable "leak proof" pressure compartment would result.

(4) Self-sealing cannot be achieved at the metallic inner shell of a multi-wall configuration once it sustains a puncture resulting from a hypervelocity particle impact. Ballistic tests have demonstrated that irrespective of interior wall construction, the inner shell of a multi-sheet metallic wall can be expected to petal once its ballistic limit is exceeded.

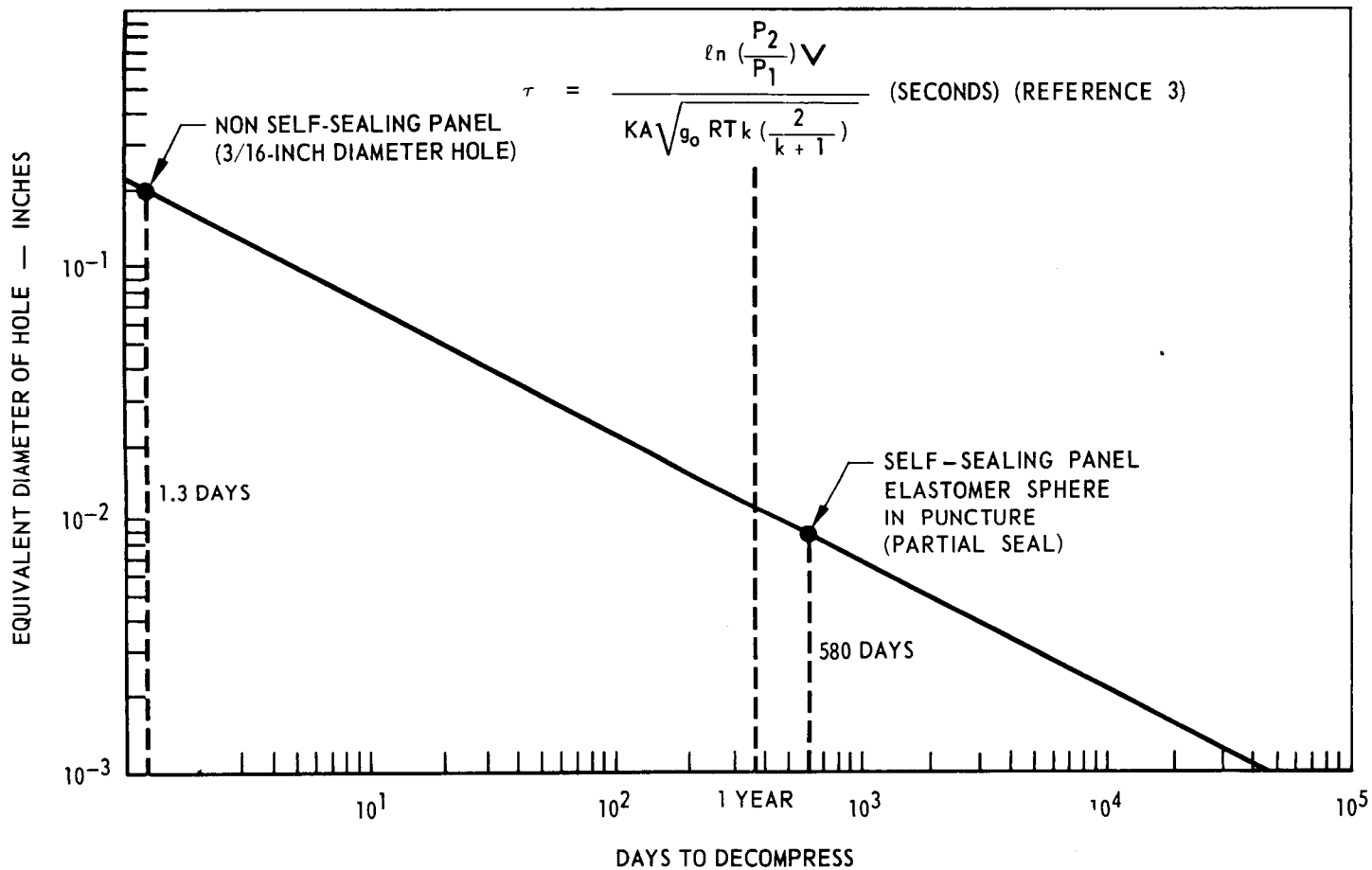

FIGURE 28 DECOMPRESSION OF 10,000 CUBIC FOOT SPACE VEHICLE FROM 14.7 TO 5.0 PSI (NO AIR AUGMENTATION)

(5) In wall configurations consisting of metallic face sheets, self-sealing can best be achieved at the front face where, by the proper use of shock wave damage control techniques, impact damage can be limited to a simple sealable hole.

(6) Shock wave damage control to the front fact sheet of a metallic wall configuration can best be achieved by isolating the outer shell from nearly incompressible material (solids or liquids) by an air gap or by the interposition of low density and highly compressible materials. However, these same techniques prove ineffective in preventing petalling of the rear metallic shell of a wall configuration once its ballistic limit is exceeded.

(7) If sealing is to be achieved at the inner shell of a multi-sheet wall configuration by use of the "self-sealing tile" concept, then the sealing surface of the inner shell of the basic wall structure should be a nonmetallic laminate or a bonded composite of nonmetallic laminate and metallic face sheet. In this latter case the metallic face sheet can still be expected to petal (once its ballistic limit is exceeded) but limited damage to the nonmetallic laminate permits sealing of the puncture at that face.

(8) For the self-sealing tile to be consistently effective in obtaining a complete seal, the combined sphere-chemical sealing system should be used, since the elastomer sphere cannot, by itself, seal completely the irregular shaped hole sustained at the nonmetallic sealing surface of the inner shell. While the tile sealing concept requires that only the inner shell be airtight (similar to conventional space vehicle wall construction) greater "leak-proof" reliability for the pressure compartment could be obtained if both shells were made airtight. In such a wall configuration, some loosely packed elastomeric spheres could be placed close to the outer shell to provide a backup system for the tile by permitting sealing at the metallic outer shell should the tile sealing system achieve only a partial seal.

(9) Based on the present state of development of the self-sealing wall concepts investigated, the elastomer sphere concept, when used in an "integral self-sealing wall" configuration, is the simplest in design and the most conpetitive, weightwise, with non-self-sealing wall configurations, since a weight addition of approximately 0.40 lbs/ft^2 will provide self-sealing capability. The combined sphere-chemical concept when used either in the integral wall or tile configuration requires a weight addition of 1.04 lbs/ft^2 and 1.45 lbs/ft^2 respectively. However, the weight of these latter two concepts could be appreciably reduced by a weight optimization program.

(10) On the basis of the assumptions made for determining the penetration flux of multi-wall composite structures, preliminary analysis indicates that for a design probability of zero penetrations equal to 0.990 the weight tradeoff point between self-sealing and non-self-sealing structures will occur at a mission parameter $A\tau$ * equal to 8.2 x 10^6 ft^2-days. If reliability requirements for long duration manned space missions require that the probability of zero penetration be increased to 0.999, then the weight tradeoff point will occur at a value of $A\tau$ equal to 8.2 x 10^5 ft^2-days. For a 10,000 ft^2 space station, these values of $A\tau$ imply a mission time of 2.24 years and 82 days, respectively. These weight tradeoff points will occur at lower values of $A\tau$ if the recently launched meteoroid detection satellite (Pegasus) reveals a less optimistic penetration flux than that assumed in the analysis. In this respect, it should also be noted that the Mariner IV Mars probe has encountered a continuing increased micrometeoroid activity at some 60 million miles from earth with the spacecraft experiencing an average of four impacts per day. Therefore, self-sealing wall structures can be expected to become increasingly competitive, weightwise, with non-self-sealing structures as the vehicle size and reliability requirements for a "leak-proof" space vehicle increases with increasing mission times and as the spacecraft ventures farther from the vicinity of the earth.

---

*A = Vulnerable area of space vehicle (ft^2)

τ = Exposure time in meteoroid environment (days)

Recommendations

In order to further enhance the development and evaluation of self-sealing wall structures for potential application to future manned space vehicles, the following recommendations are offered.

(1) Optimization, for minimum weight, of the most promising self-sealing concepts developed during this program (e. g. the elastomer sphere and the combined sphere-chemical concepts). The evaluation of candidate self-sealing wall configurations should be conducted with particle sizes more representative of meteoric particles (1/16-inch diameter and smaller). Particle velocities should be in excess of 30, 000 fps.

(2) Investigation of the design and fabrication problems associated with incorporating self-sealing capability into realistic pressure wall configurations. The following factors should be considered:

- Lightweight wall construction that will satisfy both the structural and thermal requirement of a space vehicle.
- The feasibility of using nonmetallic laminates or composites of nonmetallic laminates and metallic sheets in the construction of a space vehicle pressure wall.
- The feasibility of constructing a space vehicle multi-sheet wall with both shells airtight in order to increase the reliability of the sealed integrity of a pressurized compartment.
- Potential areas of application for space vehicles, space stations, lunar shelters, lunar roving vehicles, etc.

(3) In order to permit a more realistic comparative analysis and evaluation with non-self-sealing techniques, the following should be determined for the most successful weight optimized self-sealing wall configurations.

- Ballistic limits so that the penetration resistance of the self-sealing wall configurations may be compared to an equivalent weight non-self-sealing wall configuration.
- The reliability of the self-sealing wall concepts to maintain zero leakage for extended periods of time under sustained realistic operating conditions of pressure, temperature and radiation exposure.
- Multifunctional properties of the self-sealing elements used in a wall configuration (e. g. thermal and radiation protection).

REFERENCES

1. NASA CR-120 - Self-Sealing Structures for Control of Meteoroid Hazard to Space Vehicles - P. J. D'Anna, R. M. Heitz, J. J. Piechocki, October 1964.
2. "Self-Sealing Structures for Control of the Meteoroid Hazard to Space Vehicles," Northrop Report NSL 62-132-7 (Part II) March 1964, - Confidential.

3. "Self-Sealing Structures for Control of the Meteoroid Hazard to Space Vehicles," Northrop Report NSL 62-132-3, March 1963.

4. "Self-Sealing Structures for Control of the Meteoroid Hazard to Space Vehicles," Northrop Report NSL 62-132-4, June 1963.

5. "Self-Sealing Structures for Control of the Meteoroid Hazard to Space Vehicles," Northrop Report NSL 62-132-1, October 1962.

6. "A Report on the Research and Technological Problems of Manned Rotating Spacecraft," By Langley Research Center Staff - NASA TN-D-1504, August 1962.

7. NASA TN D-1493 - Environmental Problems of Space Flight Structures II. Meteoroid Hazard - January 1963, John R. Davidson, Paul E. Sandorf.

8. NASA TM X-899 - The Explorer XVI Micrometeoroid Satellite, Supplement II, Preliminary Results for the Period March 3, 1963 through May 26, 1963 - Compiled by Earl C. Hastings, Jr., Langley Research Center, Langley Station, Hampton, Va.

9. Handbook of Mathematical Functions - U.S. Department of Commerce, National Bureau of Standards, Applied Mathematics Series 55, June 1964.

10. Herrman, W., and Jones, A.H. "Correlation of Hypervelocity Impact Data," Proc. 5th Symposium on Hypervelocity Impact by the Tri-Service.

APPENDICES

The four appendices that follow contain a more thorough treatment of certain related subject matter that was either not included or discussed only briefly in the main body of this report. Appendices A and B discuss the state of materials subjected to impact shock and the consequences of high velocity particle penetration into compartments containing nearly incompressible materials. Appendix C discusses the relationship of the physical and chemical properties of materials to successful self-sealing. Appendix D summarizes the ballistic test results obtained in an attempt to determine the ballistic limit of a composite non-self-sealing wall structure.

LIST OF APPENDICES

APPENDIX A

STATE OF MATERIAL SUBJECTED TO IMPACT SHOCK

When two surfaces collide with sufficient speed, portions of both the projectile and target local to the interface are compressed to a great degree. Shock waves are generated in both target and projectile, radiating outward from the point of contact. A most simple description of this incident condition can be visualized by considering the one-dimensional impact situation wherein all motion is unidirectional and normal to the plane of the disturbance. For purposes of determining the severity of impact, it is of interest to know the pressures and associated velocities. Referring to Figure A-1, incident conditions are shown for a target material, initially at rest, impacted by a projectile moving to the right at a speed of V_i. The description of the target material in the shocked state can be defined by the classical Rankine-Hugoniot equations:[1]

$$\left(\frac{\rho}{\rho_o}\right)_t = \frac{U_{s_t}}{U_{s_t} - U_{p_t}} \qquad \text{(conservation of mass)} \qquad (1)$$

$$P_t - P_{o_t} = \rho_{o_t} U_{s_t} U_{p_t} \qquad \text{(conservation of momentum)} \qquad (2)$$

$$E_t - E_{o_t} = \frac{1}{2}(P_t + P_{o_t})(\nu_{o_t} - \nu_t) \qquad \text{(conservation of energy)} \qquad (3)$$

where

P = pressure

ρ = density

U_s = shock wave front velocity of propagation

U_p = material particle velocity in the shocked region

E = specific internal energy

ν = specific volume ($= 1/\rho$)

subscripts:

o refers to initial (unshocked) state

t refers to target material

The above three equations in five unknowns (assuming that the unshocked state is defined) are augmented by the equation of state of the material,

$$P = f(\rho, E) \qquad (4)$$

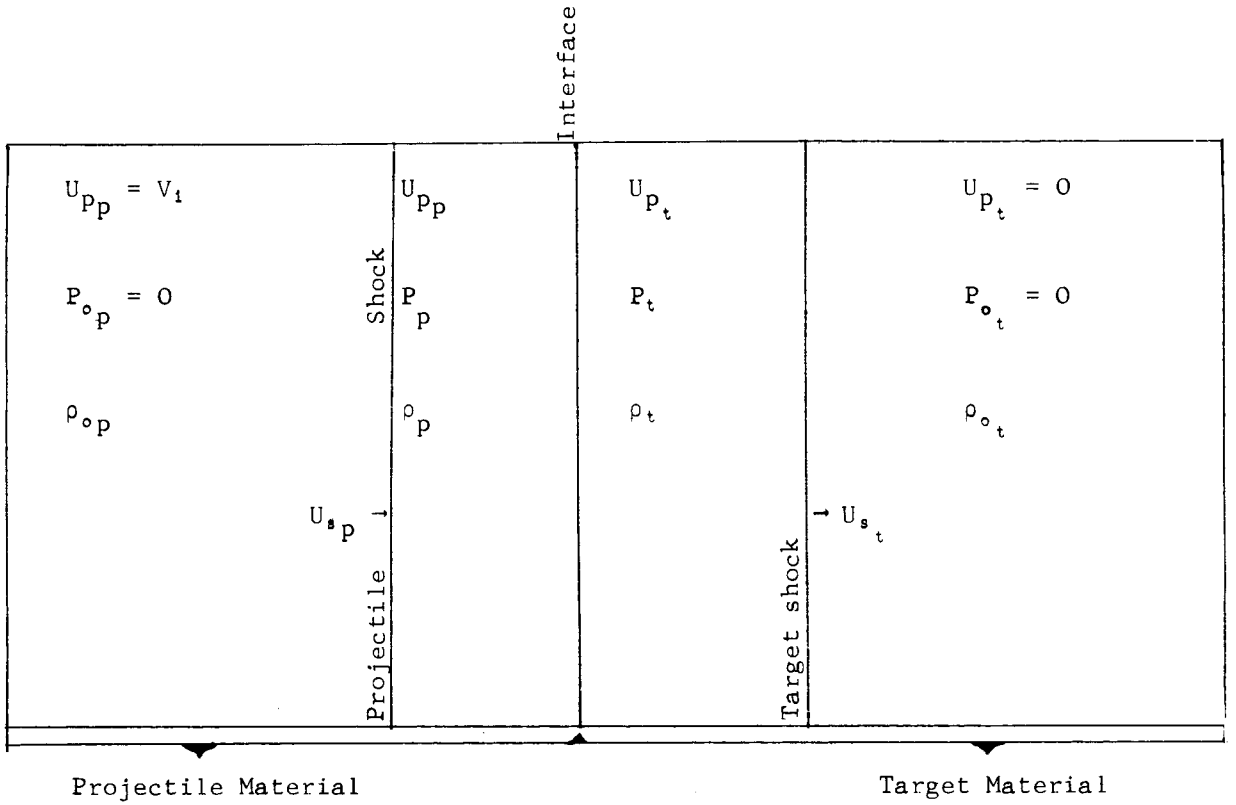

U_p = material particle velocity

U_s = shock propagation velocity

P = pressure

ρ = density

V_i = projectile impact velocity

Subscripts:

$_p$ refers to projectile

$_t$ refers to target

$_o$ refers to initial (unshocked) conditions

FIGURE A-1 ANALYTICAL MODEL OF ONE-DIMENSIONAL IMPACT CONDITIONS

Equation (4) is often replaced by an empirical relation found by experiment to be very accurate for most metals, viz.,[2]

$$U_{s_t} = Co_t + \lambda_t U_{p_t} \tag{5}$$

where

Co_t = adiabatic bulk sonic velocity

λ_t = empirical constant

This system of equations (1), (2), and (5) with four unknowns, $(U_s, U_p, P, \rho)_t$ is conventionally solved by considering similar conditions applicable to the projectile material, viz.,

$$\frac{\rho_p}{\rho_{op}} = \frac{V_i - U_{s_p}}{V_i - U_{s_p} - U_{p_p}} \tag{6}$$

$$P_p - P_{op} = \rho_{op} (V_i - U_{s_p}) (V_i - U_{p_p}) \tag{7}$$

$$U_{s_p} = Co_p + \lambda_p (V_i - U_{s_p}) \tag{8}$$

where the subscript $_p$ refers to projectile properties. Two additional stipulations are necessary to make the system determinant. These are the conditions that insure that both surfaces remain in contact, viz.,

$$P_p = P_t = P \tag{9}$$

$$U_{p_p} = U_{p_t} = U_p \tag{10}$$

The solution for impact pressure, P, is of greatest interest from the standpoint of target damage and will now be discussed. From equations (2), (5), (7), (8), one may write

$$P = \rho_{o_t} Co_t U_p + \lambda_t \rho_{o_t} U_p^2 \tag{11}$$

$$P = \rho_{op} Co_p (V_i - U_p) + \lambda_p \rho_{op} (V_i - U_p)^2 \tag{12}$$

Explicit solutions for P and U_p from equations (11) and (12) result in cumbersome expressions. For this reason, a graphical solution in the P-U_p plane is employed. This simple solution is executed as shown in Figure A-2. It can be seen that one merely offsets the projectile material curve on the horizontal scale by an amount equal to V_i, reflecting it about the vertical scale. (It can be seen that for impact of identical materials, the target material is accelerated to one-half the impact velocity due to the symmetry of the problem.) This graphical method of solution is used by experimenters for determining previously undefined Hugoniot properties of solids[3, 4] and liquids.[5]

The same procedure may be used for shocks traversing layered media. The problem is merely "re-started" when an additional interface is encountered, using as initial conditions the results from the previous cycle. To extend the previously cited example, the pressure of a second layer of target material behind the first requires that we "start" the solution for this next interface at the intersection point shown in Figure A-2. This is done by reflecting the initial target layer material curve about a vertical line through (P_1, U_{p_1}), since the initial target layer is effectively a "projectile" impacting the sublayer. The intersection of this reflected curve with the Hugoniot for the sublayer defines the new values of P_2 and U_{p_2} for this interface. This procedure is outlined in Figure A-3.

For the condition, $P_2 > P_1$, the first target layer is additionally compressed by a shock pressure jump ($P_2 - P_1$). In this instance, the compression follows the Hugoniot curve as presented. It is in the existence of the alternative, $P_2 < P_1$, that questions arise concerning the accuracy of the reflection method. In this case, the incident target layer expands upon rarefaction along approximately the adiabatic curve rather than the Hugoniot as assumed here. However, this inconsistency is disregarded for the calculations used in this study. In all instances, shock attenuation is neglected and, accordingly, results apply only to incident conditions. Factors of geometry which affect the one-dimensional motion assumption have been similarly disregarded, and the usual conditions of isotropy have been assumed.

This calculation method was used in this study for the determination of impact and interfacial pressures. Hugoniot data are available for approximately 27 basic metals, some common alloys, and a few organic and inorganic solids and liquids. In general, no Hugoniot data exist for the class of polymers used in the self-sealing program. However, it is still possible to utilize the analysis with polymers in the configurations (e.g., for the metal/polymer/liquid interface problem).

REFERENCES FOR APPENDIX A

1. Courant, R. and Friedrichs, K. O., "Supersonic Flow and Shock Waves, Vol. I," Interscience Publishers, Inc., New York, 1948.

2. Herrmann, W. and Jones, A. H., "Survey of Hypervelocity Impact Information," A.S.R.L. Report No. 99-1, Aeroelastic and Structures Research Laboratory, MIT, September (1961).

3. Walsh, J. M., et al., Phys. Rev., 108, 196-216 (1957).

4. McQueen, R. G. and Marsh, S.P., J. Appl. Phys., 31, 1253-1269 (1960).

5. Walsh, J. M. and Rice, M. H., J. Chem. Phys., 26, 815-823 (1957).

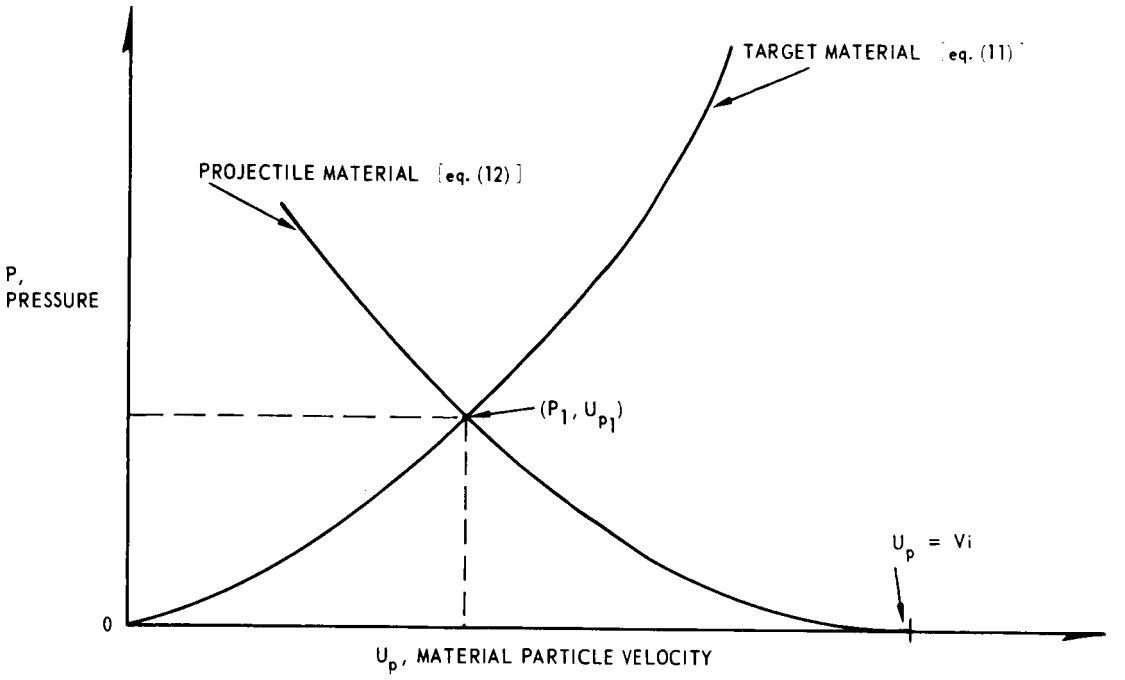

FIGURE A-2 GRAPHICAL SOLUTION TO IMPACT PROBLEM

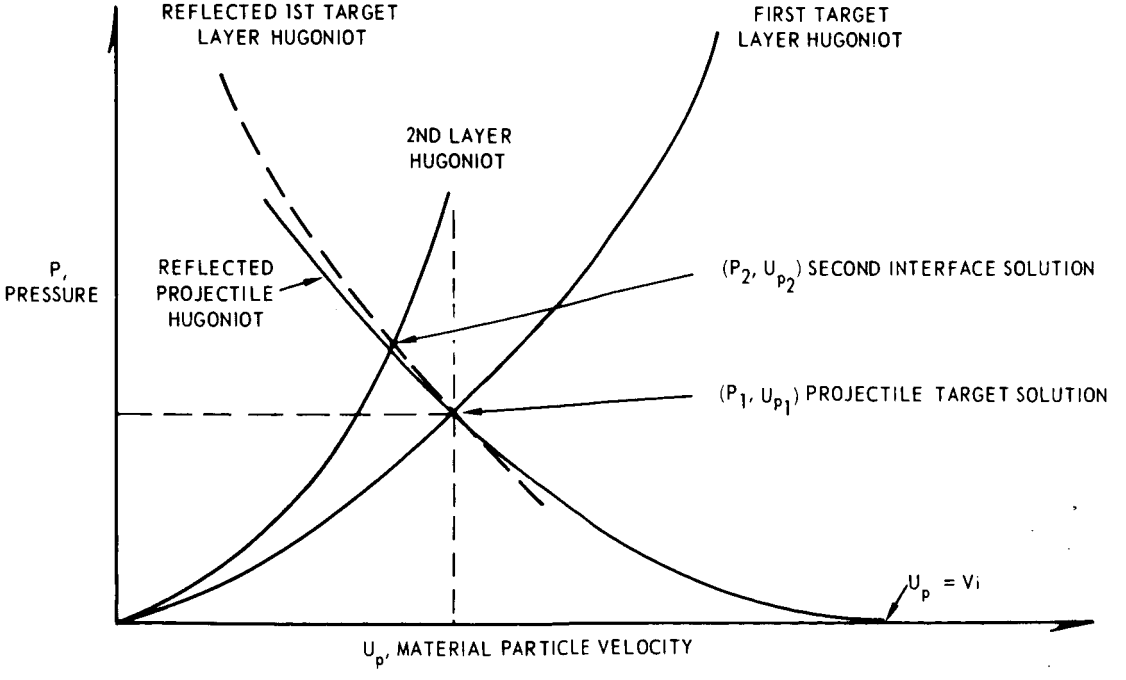

FIGURE A-3 SHOCK SOLUTION: TWO-LAYERED TARGET

APPENDIX B

HIGH VELOCITY PARTICLE PENETRATION INTO COMPARTMENTS CONTAINING A NEARLY INCOMPRESSIBLE MEDIUM

When a high velocity particle penetrates a compartment containing a nearly incompressible material (liquid or solid), the incident shock wave induces extremely high pressures at the compartment wall interface which may exceed the dynamic rupture strength of the penetrated wall. If the penetrated wall material is metallic or prone to rapid crack propagation, when loaded at high strain rates, then, the consequence may be petalling and/or explosive rupturing of the penetrated face sheets. This was dramatically demonstrated during the ballistic testing of one of the earlier panel configurations. The panel construction was basically a honeycomb core sandwich, with the core cells filled with a nearly incompressible elastomer. The pellet entry face of the panel was an 0.032-inch aluminum sheet while the pellet exit face was a 1/16-inch asbestos cloth (wire reinforced) neoprene sheet. The aluminum face sheet petalled while the neoprene sheet did not (see Figure B-1).

The chemical compartments used in the chemical self-sealing panel configuration are in essence liquid-filled tanks and, as a consequence, are also subject to such failures. An example of the explosive rupturing of an aluminum face sheet used as the penetrated wall of a liquid (water) filled tank is shown in Figure B-2.

In order to obtain a better understanding of the magnitude of the pressures that may be generated by a high velocity particle penetrating the chemical compartments of a chemical self-sealing panel, the method of analysis described in Appendix A is used to determine the pertinent interface pressures. The required Hugoniot shock data for the chemicals and face sheet materials used in the self-sealing panels were not available. Therefore, existing shock data of materials with densities approximately equal to those of interest were selected for this analysis. This approach, although yielding an approximate solution, is sufficiently accurate to indicate the pertinent pressures within a factor of two or less. For this analysis, an aluminum projectile was assumed to impact a water-filled nylon wall compartment at an impact velocity of 20,000 fps. The graphical solution for the interface pressures is illustrated in Figure B-3.

An aluminum projectile impacting a nylon compartment wall at 20,000 fps will result in an Al/nylon interface pressure of 425 kilobars (Pt. A) while the Nylon/H_2O interface pressure would be 370 kilobars ($\sim 5.44 \times 10^6$ psi) (Pt. B).

It is this latter pressure then that loads up the compartment wall. This pressure, when combined with initial impact induced damage to the wall, results in rupture of the penetrated face sheet. It is interesting to note that, for the ballistic conditions cited, an aluminum compartment wall gives an Al/H_2O interface pressure of 360 kilobars (Pt. C) or 10 kilobars lower than when a lower density (Nylon) material is used for the compartment wall. On the other hand, the initial impact pressure of the aluminum projectile on the aluminum wall (Al/Al) is about twice that of the aluminum projectile on the nylon wall (Al/Nylon). This apparent anomaly can be explained by the fact that the impedance* mismatch between the aluminum and water is greater than between nylon and water. This results in a smaller percentage of the

*Impedance = $(\rho_0 C_0 + \rho_0 \lambda Up)$ where ρ_0 = unshocked mass density, C_0 = bulk acoustic velocity, λ = empirical compressibility factor and Up = material particle velocity

PELLET IMPACT FACE

1/8″ DIA. GLASS SPHERE
V = 21,000 FPS

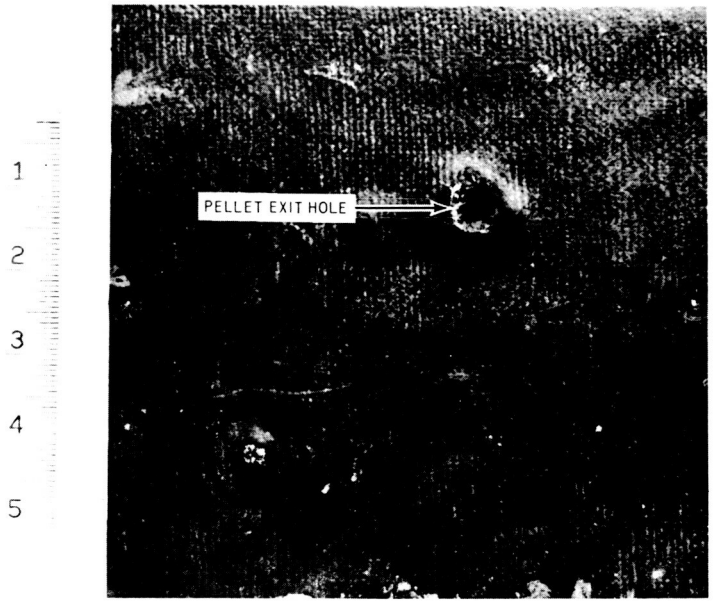

PELLET EXIT FACE

FIGURE B – 1 RUPTURED HONEYCOMB CORE – ELASTOMER PANEL

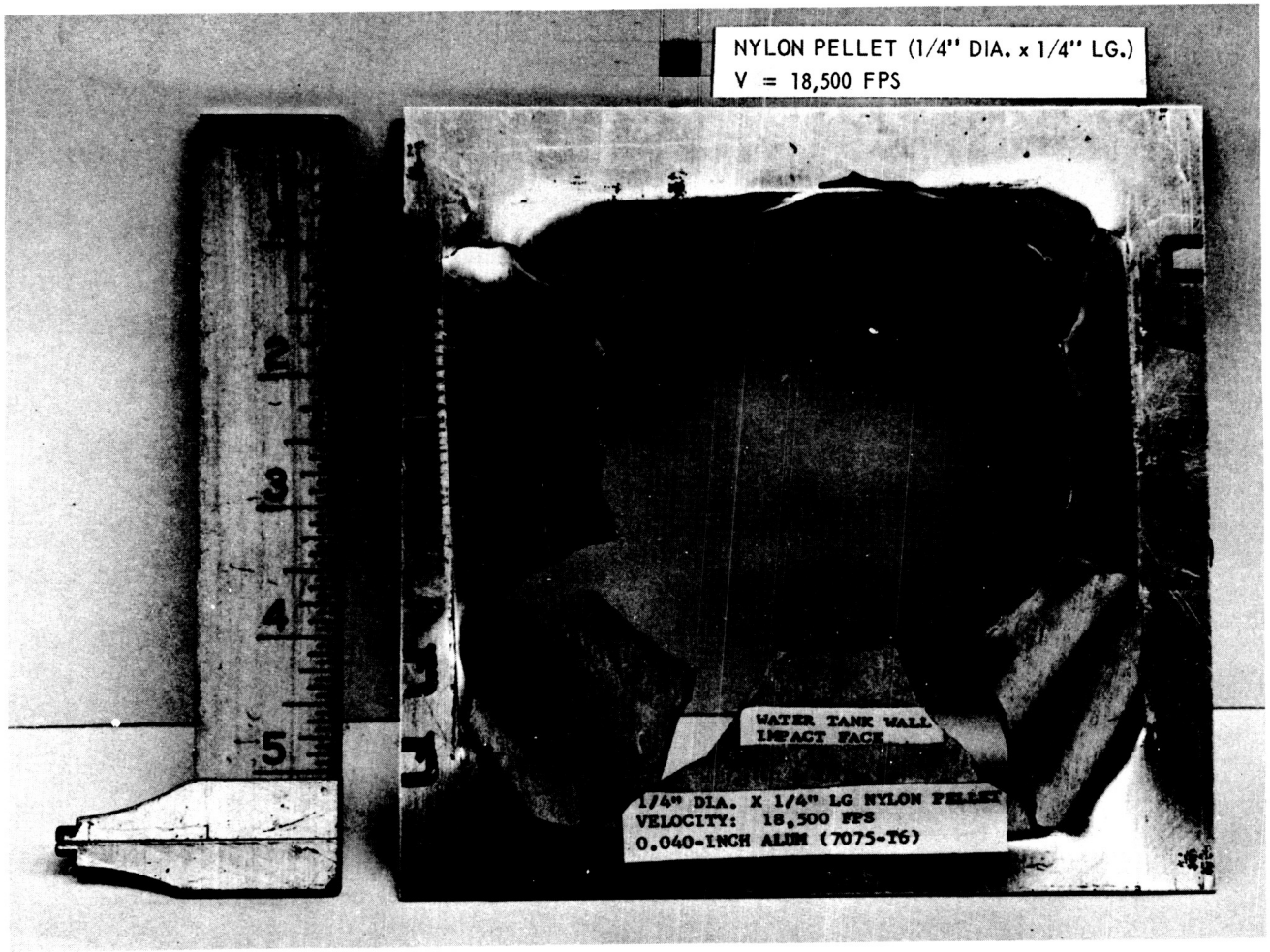

FIGURE B-2 RUPTURED ALUMINUM PANEL (WATER FILLED TANK)

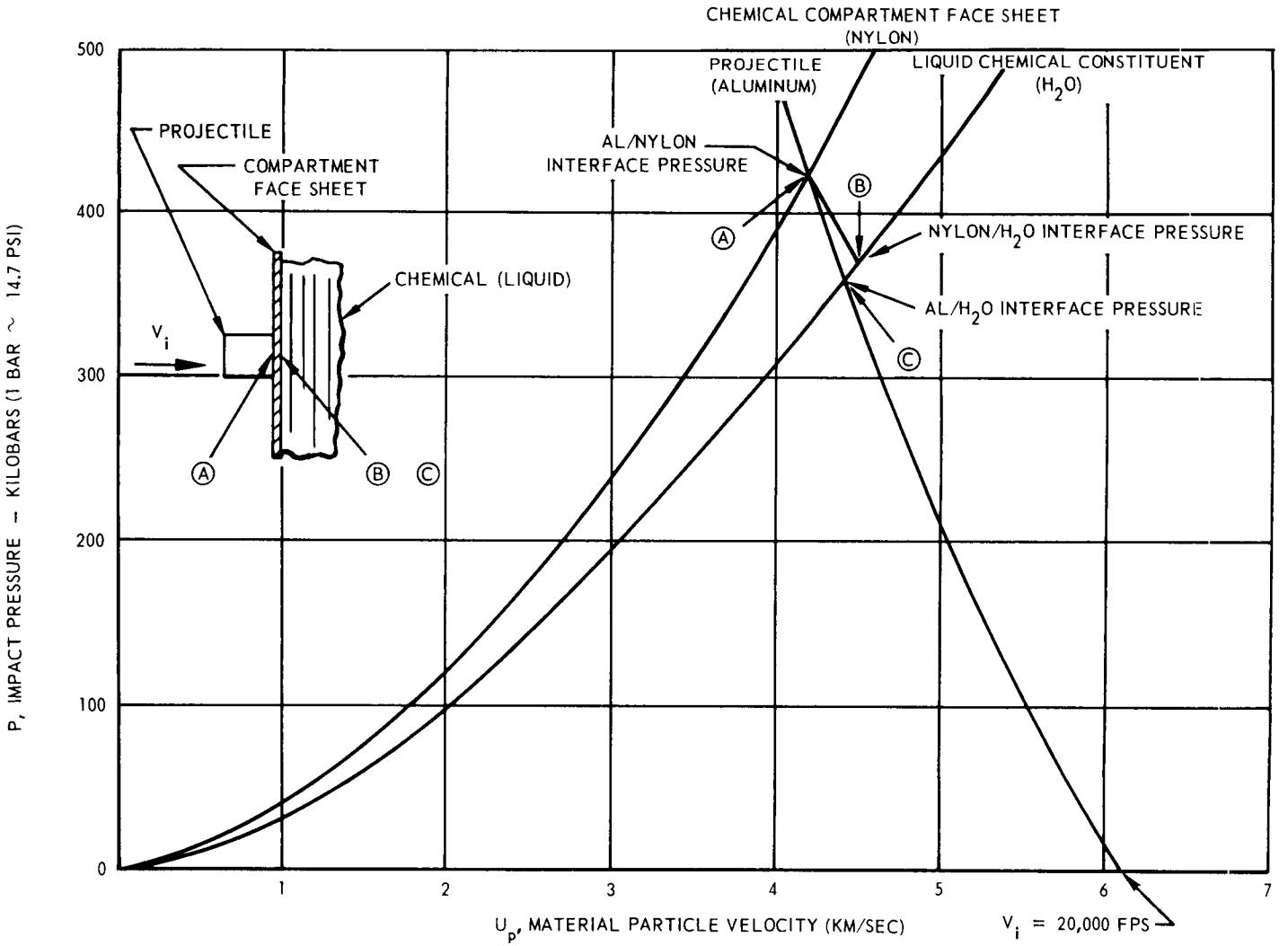

FIGURE B-3 APPROXIMATE SOLUTION OF SHOCK PRESSURE IN CHEMICAL COMPARTMENT

incident pressure being transmitted to the water for the Al/Al/H_2O impact conditions. However, it should not be concluded that an aluminum wall compartment would be more effective for damage control, than an appropriate structural non-metallic wall. Metals in general are more sensitive than non-metallics to rapid crack propagation when subjected to loading conditions under high strain rates (e.g., hypervelocity impact conditions). They would be expected to sustain more extensive damage than non-metallics when tested under similar ballistic conditions. Therefore in order to mitigate this hazard, non-metallic face sheets should be used for the chemical compartment of chemical self-sealing configurations and the compartment should be isolated from the pellet entry face of the panel.

APPENDIX C

PHYSICAL AND CHEMICAL PROPERTIES OF CURING AND FOAMING COMPOUNDS USED IN THE CHEMICAL SELF-SEALING CONCEPTS FOR METEOROID PROTECTION

The principle of the chemical self-sealing concepts investigated during this research program was based upon the dynamic action of a penetrating projectile initiating chemical reactions which result in a fast chemical seal. The existing pressure differential of approximately one atmosphere across the panel faces at the time of puncture was an important contributing factor in this fast chemical seal.

To attain the best response to the dynamic action of the penetrating projectile as well as to the turbulent mixing action due to the pressure differential, appropriate chemical constituents had to be selected. The selection of these constituents was dictated principally by the following factors.

(1) Selection of reactive components which cure and/or foam and cure very rapidly upon mixing in order to avoid heavy extrusion of the materials through the puncture during the chemical reaction.

(2) Selection of reactive fluids with a viscosity allowing proper flow and mixing inside the self-sealing structure once punctured.

(3) Selection of reactive fluids which form an elastomeric or foam material of sufficient strength and adhesion to the self-sealing structure walls to withstand the pressure differential of one atmosphere across the panel faces.

(4) Selection of reactive fluids which are the least toxic or nontoxic and do not undergo explosive reactions or highly exothermic reactions with the formation of highly volatile and toxic products.

(5) Selection of reactive fluids for which the mixing ratio should not be critical in order to give suitable cured elastomeric or foamed materials.

The preceding criteria were dependent upon other factors or parameters such as the type of self-sealing panel configuration investigated which included either strictly chemically self-sealant or combined mechanically and chemically self-sealant concepts. The type of materials used to make up the self-sealing panel configuration other than the chemical components was another important factor on which the selection of the chemical constituents was dependent. For example, the type of compressible material (such as elastomeric balls, fibers, and foams) used to minimize structural damage at the higher velocity impacts, influenced greatly the rate of formation of the elastomeric mass and its physical properties. In the case of the strictly chemical self-sealing concept, the degree and rate of mixing, the viscosity of the reactive fluids, and the rate of reactions of the mixed reactive fluids had to be higher than that of the combined mechanical-chemical self-sealing, if the extrusion of the reacting chemical constituents was to be kept low and thus attain a more successful seal. Finally, other important factors which influenced the selection of the chemical reactive fluids were: the method of encapsulation used for separating these fluids from each other to prevent reaction prior to being mixed upon impact; the velocity at which the panel was impacted; the temperature of the target.

With these varied criteria in mind, a variety of elastomeric materials were investigated. The two classes of materials which were felt to be satisfactory were the polyurethanes and the silicones. Because the expanding materials or foams were found to be the most promising self-sealants during this study, the discussion on physical and chemical properties of the chemical constituents investigated will be centered on the polyurethane and silicone foams.

Investigation of Polyurethane Foams

Recent advances in the development of polyurethane foams and their generally attractive properties suggested a possible application to self-sealing structures. The polyurethane foams are diisocyanate-linked condensation polymers which involve, in their preparation, a device for the formation of high polymeric molecules of predetermined structure. This device is a two-step reaction in which primary polymer chains terminating in reactive groups are treated with a bifunctional reagent adapted to react with these terminal groups and, thus, by uniting the primary chains, lead to molecules of a higher molecular weight. The material in the first step consists of polyester or polyether resins and the material in the second step is a diisocyanate which reacts with the terminal group and, in presence of a blowing agent, forms the polyurethane foam.

The polyester resins are produced by the reaction of a dibasic acid and a polyol with the elimination of water. These resins, when used for polyurethane foam systems, have a number of alcohol groups which react with the polyisocyanate in converting the low molecular weight-liquid polymer into a high molecular weight elastomer. Simultaneously, the excess of polyisocyanate reacts with water to generate the foaming agent, carbon dioxide (CO_2). The reaction of the polyisocyanate and water also contributes to the cross-linkage of the structure and its final chemical composition. Less cross-linkage or less branching produces a flexible foam. More cross-linkage or more branching produces a less eleastic structure; semi-rigid or rigid foam.

The polyether resins are produced by the catalyzed addition of propylene oxide to an alcohol by a reaction similar to the curing of epoxy resin systems. In the case of rigid foams, a few molecules of propylene oxide are added to the basic alcohol, while for flexible foams, many hundreds are added.

The polyisocyanates are chemicals derived from basic raw materials. Being very active and able to react readily with compounds containing active hydrogen atoms (i.e. polyesters and polyethers) they permit combinations leading to many new synthetics. Differences in reactivity with other chemical groups enable control of the formulation and characteristics of the resulting synthetic foams with an infinite range of physical, thermal, and chemical properties. These reactions usually take place quite readily at room temperature or with only moderate heating and the absence of catalysts. However, most of the reactions are greatly accelerated by small amounts of catalyst. The reactivity is usually more pronounced with aromatic diisocyanates than with the aliphatic derivatives. By choosing the right catalyst, the reaction can take place within 5 to 30 seconds. The diisocyanates have a tendency to form the dimers at room temperature when stored for long periods of time and, particularly, when exposed to moisture. The addition of small amounts of phosphorous chlorides and acyl chlorides has been recommended to prevent any loss in reactivity.

In the original foaming method for polyurethanes, carbon dioxide is used as the blowing agent. In the new method, a low boiling chlorofluorinated hydrocarbon (Freon) is introduced into the catalyst portion of the components. When the catalyst is added to the polyurethane resin, an exothermic reaction takes place, raising the temperature of the mass above the boiling point of the Freon, causing it to expand and fill the cells. Freon blown foams are, in general, considered more stable than the carbon dioxide blown foams.

Because a basic understanding of the polyurethane foams chemistry is helpful in realizing the limitations of their application to self-sealing panels, a brief description will be given here. Two of the most important primary reactions involved in the polyurethane formation are given below.

As an initial step, the polyfunctional compounds, diisocyanate (in excess), and polyester resin (or polyether resin), having alcohol groups react to form molecular chains terminated with isocyanate groups:

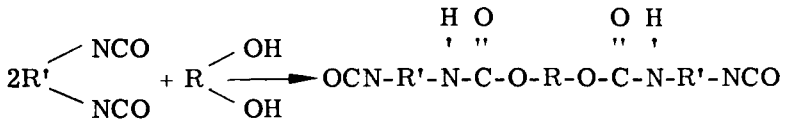

Diisocyanate + Polyester or Polyether ⟶ Liquid Adduct (Prepolymer)

The obtained liquid adduct contains both active hydrogens and reactive isocyanate groups which continue to react with hydroxyl groups to form long chains. This reaction frequently has an induction period of from 5 to 10 minutes followed by a rapid evolution of heat. The rate of this reaction can be increased; the degree of increase depending on the base used. Strong bases can cause the reaction to become violent. Generally, when a base is used, a mildly basic tertiary amine is recommended.

The rate of the foam and cure reactions required, for the chemical self-sealing system under discussion, should be in the order of seconds depending upon the type of self-sealing panel configuration investigated. Adding small amounts of stannous octoate catalyst to the reaction mixture will allow close control of the rate within the span of time indicated.

In the second step, the foaming reaction takes place. The free isocyanate groups react very readily with water in the following manner:

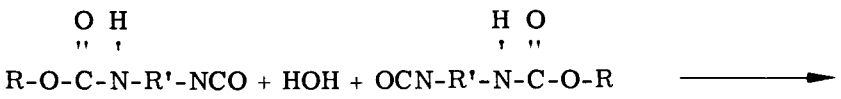

Urethane linkage + Water + Urethane linkage

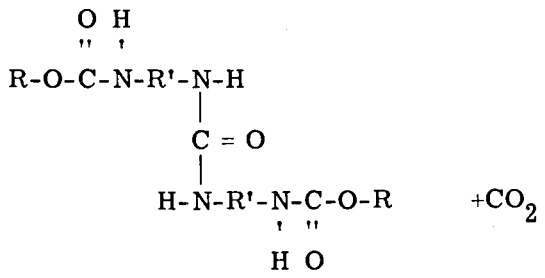

Polyurethane Foam + Foaming Agent

The carbon dioxide (foaming agent) is controlled by the quantity of water or amine present in the reaction mixture.

Among the polyurethane foam systems studied, concentrated effort was placed upon Freon blown foams. This type of foam does not necessitate an excess of diisocyanate as in the case of the CO_2 blown foams. In the preliminary study of the polyurethane foam application to self-sealing concepts, it was noted that careful control of the rise time property was important.

The rise time is a measure of the time elapsed between initial mixing of the foam ingredients and the completion of the rapid expansion of the foam sample. This time is a function of the generated heat and the Freon and stannous octoate concentrations. The amount and rate of the generated heat will depend upon the ratio of resin to diisocyanate and the degree and rate of mixing. This will determine a very important parameter, namely, the ratio of the rate of curing to the rate of blowing. If this latter ratio is too low, the foam will blow itself apart, that is the formed cell ribs and membranes will not have sufficient strength during the rise to withstand the forces caused by the gas evolution. Conversely if the ratio is high the polymer is rigidizing prior to sufficient foaming or rising, resulting in inadequate volume expansion. From this simple description, it can be seen that the reaction kinetics of any formulation are extremely sensitive to the chemical composition. Successful systems usually employ numerous additives whose quantity and function are determined mainly by experiment.

During a series of test where several self-sealing structures using a polyurethane system were impacted with 1/8-inch steel pellets at the lower velocities (~7,000 fps), the following disadvantages were noted.

(1) The high reactivity of the diisocyanate with compounds containing active hydrogen atoms. As mentioned above, it polymerizes at room temperature when exposed to moisture which makes it less reactive. However, this can be remedied by using small amounts of specific chemicals.

(2) The impracticability of most of the polyurethane foams being blown by either carbon dioxide or by Freon which will affect the shelf-life of the material and the sealing effectiveness of the self-sealing structures.

In the case where carbon dioxide is used as the blowing agent, an excess of diisocyanate is necessary in order to have free isocyanate groups to react with water and form the carbon dioxide. However, upon impact of the self-sealing structure containing such a foaming system, the proportion of diisocyanate to resin cannot be controlled, and therefore, in some cases, no excess of diisocyanate is present and no blowing agent is formed.

In the case where Freon is used as the blowing agent, the problem is the escape of the Freon from the foaming ingredients. The degree of escape of the Freon will depend upon the environment in which the foaming ingredients will be before or during the foaming activity. Most severe degassing takes place when the Freon containing ingredients are exposed to vacuum and to temperature variations, particularly to high temperatures for a long period of time. The loss of Freon under such conditions, prior to or during the foaming action, could create a serious problem to the point where no foaming could take place upon mixing of the two reactive fluids (resin and diisocyanate). However, the problem of degassing could be prevented to some extent by encapsulating the Freon-containing liquid. For higher temperatures a higher boiling Freon could be used. Upon foaming, the Freon would then either be expanded by the heat surrounding the foaming ingredients at the time of the foaming activity, or by the heat generated from the chemical reaction, depending on which of the heat sources would give the temperature at or above the Freon boiling point.

(3) The collapsing of the formed foam due to the reaction between, for example, the polyether and diisocyanate which had not proceeded far enough for the foam to support its own weight in the case where carbon dioxide is used as the blowing agent. However, today a remedy exists to correct this condition. A number of copolymers of polyethers and silicones can be

used. These retain the surface activity of the silicones (low surface tension, low internal energy, low polarity) and play the role of stabilizers in polyether urethane foams because of their stability and solubility in water, alcohols, and other organic solvents. Once the foam is formed they stabilize the foam and prevent a collapse.

Actual tests, where some selected polyurethane foams using Freon as the blowing agent were incorporated into self-sealing panel configurations punctured by projectiles simulating meteoroid impacts, demonstrated the feasibility of this type of foam.

Investigation of Silicone Foams

The silicones are a class of polymers of considerable commerical importance. They are based on a linear, cyclic, or cross-linked arrangement of alternating silicon and oxygen atoms, where the silicon is substituted by organic radicals or hydrogen. This class polymers is formulated as follows:

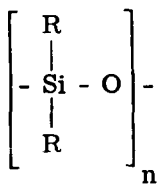

$R = (CH_3,\ C_2H_5,\ C_6H_5,\ \text{etc.})$

Organopolysiloxanes

The usual procedure for preparing silicone polymers is to hydrolize compounds such as $R_3SiC\ell$, $R_2SiC\ell_2$, $RSiC\ell_3$, and $SiC\ell_4$. The intermediates in the reaction are believed to be the corresponding silanols $R_2Si(OH)_2$ which condense very rapidly with elimination of water and formation of the -Si-O-Si- link. If (n) ranges from 3 to 9, cyclic systems are obtained which in the presence of alkaline catalysts open and give high molecular weight, linear silicone gum and, subsequently, elastomers. Various curing techniques are available for converting linear and cyclic materials to cross-linked elastomers and resins.

The manufacture of silicone elastomers is divided essentially into two steps; compounding and cross-linking. The first step consists of the intimate mixing under high shear or milling of the polysiloxane gum, a filler, and usually a cross-linking agent, together with miscellaneous additives for obtaining desired physical properties. The second step involves the cross-linking and curing processes that connect the polymer molecules with one another into an elastomeric mass of the desired properties. It is this second step which was of importance to us in the evaluation of elastomeric ingredients to be incorporated into self-sealing structures.

In the second step, the compounded stock may be cross-linked by the action of organic peroxides such as benzoyl peroxide. The number of cross-links can be controlled by varying the amount of peroxide (catalyst) used.

Of the materials evaluated for self-sealing purposes, the silicone foams were of particular interest. These are obtained by catalyzing either a fluid silicone rubber or a fluid silicone resin, each containing hydrogen as a foaming source and giving, respectively, a flexible silicone foam and a rigid silicone foam. In this foaming system, the foaming agent (hydrogen) is released upon mixing of either of these two fluids with the appropriate catalyst. A large variety of hydrogen sources exists, but the most interesting one has a releasing mechanism that is

initiated at room temperature and then accelerated with the exothermic chemical reaction taking place when the silicone base fluid and catalyst are mixed. Such a hydrogen foaming source could be obtained by the following chemical system:

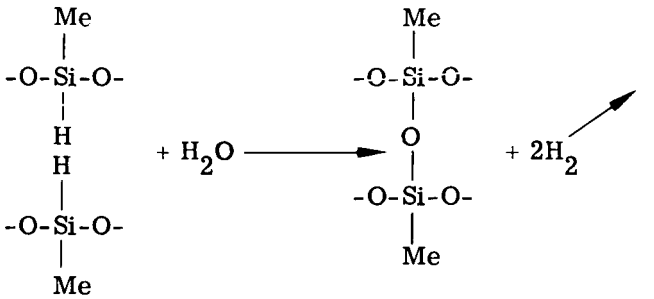

This reaction is very feasible due to the sensitivity of the silicone-hydrogen bond to acid and especially to base catalysts.

In the course of this investigation a silicone foaming system was discovered which yielded excellent results when incorporated in our chemical self-sealing concepts. It is a two-phase system where no excess of one of the foaming ingredients is necessary for formation of the blowing agent and where the blowing agent is chemically formed upon mixing of the fluid foaming base and a catalyst. Because of the proprietary nature of this material, the nature of the hydrogen source and the release mechanisms are unknown. The material is an RTV (Room Temperature Vulcanizing) silicone foam, either flexible or rigid.

The flexible silicone foam is a low-density resilient rubber over a temperature range of -100 to +500° F which cures at room temperature. When the fluid silicone rubber base and catalyst are mixed together in the proper proportions, expansion and curing actions begin immediately at room temperature. The foam will expand approximately seven times its original volume in the case where the foaming activity is not confined to a restricted area. During the expansion period, a small amount of hydrogen gas (blowing agent) is evolved from the reacting material.

The rigid silicone foam is a low-density foam which is a two-phase system (fluid silicone resin and catalyst). Here, too, if the two phases are mixed properly, expansion and curing begin immediately at ambient temperature. The blowing agent (hydrogen) is generated from the reacting material, similar to the flexible foam. By using stannous 2-ethylhexoate tin octoate as the catalyst, the expansion is accelerated appreciably, the curing time is shortened, and the reactions take place within seconds. However, by using the same catalyst for the formation of the flexible foam, the expansion and cure were accelerated only slightly and were below the rate of expansion and cure of the rigid foam.

In a further investigation of catalysts an even more effective material, that is, giving even faster foaming and curing actions, was found. This catalyst is of the stannous type (T-9) which gave significant improvement in higher curing and foaming rates making the chemical self-sealing systems even more effective. With this catalyst, the rates were almost identical for the flexible and rigid foams. It was found to be more uniform in its activity and possessing superior performance to the other stannous octoate catalysts in "one-shot" foams. It also maintained its activity for a longer period of time.

Within the chemical reactions taking place for the formation of the silicone foams, two actions occur; a curing action and a foaming action. In order that the formation of these foams can be used in the most effective way in chemical self-sealing concepts, the ratio of curing rate/foaming rate should be kept within a reasonable range. This ratio will vary drastically

depending upon; the type of catalyst used, the mixing proportion of the fluid silicone base and catalyst, the degree of mixing (or dispersion) of these two components, the heat generated upon mixing, and the size of the puncture obtained in the self-sealing structure after impact. The ratio should always be lower than one, but not excessively lower, since too low a value will cause heavier losses of foaming materials through the punctured hole. In the case where the ratio is too high, the silicone foam will set itself prior to sufficient foaming resulting in inadequate volume expansion. It can be seen that the closer the ratio approaches one without exceeding it, the more effective the self-sealing action will be at higher projectile impact velocities.

Preparation of Microcapsules Containing the Reactive Fluids

Southwest Research Institute (San Antonio, Texas) performed the task of microcapsule preparation. This effort called for a detailed program involving; encapsulation equipment set-up, selection of shell materials compatible with the reactive fluids, and actual encapsulation of the reactive fluids.

Encapsulation equipment. — Two types of encapsulation equipment were employed. These were the gravity extrusion device and the ten-orifice extrusion device. The gravity extrusion device consists of two concentric orifices. The filler material is pressure-fed through the inner orifice and the shell solution is pressure-fed through the outer orifice to form an extruded rod of filler material within a liquid tube of shell solution. Gravitational force acts on this stream of liquids to form capsules which are allowed to fall into a liquid hardening bath. The centrifugal device operates in a similar manner, with the exception that centrifugal force is used to form the capsules.

Hardening and treatment of capsules. — With shell formulations containing align, the capsules are hardened in a bath composed of 95 wt % water and 5 wt % calcium chloride which reacts with the algin to form a water-insoluble shell. The wet capsules are removed from the bath, rinsed with water and, in some cases, are also rinsed with a 5% glycerol solution. The capsules are then air dried until free flowing. As a safety precaution, the dried capsules are rinsed with a chlorinated solvent such as chloroform to remove any catalyst that might have inadvertently contaminated the surface of the capsules.

Compatibility of shell material with silicone resin. — Small solid spheres were prepared from a mixture of algin, poly(vinyl alcohol), gelatin, Tergitol TMN, and sodium benzoate and hardended in a 5 wt % calcium chloride solution. The spheres were washed with water, 5 wt % glycerol, and air dried. It was found that these spheres had no effect on either of the reactive fluids. As a consequence, the T-9 catalyst was encapsulated in shell materials formulated from the above polymers. Shell formulations are listed in Table C-1.

Encapsulation of catalyst T-9. — Eight shell formulations (Table C-1) containing algin were evaluated for the encapsulation of catalyst T-9. Several formulations were satisfactory, but formulation No. 6 was chosen because of the good quality of capsules produced and its smooth operation in the encapsulation equipment. The results of the encapsulation runs and the type of equipment used for the various runs are listed in Table C-2. The samples retained for their evaluation in the self-sealing structures were from run 27. These capsules were rinsed with 5% glycerol before air drying.

Three other polymers were evaluated for the encapsulation of catalyst T-9. They were poly (vinyl alcohol), gelatin, and carboxymethyl cellulose. These are well known for their impermeability to hydrocarbons.

The shell formulation used for poly(vinyl alcohol) consisted of 25 wt % poly(vinyl alcohol), 0.3 wt % Tergitol TMN, 1.0 wt % calcium acetate, and 73.7 wt % distilled water. The capsules

of T-9 from the encapsulation equipment were received in a 1.0 wt % algin XRA-10 solution. The calcium salt in the shell causes a thin layer of insoluble calcium alginate to form around the capsule and permits it to be handled during the subsequent washing and drying operations. The capsules were not satisfactory in the rigid liquid foam and as a consequence this system was not investigated further.

A similar system was tried with gelatin. The shell formulation was 30 wt % 300-bloom gelatin, 1.5 wt % calcium acetate, 0.3 wt % Tergitol TMN, and 68.2 wt % water. It was used at about 120°F. The hardening bath was a cold 1.0% algin XRA-10 solution. In several encapsulation runs the capsules formed readily and could easily be handled in the subsequent treatments but upon drying they became badly misshaped.

A different system was employed with the carboxymethyl cellulose. The encapsulation equipment consisted of three concentric orifices. A stream of liquid containing T-9 within a carboxymethyl cellulose solution with an outer surface of an algin-containing solution was extruded from this equipment. The double-shelled capsules were hardened in a 5 wt % calcium chloride solution. Several shell formulations were evaluated, the following being the most satisfactory.

(1) Outer shell:
- 1.5 wt % Algin XRA-10
- 1.5 wt % Algin XRA-20
- 2.0 wt % Elvanol 70-05
- 1.0 wt % Gelatin
- 0.3 wt % Tergitol TMN
- 0.2 wt % Sodium benzoate
- 93.5 wt % Distilled water

(2) Inner shell:
- 4.8 wt % Carboxymethyl cellulose
- 0.3 wt % Tergitol TMN
- 94.9 wt % Distilled water

Good capsules which had no effect on the liquid silicone foam resins were prepared. This system was abandoned when satisfactory capsules were prepared from the simpler single-shell system.

Encapsulation of liquid rigid silicone foam resin. — The liquid rigid silicone resin was encapsulated without any difficulty. Properties of the capsules are listed in Table C-3.

TABLE C-1 SHELL FORMULATIONS CONTAINING ALGIN

Shell Formulation Number	Algin wt %	Elvanol 70-05, wt %	Gelatin, wt %	Tergitol TMN wt %	Sodium Benzoate, wt %	Distilled Water wt %	Viscosity, centistokes
1	4.5	2.0	0.5	0.2	-	to 100%	275
2	5.0	2.0	0.5	0.3	-	"	470
3	5.0	-	0.6	-	-	"	430
4	5.0	3.5	0.5	0.3	0.2	"	550
5	4.0	4.0	1.0	0.3	-	"	300
6	5.0	3.0	1.0	0.3	0.2	"	630
7	1.3	6.0	0.5	0.3	0.2	"	
8	4.5	2.0	1.0	0.3	0.2	"	-

TABLE C-2 ENCAPSULATION OF CATALYST T-9

Ref. No.	Shell Formulation Number	T-9 Payload, wt %	Encapsulation Equipment[1]	Capsule Size, microns	Effect of Capsules on Silicone Resins	
					Rigid	Flexible
1	1	65	G	-	Hardened in 3 days, slight foaming.	Gelled in 3 days.
2	1	44	G	500-1000	Slight foaming and viscosity increase after 5 days.	Viscosity increase after 5 days.
4	1	68	G	1200-1400	Slight viscosity increase and gas bubbles after 11 days.	Few gas bubbles after 11 days.
5	2	65	G	950-1200	Slight viscosity increase and few gas bubbles in 10 days.	Slight viscosity increase in 10 days.
6	3	58	G	800-1000	Gelled in 9 days.	Slight viscosity increase in 9 days.
8	4	44	G	900-1100	Slight viscosity increase after 4 months.	No change after 4 months.
9	5	20	G	900-1100	Slight viscosity increase after 4 months.	No change after 4 months.
10	6	34	G	900-1100	Slight viscosity increase after 4 months.	No change after 4 months.
12	7	44	G	900-1100	No change after 4 months.	No change after 4 months.

TABLE C-2 ENCAPSULATION CATALYST T-9 (Continued)

Effect of Capsules on Silicones Resins

Ref. No.	Shell Formulation Number	T-9 Payload, wt %	Encapsulation Equipment(1)	Capsule Size, microns	Rigid	Flexible
13	8	-	G	900-1100	Immediate reaction.	-
22	9	60	G	900-1100	Immediate reaction.	-
23	6	35	G	900-1100	No change after 3 months.	-
24a	6	32	C	900-1100	Slight viscosity increase after 3 months.	-
24b	6	35	C	900-1100	No change after 3 months.	-
25	6	33	C	900-1100	No change after 2 weeks.	-
27	6	33	G	900-1000	No effect.	No effect

(1) G - Gravity extrusion equipment, C - Centrifugal extrusion equipment.

TABLE C-3 ENCAPSULATION OF LIQUID RIGID SILICONE FOAM RESIN

Equipment - Gravity Extrusion

Ref. No.	Sample Shipment Number	Shell Formulation	Resin Payload, wt %	Capsule Size, microns	Capsule Treatment
26a	1-788	6	81	1000-1600	Glycerol rinse.
26b	1-789	6	85	1000-1600	Glycerol rinse.

APPENDIX D

SUMMARY OF TEST RESULTS FOR DETERMINING THE BALLISTIC LIMIT OF A COMPOSITE WALL STRUCTURE

In the section of this report entitled "Technical Discussion and Analysis" (page 40), an analytical procedure was presented for conducting a comparative evaluation between self-sealing and non-self-sealing wall structures. However, before this analysis could be applied to composite wall structures, the ballistic limit* of the candidate wall had to be known or experimentally determined so that a penetration resistance efficiency factor (r) of the composite wall, as compared to a homogenous single wall (having the same ballistic limit), could be calculated. Therefore, in line with this requirement a ballistic test program was initiated in an attempt to experimentally determine the ballistic limit of a representative non-self-sealing composite wall configuration. A summary of the results of this test program including details of the wall configuration tested are given in Figure D-1. The figure inserted to the right of each datum point indicates the accuracy to which each velocity was determined. Three different diameter (1/16", 3/32", and 1/8") steel spheres and 1/8" diameter aluminum spheres were used for projectiles, thus permitting variation of the mass by a factor of 8 and the mass per unit projected area of the projectile by a factor of approximately 3.

At the respective velocities indicated, the rear sheet of the wall specimen was punctured each time it was impacted with either the 1/8-inch diameter or 3/32-inch diameter steel spheres. Since it became apparent that the ballistic limit would occur at some velocity below the velocity range of interest for our study ($V \geq 20,000$ fps), further testing with these projectiles was discontinued. On the other hand, while the rear sheet of the wall specimen was perforated with the 1/16-inch diameter steel and 1/8-inch diameter aluminum spheres, at the lower impact velocities indicated, perforation of the rear sheet ceased as the impact velocity approached 20,000 fps.

Evaluation of these test results plus consideration of the phenomena associated with hypervelocity impact indicates that for certain combinations of wall structure and projectile there may exist more than one ballistic limit. This may become more apparent if we first consider the manner in which Charters and Summers (References 1 and 2) classified impacts into thick targets into several categories. These categories, which depend primarily on projectile material and velocity, are defined as the unfragmented projectile region, the transition region in which the projectile is broken, and the fluid impact region in which both projectile and target behave like fluids. It is to be noted that any penetration relations obtained in one region are not applicable to other regions of impact.

In a similar manner, impacts into multi-sheet composite targets may be classified simply into the low-speed region, the transition region, and the high-speed region. Figure D-2 qualitatively illustrates how, depending on the projectile and wall configuration specified, a ballistic limit for a given projectile may exist at one or more regions of impact. In the low speed region of curve ①, V_a represents the lower ballistic limit or minimum velocity at which an unfragmented projectile will perforate the rear sheet of a multi-wall target. For the composite multi-sheet wall configuration used in these tests, this point will occur at some velocity

* The ballistic limit, as defined here, is the velocity above which a given projectile will damage the rear shell of a multiwall composite structure to the extent that air leakage (assuming no self-sealing capability) will occur through the wall when it is subjected to a pressure differential of approximately one atmosphere.

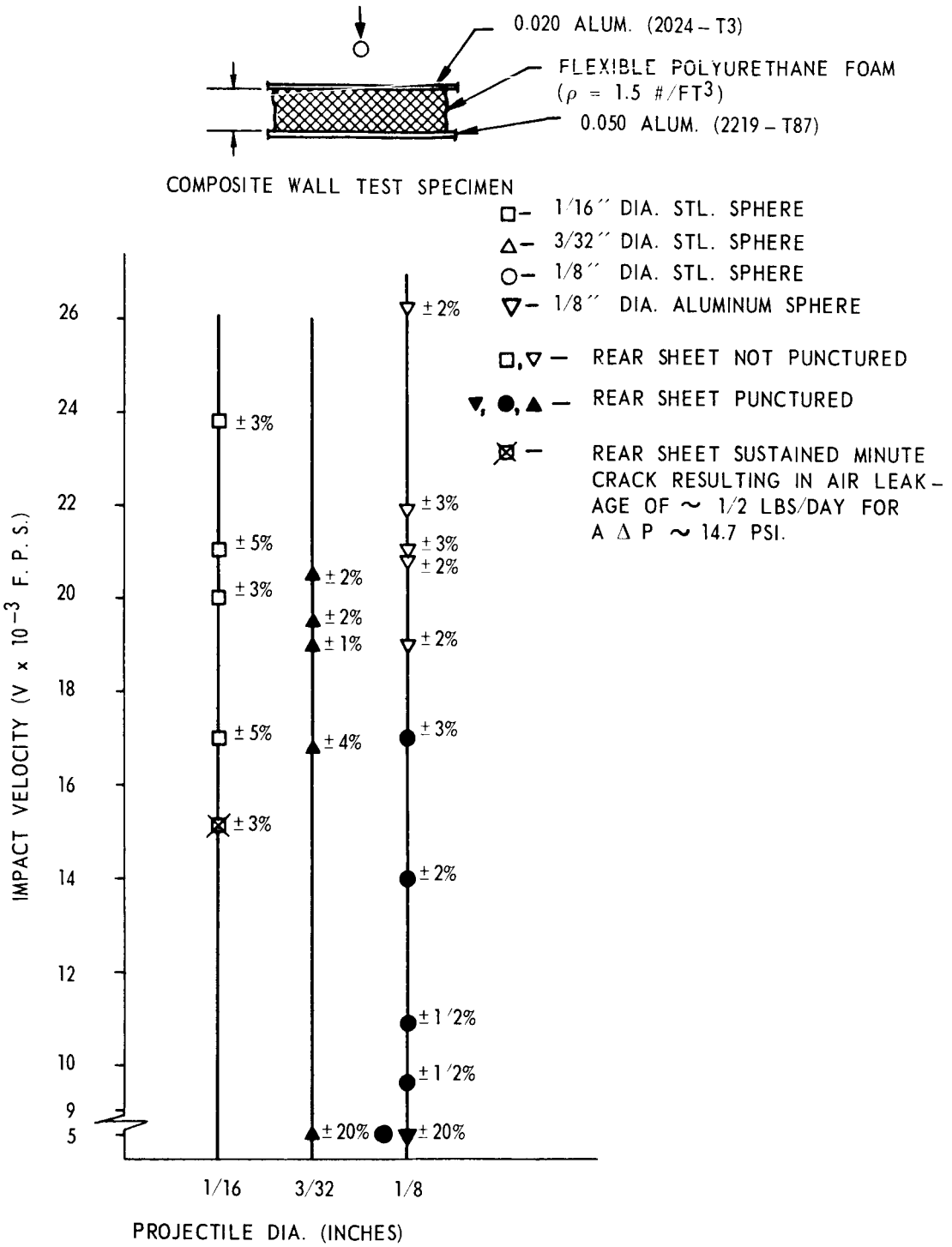

FIGURE D – 1 SUMMARY OF BALLISTIC TEST RESULTS

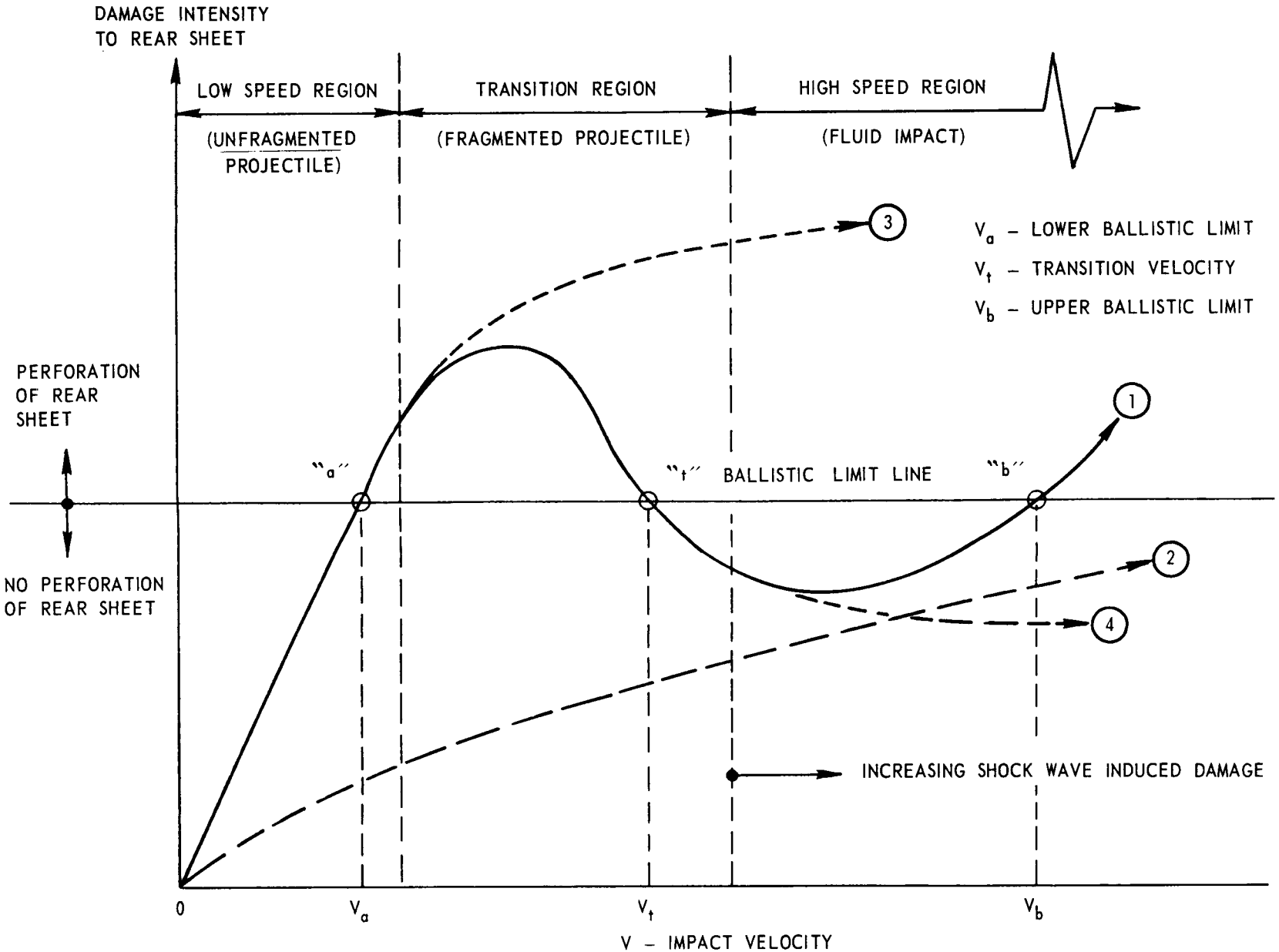

FIGURE D–2 BALLISTIC LIMIT VS IMPACT REGION

below 5000 fps for both the 3/32 and 1/8-inch diameter steel and 1/8-inch diameter aluminum projectiles. For the 1/16-inch diameter steel projectiles, the lower ballistic limit would occur at some velocity below 15,000 fps.

As the above projectile velocities are increased above their respective lower ballistic limit, a point will be reached beyond which the projectiles will start to fragment. Initially, the projectile and target material punched out of the front sheet form a tight cluster of relatively large fragments with each fragment possessing sufficient energy to punch a hole in the rear sheet. With increasing velocity this cluster of material will be fragmented further into finer particles, which, upon passing through the front sheet, will expand into a circular cross-section conical spray before impacting the rear sheet. The impact pattern observed on the rear sheet indicates that the spray cone is divided into two zones. A central or inner zone, with high particle concentration, composed of the larger particles from the projectile and front sheet material, that was in line with the projectile, and an outer zone of lower particle concentration composed mainly of finer particles ejected from the front sheet. For a given projectile and wall configuration, the diameter of the spray cone impacting the rear sheet increases with increasing velocity, to some limiting value, while the individual particle sizes decrease. In general, the penetration capability of the particle spray would be expected to decrease as one moves radially outwards from the center of impact at the rear sheet.

Depending on the size and structure of the projectile, the rear sheet of a wall configuration may be perforated at a low velocity but not at some higher velocity. This will occur if at the lower impact velocity, where the projectile is either unbroken or slightly fragmented, the resulting relatively large particles of projectile and/or front sheet retain sufficient energy to perforate the rear sheet. At higher impact velocities, the resulting finer fragments are either absorbed by the filler material of the wall configuration or dispersed over a larger area of the rear sheet so that the intensity of pressure loading by the spray of particles falls below that required to perforate or rupture the rear sheet. The velocity V_t at which this occurs (see curve ① of Figure D-2) is called the transition velocity or the velocity at which perforation of the rear sheet ceases with a further limited increase in impact velocity. In the ballistic tests conducted, this transition point "t" was bracketed with both the 1/16-inch diameter steel and 1/8-inch diameter aluminum projectile. The 1/16-inch diameter steel sphere cracked the rear sheet at a nominal impact velocity of 15,000 fps while at a velocity of 17,000 fps, the rear face of the rear sheet was undamaged. Therefore, the transition velocity for this projectile would occur at approximately 16,000 fps. The 1/8-inch diameter aluminum sphere perforated the rear sheet at a nominal velocty of 5,000 fps while at 19,000 fps, the rear face of the sheet was undamaged. Therefore, the transition velocity for this projectile must occur somewhere between 5,000 and 19,000 fps. Within the transition region, the character of the projectile and front sheet material breakup changes so rapidly with velocity that it becomes extremely difficult to accurately locate the transition velocity. It should also be noted that V_t cannot be considered a ballistic limit since it is a velocity above which perforation of the rear sheet ceases rather than, by definition of ballistic limit, a velocity above which perforation occurs.

With increasing velocity, above the transition point, the spray cone angle formed by the impact-induced particles will continue to increase and finally stabilize at some relatively constant value. As the spray cone angle increases, the particles are spread over a larger area so that the effective particle pressure induced on the rear sheet will decrease. When the spray cone angle reaches a constant value, and if the mass of the impact-induced material being accelerated towards the rear sheet remains relatively constant, the effective particle pressure on the sheet will start to increase with increasing velocity and ultimately ruptures the rear sheet. On the other hand, if the total mass of the impact-induced particles that reaches the rear sheet decreases, due to some of the particles being absorbed by the filler material of the wall configuration, and/or a rearward ejection of projectile material at the front sheet (due to rarefaction wave interaction at the projectile free surfaces), then the effective particle pressure at the rear sheet may decrease with increasing velocity. However, as the high speed

region is transversed, shock wave induced damage will play an increasingly important part in inducing failure of the rear sheet and depending on the mass of the projectile, it is expected that another ballistic limit will be reached at some velocity V_b as is indicated in Figure D-2. At the highest velocities attained with the 1/16-inch diameter steel and 1/8-inch diameter aluminum projectiles, it was not possible to reach this second or upper ballistic limit. This indicates that if this limit does exist for the above projectiles it must lie at some impact velocity higher than those achieved during these tests. In support of this it was observed that the aluminum projectile at 21,900 fps did not damage the rear face of the rear sheet while at the highest velocity achieved (26,200 fps) the rear sheet was bulged.

If, within the velocity range of interest, a specific projectile does not induce shock wave pressures of sufficient intensity to rupture the rear sheet then the upper ballistic limit V_b would never be reached and only the lower ballistic limit V_a (if it lies within the velocity range of interest) will have any significance in determining the vulnerability of a wall structure. Curve ② of Figure D-2 illustrates the situation where a projectile is of such size and structure that it does not perforate the rear sheet of a given wall configuration, neither in the low speed and transition region where effective particle pressure is the predominant damage mechanism, nor in the high speed region where shock wave damage predominates. This curve may exemplify the situation for the majority of dust-like meteoric particles that may be encountered during a space mission. Curve ③ on the other hand exemplifies the situation for the larger mass particles where, if a particle causes perforation of the rear sheet (in the low speed region), a similar particle will also rupture the sheet with any further increase in velocity in all three impact regions. Curve ④ illustrates the situation for an intermediate mass particle in which the rear sheet is perforated in both the low speed and transition region, but once it transverses the transition velocity, it ceases to rupture the rear sheet for any further increase in velocity in both the transition and high speed regions. This could occur, at the higher impact velocities, when the geometry and structure of projectile and bumper (front face sheet) are such that interaction of rarefaction waves at the projectile free surfaces results in most of the projectile mass being ejected rearwards at the bumper face.

Figure D-3 illustrates how damage to the rear sheet of the wall configuration, depicted in Figure D-1, varies with increasing impact velocity of 3/32-inch diameter steel spheres. At a nominal velocity of 5,000 fps the impact is in the low speed region where the unfragmented projectile shears a plug from the rear face sheet of approximately the same diameter as the projectile. At 16,800 fps, the transition region is entered where the projectile has fragmented and the cluster of impact induced particles has punched a hole in the rear sheet of approximately the same diameter (1/2-inch) as the cluster of particles impacting the sheet. In this velocity range each fragment in the cluster possesses sufficient size and energy to perforate the rear sheet individually, as is evidenced by the jagged periphery of the hole. As the impact velocity increases to 19,000 fps, the amount of material removed from the rear sheet decreases, but the sheet bulges outwards, local to the hole, in a 1-inch diameter area and cracks radiate from the hole boundary. This can be attributed to the fact that as the diameter of the outer zone or spray of impact-induced particles increases (with increasing velocity) the diameter of the inner zone or cluster of larger particles, possessing sufficient energy to perforate the rear sheet, decreases. While this results in less material being removed from the rear sheet, the spray of particles forming the outer zone induces a shock wave pressure pulse to the rear sheet of sufficient intensity to cause outward bulging of the sheet and the formation of cracks local to the hole. With the impact velocity increasing to 20,500 fps, the shock wave induced pressure pulse to the rear sheet also increases so that petalling of the cracked sheet segments occurs local to the hole. Therefore, while the overall hole size in the rear sheet has now increased with an additional increase in velocity, the amount of material removed from the sheet has continued to decrease. On the basis of these observations, it would be reasonable to assume that by increasing the impact velocity further into the high speed region, a limiting velocity would ultimately be reached where perforations of the rear sheet by clusters of individual particles would cease. Any rupturing of the sheet would then occur from the

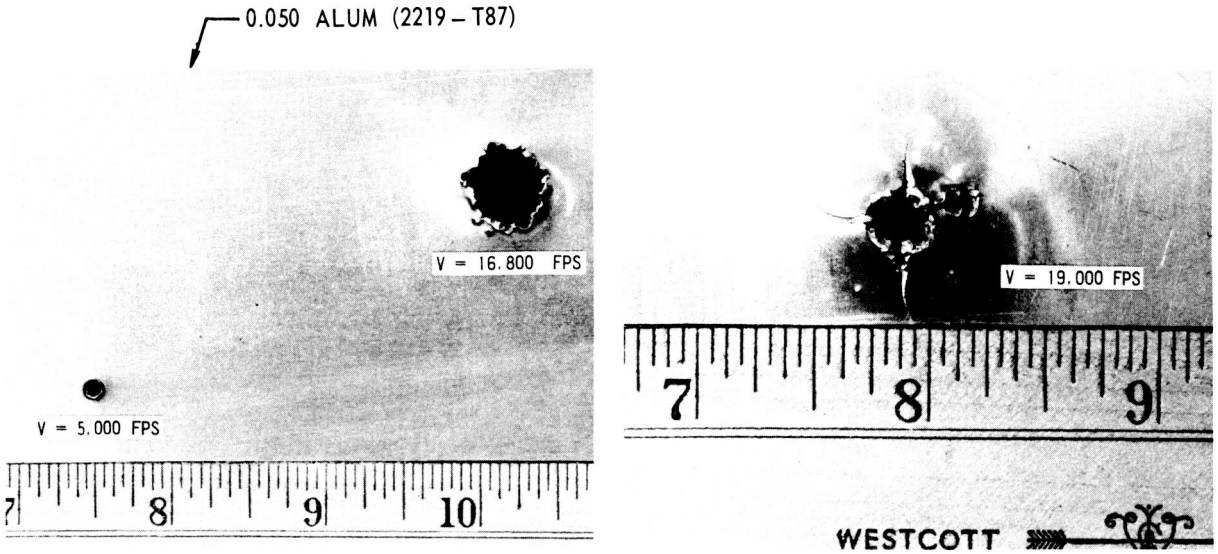

REAR FACE SHEET (PELLET EXIT FACE) SHOWN

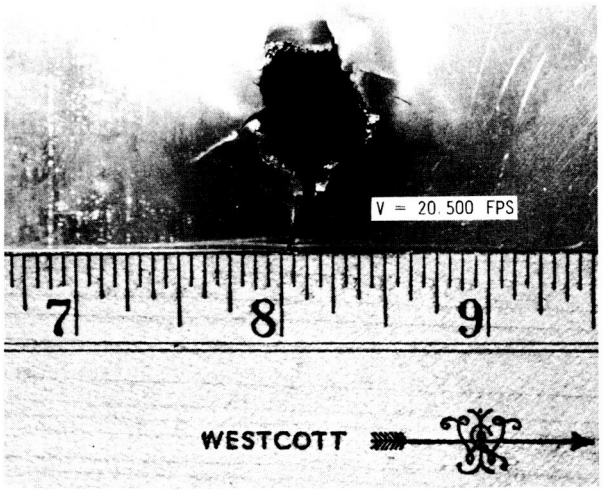

PROJECTILE: 3/32 – INCH DIA. STEEL SPHERE

FIGURE D – 3 COMPARISON OF DAMAGE TO REAR FACE SHEET OF DOUBLE WALL STRUCTURE AT VARIOUS IMPACT VELOCITIES

shock-induced pressure pulse transmitted by the filler material or in its absence by the fine spray of impact-induced particles. While the diameter of such punctures would be larger than those occuring at lower velocities, it might be expected that no material would be removed from the rear sheet. However, reflection of the shock compression waves from the free surface of the rear sheet induces exceedingly high tension stresses in the sheet which would result in material removal by spalling.

REFERENCES FOR APPENDIX D

1. Charters, A.C., and Locke, G.S., Jr., "A Preliminary Investigation of High-Speed Impact," NACA RM A58B26, 1958.

2. Summers, James L., "Investigation of High Speed Impact-Regions of Impact and Impact at Oblique Angles," NASA TN D-94, 1959.